

Linköping Studies in Science and Technology
Dissertation No. 484

Driveline Modeling and Control

Magnus Pettersson



Department of Electrical Engineering
Linköping University, S-581 83 Linköping, Sweden

Linköping 1997

Driveline Modeling and Control

© 1997 Magnus Pettersson

magnusp@isy.liu.se
Department of Electrical Engineering
Linköping University
S-581 83 Linköping
Sweden

ISBN 91-7871-937-2 ISSN 0345-7524

Printed in Sweden by LTAB Linköpings Tryckeri AB 1997.548

To Anna and Oscar

Abstract

A vehicular driveline is the system used to transfer engine torque to the wheels. Resonances in the elastic parts of the driveline are important to handle when control of the engine and the transmission is optimized.

Gear shifting by engine control is a new approach for automatic gear shifting with disengaging the clutch replaced by engine control. Resonances are excited in an uncontrolled driveline if the time for shifting to neutral gear is decreased. This leads to problems with disengaging the old gear and synchronizing speeds for engaging the new gear. Internal driveline torque control is a novel idea for handling resonances and increasing shift quality. By estimating the transmitted torque and controlling it to zero by engine control, the gear can systematically be disengaged with minimized driver disturbances and faster speed synchronization. Field trials show fast shifts to neutral gear, despite disturbances and driveline oscillations at the start of the gear shift. The control scheme is simple and robust against variations among different gears. Furthermore, damping of driveline resonances can be obtained with an observer in combination with a PID feedback structure, despite the higher order driveline system.

Traditional diesel engine speed control maintains a well damped engine speed set by the driver. However, the resonance modes of the driveline are easily excited by accelerator-position changes or by road disturbances. A speed-control strategy is proposed that includes the behavior of the driveline, and reduces driveline resonances and vehicle shuffle by engine control. Implementation shows significant reduction, also when facing nonlinear torque limitations from maximum torque and diesel smoke delimiters.

A basis for both applications is a driveline model with a drive-shaft flexibility, and an analysis of the control problem. The model captures the first main resonance mode of the driveline and is sufficiently detailed for control design. Furthermore, the response time of the diesel engine is shown to be sufficient for reducing the first resonance mode.

Acknowledgment

This work has been carried out under excellent guidance of Professor Lars Nielsen at Vehicular Systems, Linköping University. By inspiring me and taking time for many discussions he has contributed to this work in many ways. I would also like to thank all colleagues at Vehicular Systems for creating a positive atmosphere for research and discussions.

I greatly acknowledge NUTEK (The Swedish National Board for Industrial and Technical Development) and Scania AB for fundings.

I am indebted to Sven-Åke Edström and Lars-Gunnar Hedström at Scania in Södertälje for believing in my ideas for driveline modeling and control. I particularly acknowledge Lars-Gunnar Hedström for the many discussions which have made me understand the problems and challenges with driveline control. Thanks also for the help with providing trucks for experiments.

I would like to thank Anders Björnberg and Anders Eskilsson at Scania for the driving assistance during the experiments. Thanks also for the help with adjusting the interface of the control units on the trucks for external control. I also acknowledge Simon Edlund for support on PC and real-time programming during the implementation work.

I am indebted to Simon Edlund, Lars Eriksson, Erik Frisk, Dr Peter Lindskog, and Dr Joakim Petersson for reading the manuscript. Thanks for the remarks and suggested improvements. Dr Peter Lindskog is also acknowledged for support on L^AT_EX, and Mattias Olofsson for keeping the computers running.

Dr Bo Bernhardsson read an earlier version of the material which led to valuable improvements of the thesis and the implementations, which I am grateful for.

My parents Birgitta and Nils together with my sister Katharina are always supporting and carrying, which means a lot to me. For this I will always be grateful.

Finally, I would like to express my appreciations to my wife Anna. Thanks for sharing life with me and constantly being at my side to encourage and support me. To Anna and our son Oscar I dedicate this work.

Linköping, April 1997

Magnus Pettersson

Contents

1	Introduction	1
1.1	Outline and Contributions	2
2	Problems with Driveline Handling	5
2.1	Background	5
2.2	Field Trials for Problem Demonstration	6
2.3	Goals	9
3	Experimental Platform	13
3.1	Trucks	13
3.1.1	Engine	16
3.1.2	Sensor System	17
3.2	Measurement and Control Platform	18
3.3	Experiments for Driveline Modeling	19
4	Driveline Modeling	23
4.1	Basic Driveline Equations	24
4.2	Engine Friction Modeling	28
4.3	Modeling the Driveline of the 144L Truck	30
4.3.1	Model with Drive-Shaft Flexibility	30
4.3.2	Influence from Propeller-Shaft Flexibility	33
4.3.3	Deviations between Engine Speed and Transmission Speed	37
4.3.4	Model with Flexible Clutch and Drive Shaft	38
4.3.5	Nonlinear Clutch and Drive-Shaft Flexibility	43

4.3.6	Model Validity	45
4.4	Modeling the Driveline of the 124L Truck	47
4.5	Summary	48
5	Architectural Issues for Driveline Control	49
5.1	State-Space Formulation	50
5.1.1	Disturbance Description	51
5.1.2	Measurement Description	51
5.2	Controller Formulation	52
5.3	Some Feedback Properties	54
5.4	Driveline Control with LQG/LTR	54
5.4.1	Transfer Functions	54
5.4.2	Design Example with a Simple Mass-Spring Model	57
5.5	Summary	62
6	Speed Controller Design and Simulations	63
6.1	RQV Control	64
6.2	Problem Formulation	64
6.3	Speed Control with Active Damping and RQV Behavior	67
6.3.1	Extending with RQV Behavior	70
6.4	Influence from Sensor Location	71
6.4.1	Influence from Load Disturbances	73
6.4.2	Influence from Measurement Disturbances	74
6.4.3	Load Estimation	76
6.5	Simulations	77
6.6	Summary	80
7	Speed Controller Experiments	83
7.1	Controller Implementation	83
7.1.1	Controller Discretization	84
7.1.2	Tuning the Controller Parameters σ and β	85
7.1.3	Tuning the Controller Parameter η	85
7.1.4	Tuning the Controller Parameter ρ	86
7.1.5	Influence from Sampling Time and Bus Delay	90
7.2	Experiments without Smoke Delimiter	90
7.3	Experiments with Smoke Delimiter	93
7.4	Controller Robustness	94
7.5	Summary	95
8	Gear-Shift Controller Design and Simulations	97
8.1	Internal Driveline Torque	98
8.1.1	Transmission Torque	98
8.1.2	Transmission Torque for the Drive-Shaft Model	98
8.1.3	Transmission Torque for the Clutch and Drive-Shaft Model	101

8.1.4	Transmission Torque for the Nonlinear Clutch and Drive-Shaft Model	102
8.2	Transmission-Torque Control Criterion	103
8.3	Transmission-Torque Control Design	108
8.4	Influence from Sensor Location	110
8.4.1	Influence from Load Disturbances	112
8.4.2	Influence from Measurement Disturbances	113
8.5	Simulations	114
8.6	Summary	117
9	Additional Modeling and Analysis for Gear-Shift Control	119
9.1	Open-Loop Gear-Shift Experiments	119
9.1.1	Stationary Trials	120
9.1.2	Dynamical Trials	120
9.2	Predicting Gear-Shift Quality	121
9.2.1	Quality of the Decoupled Model	124
9.2.2	Simulation of Gear Shifts with Stationary Driveline	124
9.2.3	Simulation of Gear Shifts with Driveline Oscillations	125
10	Gear-Shift Controller Experiments	127
10.1	Internal Driveline Torque	128
10.2	Virtual Drive-Shaft Torsion Sensor	129
10.2.1	Validation in Stationary Trials	131
10.2.2	Validation in Dynamical Trials	131
10.3	Drive-Shaft Torsion Control	134
10.3.1	Controller Structure for Active Damping	134
10.3.2	Demonstration of Active Damping in Field Trials	135
10.3.3	Validation of Controller Goal	136
10.3.4	Gear Shifts with Initial Driveline Oscillations	137
10.4	Summary	141
11	Conclusions	143
	References	145
	Notations	147
	Index	149

Introduction

The main parts of a vehicular driveline are engine, clutch, transmission, shafts, and wheels. Since these parts are elastic, mechanical resonances may occur. The handling of such resonances is basic for functionality and driveability, but is also important for reducing mechanical stress and noise. New driveline-management applications and high-powered engines increase the need for strategies for how to apply engine torque in an optimal way. Two systems where driveline oscillations limit performance are fuel injection for speed control and automatic gear shifting by engine control.

Low-frequent driveline resonances can be damped by having a strategy that applies engine torque so that the engine inertia is forced to work in the opposite direction of the oscillations. This is referred to as active damping or engine controlled damping of driveline resonances. In order to derive these strategies, models of the driveline are developed. The aim of the modeling and experiments is to find the most important physical effects that contribute to driveline oscillations. The frequency range of interest includes the first main resonance modes of the driveline. Experiments are performed with a heavy truck with different gears and road slopes in order to excite driveline resonances for modeling. Some open questions are discussed, regarding influence of sensor dynamics and nonlinear effects.

The first problem treated is wheel-speed oscillations following from a change in accelerator pedal position or from impulses from towed trailers and road roughness, known as vehicle shuffle [16, 21].

Traditional fuel-injection strategies are of torque control type or speed control type. Control performance is limited by driveline resonances for both control schemes. For diesel engines, speed control is often referred to as RQV control [2].

With RQV control there is no active damping of driveline resonances, and for low gears this leads to wheel-speed oscillations and vehicle shuffle. A desired property with RQV control is a load dependent velocity lag resulting from downhill and uphill driving. Model based control is used to extend the RQV control concept with engine controlled damping of wheel-speed oscillations, while maintaining the desired velocity lag characteristic for RQV control.

In today's traffic it is desired to have an automatic gear shifting system on heavy trucks. One approach at the leading edge of technology is gear shifting by engine control [19]. With this approach, disengaging the clutch is replaced by controlling the engine to a state where the transmission transfers zero torque, and by that realizing a virtual clutch. After neutral gear is engaged, the engine speed is controlled to a speed such that the new gear can be engaged. The gear shifting system uses a manual transmission with automated gear lever, and a normal friction clutch that is engaged only at start and stop.

The total time needed for a gear shift is an important quality measure. One reason for this is that the vehicle is free-rolling, since there is no driving torque, which may be serious with heavy loads and large road slopes. The difference in engine torque before a gear shift and at the state where the transmission transfers zero torque is often large. Normally, this torque difference is driven to zero by sliding the clutch. With gear shifting by engine control, the aim is to decrease the time needed for this phase by using engine control. However, a fast step in engine torque may lead to excited driveline resonances. If these resonances are not damped, the time to engage neutral gear increases, since one has to wait for satisfactory gear-shift conditions. Furthermore, engaging neutral gear at a non-zero transmission torque results in oscillations in the transmission speed, which is disturbing for the driver, and increases the time needed to engage the new gear. These problems motivate the need for using feedback control in order to reach zero transmission torque. Two major problems must be addressed to obtain this. First, the transmission torque must be estimated and validated. Then a strategy must be derived that drives this torque to zero with damped driveline resonances.

A common architectural issue in driveline control is the choice of sensor location. Different sensor locations result in different control problems, and the influence in control design is investigated. A comparison is made between using feedback from the engine-speed sensor or the wheel-speed sensor. The investigation aims at understanding where to invest in increased sensor performance in future driveline management systems.

1.1 Outline and Contributions

Chapter 2 gives more background to the applications described above, and an outline of the goals for later derivation of various control strategies. Experiments for modeling and testing the derived strategies are performed with two heavy trucks with different engine types. One has an 8 cylinder in-line fuel-injection engine, and the other has a 6 cylinder unit pump fuel-injection engine. The experimental

platform is further described in Chapter 3.

Chapter 4 covers the derivation of three driveline models of different complexity, that can explain driveline oscillations. Experiments with the heavy trucks are described together with the modeling conclusions. The contribution of the chapter is that a linear model with one torsional flexibility and two inertias is able to capture the first main resonance of the driveline for both in-line and unit pump fuel-injection systems. Parameter estimation of a model with a nonlinear clutch and sensor dynamics explains the measured transmission speed. The difference between experiments and model is explained to occur when the clutch transfers zero torque.

Control of resonant systems with simple controllers is, from other technical fields, known to have different properties with respect to sensor location. These results are reviewed in Chapter 5. The extension to more advanced control design methods is a little studied topic. The contribution of the chapter is a demonstration of the influence of sensor location in driveline control when using LQG/LTR control [21].

Chapter 6 treats the design and simulation of the speed-controller concept. A key contribution in this chapter is the formulation of a criterion for speed control with engine controlled damping of wheel-speed oscillations, and with a retained velocity lag characteristic for RQV control [20, 22].

The implementation of the speed-control concept in a heavy truck is covered in Chapter 7. The main contribution is a demonstration of significantly reduced driveline resonances in field trials. Hence, the response time of the diesel engine is sufficient to reduce low-frequent driveline resonances and thus reducing vehicle shuffle (which is valid for both engine types). Furthermore, it is verified that the reduced linear driveline model with a drive-shaft flexibility is sufficiently detailed for control design.

Chapters 8 to 10 deal with gear-shift control by using internal driveline torque control. Two similar principles of internal torque control are covered. The first is derived in Chapter 8, where a detailed analysis of the transmitted torque in the transmission is performed. A key contribution is the derivation of a transmission-torque control strategy, based on a model describing the transmission torque, and a criterion for a controller that drives this torque to zero [20, 23]. With this approach the specific transmission-torque behavior for each gear is described and compensated for. This investigation is important as a principle study in order to understand the dynamic behavior of the transmission torque and for verifying simulation studies.

However, in order to implement gear-shift control it is of great importance to have a robust and simple control strategy with simple tuning rules for optimizing shift quality. Chapter 10 considers this and describes a second variant of internal torque control, where gear-shift control is obtained by controlling the drive-shaft torsion to zero. A key contribution is the field-trial demonstration of gear shifts by using the drive-shaft torsion controller with a short time for the torque control phase, without leading to oscillations in the driveline speeds after engaged neutral gear. Furthermore, engine controlled damping can be obtained by using an observer

together with a PID feedback structure. Chapter 9 discusses additional modeling of the driveline when separated in two parts due to engaged neutral gear. This is used for validation purposes in Chapter 10. The derivation of the gear-shift control strategies and their demonstration in field trials form the main contribution of the thesis.

Problems with Driveline Handling

As a background, the first section gives the traditionally used techniques for speed control and automatic gear shifting, which are the two vehicular applications considered. Field trials with the two applications are then shown to demonstrate the limitations in performance imposed by driveline resonances. The goals of the control strategies for performance improvement are then outlined, being the basis for later design and implementation work.

The control scheme of the traditional fuel-injection strategy is covered together with measurements of how driveline resonances give wheel-speed oscillations, resulting in vehicle shuffle. The second application is gear shifting by engine control, which utilizes engine control to engage neutral gear fast without sliding the clutch. When minimizing the time needed, the excited driveline resonances must be handled. The problem is demonstrated in field trials together with the resulting increase in shift time if neutral gear is engaged at a torque level different from zero.

2.1 Background

Fuel-Injection Strategy for Speed Control

As described in the previous chapter, fuel-injection strategy can be of torque control type or speed control type. For diesel engines, speed control is often referred to as RQV control, and torque control referred to as RQ control [2]. With RQ control, the driver's accelerator pedal position is interpreted as a desired engine torque, and with RQV control the accelerator position is interpreted as a desired engine speed. RQV control is essentially a proportional controller calculating the fuel

amount as function of the difference between the desired speed set by the driver and the actual measured engine speed. The reason for this controller structure is the traditionally used mechanical centrifugal governor for diesel pump control [2]. This means that the controller will maintain the speed demanded by the driver, but with a stationary error (velocity lag), which is a function of the controller gain and the load (rolling resistance, air drag, and road inclination). With a cruise controller, the stationary error is compensated for, which means that the vehicle will maintain the same speed independent of load changes. This requires an integral part of the controller which is not used in the RQV control concept.

Automatic Gear Shifting in Heavy Trucks

Traditionally a gear shift is performed by disengaging the clutch, engaging neutral gear, shifting to a new gear, and engaging the clutch again. In today's traffic it is desired to have an automatic gear shifting system on heavy trucks. The following three approaches are normally used:

Automatic transmission This approach is seldom used for the heaviest trucks, due to expensive transmissions and problems with short life time. Another drawback is the efficiency loss compared to manual transmissions.

Manual transmission and automatic clutch A quite common approach, which needs an automatic clutch system [17]. This system has to be made robust against clutch wear.

Manual transmission with gear shifting by engine control With this approach the automatic clutch is replaced by engine control, realizing a virtual clutch. The only addition needed to a standard manual transmission is an actuator to move the gear lever. Lower cost and higher efficiency characterize this solution.

With this last approach a gear shift includes the phases described in Figure 2.1, where the engine torque during the shift event is shown.

2.2 Field Trials for Problem Demonstration

A number of field trials are performed in order to describe how driveline resonances influence driveline management.

Driveline speed control

A specific example of how the RQV speed controller performs is seen in Figure 2.2. The figure shows how the measured engine speed and wheel speed respond to a step input in accelerator position. It is seen how the engine speed is well behaved with no oscillations. With a stiff driveline this would be equivalent with also having well damped wheel speed. The more flexible the driveline is, the less sufficient

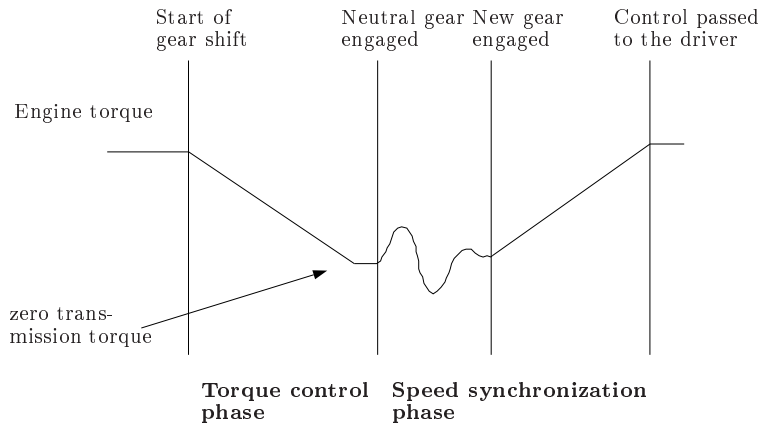


Figure 2.1 Engine torque during the different phases in automatic gear shifting by engine control. The engine torque is controlled to a state where the transmission transfers zero torque, whereafter neutral gear is engaged without using the clutch. After the speed synchronization phase, the new gear is engaged, and control is transferred back to the driver.

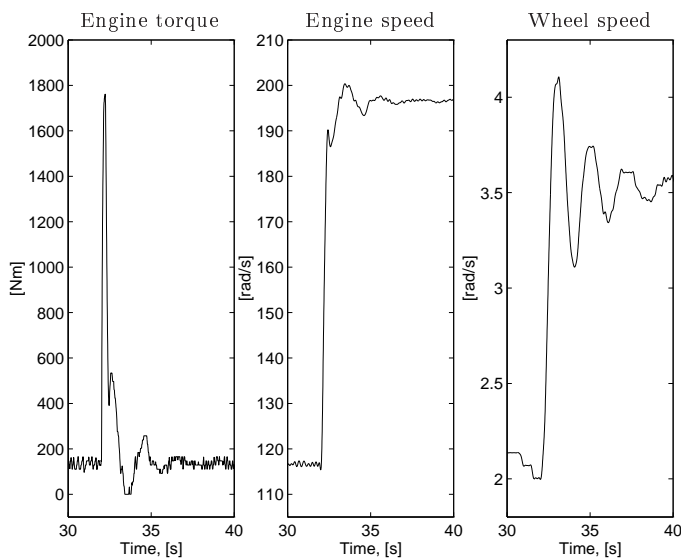


Figure 2.2 Measured speed response of a step in accelerator position at $t=32$ s. An RQV speed controller controls the engine speed to 2000 RPM. The engine speed is well damped, but the resonances in the driveline is seen to give oscillating wheel speed, resulting in vehicle shuffle.

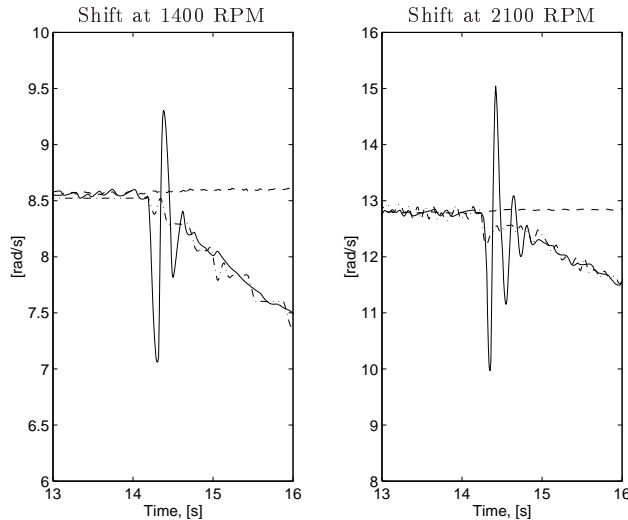


Figure 2.3 Engagement of neutral gear commanded at 14 s, with stationary driveline at 1400 RPM and 2100 RPM on a flat road with gear 1. The engine speed (dashed) and wheel speed (dash-dotted) are scaled to transmission speed (solid) with the conversion ratio of the driveline. After a short delay time, neutral gear is engaged, causing the driveline speeds to oscillate. The amplitude of the oscillating transmission speed is higher the higher the stationary speed is.

a well damped engine speed is, since the flexibility of the driveline will lead to oscillations in the wheel speed. This will be further discussed and demonstrated in later chapters.

If it is desired to decrease the response time of the RQV controller (i.e. increase the bandwidth), the controller gain must be increased. Then the amplitude of the oscillations in the wheel speed will be higher.

Driveline torque control

When using gear shifting by engine control, the phases in Figure 2.1 are accomplished. First, control is transferred from the driver to the control unit, entering the *torque control phase*. The engine is controlled to a torque level corresponding to zero transferred torque in the transmission. After neutral gear is engaged, the *speed synchronization phase* is entered. Then the engine speed is controlled to track the transmission speed (scaled with the conversion ratio of the new gear), whereafter the new gear is engaged. Finally, the torque level is transferred back to the level that the driver demands.

The total time needed for a gear shift is important to minimize, since the vehicle is free-rolling with zero transmission torque. In Figure 2.3, neutral gear is engaged, without a torque control phase, at a constant speed. This means that

there is a driving torque transferred in the transmission, which clearly causes the transmission speed to oscillate. The amplitude of the oscillations is increasing the higher the stationary speed is. This indicates that there must be an engine torque step in order to reach zero transmission torque and no oscillations in the transmission speed.

Figure 2.4 shows the transmission speed when the engine torque is decreased to 46 Nm at 12.0 s. Prior to that, the stationary speed 2200 RPM was maintained, which requested an engine torque of about 225 Nm. Four trials are performed with this torque profile with engaged neutral gear at different time delays after the torque step. After 12.4 s there is a small oscillation in the transmission speed, after 13.3 s and 14.8 s there are oscillations with high amplitude, and at 13.8 s there are no oscillations in the transmissions speed. This indicates how driveline resonances influence the transmission torque, which is clearly close to zero for the gear shift at 12.4 s and 13.8 s, but different from zero at 13.3 s and 14.8 s. The amplitude of the oscillating transmission torque will be higher if the stationary speed is increased or if the vehicle is accelerating.

One way this can be handled is to use a ramp in engine torque according to the scheme in Figure 2.1. However, this approach is no good for optimizing shift time, since the ramp must be conservative in order to wait until the transmission torque fluctuations are damped out.

The gear shift at 13.3 s in Figure 2.4 shows the effect of a gear shift at a transmission torque different from zero. This leads to the following problems:

- Disturbing to the driver, both in terms of noise and speed impulse.
- Increased wear on transmission.
- Increased time for the speed synchronization phase, since the transmission speed, which is the control goal, is oscillating. The oscillations are difficult to track for the engine and therefore one has to wait until they are sufficiently damped.

2.3 Goals

Based on the field-trial demonstration of problems with driveline handling, the goals for reducing the influence from oscillations in performance and driveability are outlined. These will be the basis when deriving strategies for driveline management, to be used in field-trial experiments in later chapters.

Speed control is the extension of the traditionally used RQV speed control concept with engine controlled damping of driveline resonances. The control strategy should maintain a desired speed with the same velocity lag from uphill and downhill driving, as in the case with traditional control. All available engine torque should be applied in a way that driveline oscillations are damped out. The response time of the controller should be made as fast as possible without exciting higher resonance modes of the driveline.

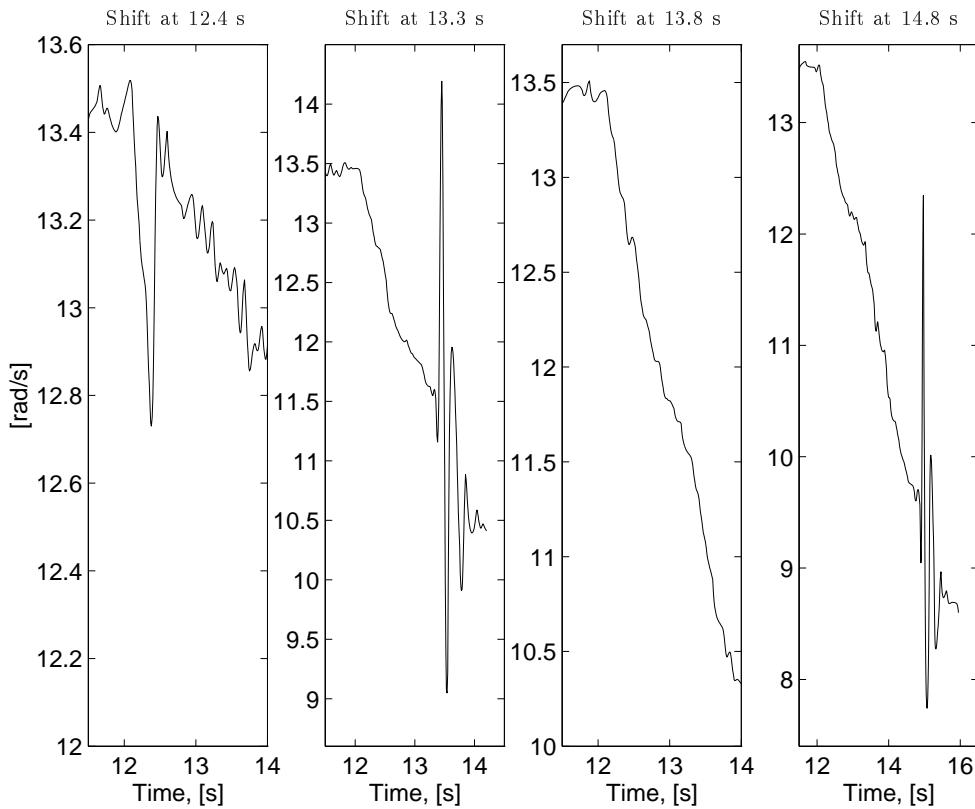


Figure 2.4 Gear shifts with the engine at the stationary speed 2200 RPM with gear 1. At 12.0 s there is a decrease in engine torque to 46 Nm in order to reach zero transmission torque. The transmission speed is plotted when neutral gear is engaged at 12.4 s, 13.3 s, 13.8 s, and 14.8 s (with the same torque profile). The different amplitudes in the oscillations show how the torque transmitted in the transmission is oscillating after the torque step. Note that the range of the vertical axes differ between the plots.

Gear-shift control is a controller that controls the internal driveline torque to a level where neutral gear can be engaged without using the clutch. During the torque control phase, the excited driveline resonances should be damped in order to minimize the time needed to complete the phase. The engagement should be realized at a torque level that gives no oscillations in the driveline speeds. Hereby, the disturbances to the driver and the time spent in the speed synchronization phase can be minimized. The influence on shift quality from initial driveline resonances and torque impulses from trailer and road roughness should be minimized.

The control problems should be formulated so that it is possible to use established techniques to obtain solutions. The designs should be robust against limitations in the diesel engine as actuator. These limitations are:

- The engine torque is not smooth, since the explosions in the cylinder result in a pulsating engine torque.
- The output torque of the engine is not exactly known. The only measure of it is a static torque map from dynamometer tests.
- The dynamical behavior of the engine is also characterized by the engine friction, which must be estimated. Many variables influence engine friction and it is necessary to find a simple yet sufficiently detailed model of the friction.
- The engine output torque is limited in different modes of operation. The maximum engine torque is restricted as a function of the engine speed, and the torque level is also restricted at low turbo pressures.

The resulting strategies should be possible to implement on both in-line pump and unit pump injection engines, with standard automotive driveline sensors.

Experimental Platform

Experiments are performed with two Scania heavy trucks. These have different number of cylinders and different fuel-injection systems. The truck used for experiments with automatic gear shifting is equipped with an actuator for moving the gear lever. Field trials are performed by controlling the driveline from a PC in the cab of the truck. Control strategies are implemented in a real-time system, controlling engine torque and gear shifts. Engine torque and temperature are measured, together with the speed of the engine, the speed of the output shaft of the transmission, and the wheel speed.

The configuration of the two trucks is described in Section 3.1. Measurement and control of driveline variables via the CAN-bus of the truck is described in Section 3.2. Finally, a few field trials with the aim of exciting driveline resonances are shown in Section 3.3.

3.1 Trucks

Two Scania heavy trucks with different configurations are used for experiments. The Scania 124L 6x2 (6 wheels, 2 driven) truck shown in Figure 3.1 has the following configuration.

- 12 liter, 6 cylinder turbo-charged DSC12 diesel engine (Figure 3.2) with maximum power of 420 Hp and maximum torque of 1930 Nm. The fuel metering is governed by unit-pump injectors [5].
- The engine is connected to a manual range-splitter transmission GRS900R (Figure 3.3) via a clutch. The transmission has 14 gears and a hydraulic



Figure 3.1 Scania 124L truck.

retarder, but no automatic gear shifting system.

- The weight of the truck is $m = 24\,000$ kg.

Figure 3.4 shows a Scania 144L 6x2 truck that has the configuration as follows.

- 14 liter V8 turbo-charged diesel engine with maximum power of 530 Hp and maximum torque of 2300 Nm. The fuel metering is governed by an in-line injection pump system [5].
- The engine is connected to a manual range-splitter transmission GRS900R (Figure 3.3) via a clutch. The transmission has 14 gears and a hydraulic retarder. It is also equipped with the automatic gear shifting system Opti-Cruise [19].
- The weight of the truck is $m = 24\,000$ kg.

The main differences between the two trucks are the engines and the transmissions. The transmission control unit in the 144L truck makes it feasible for experiments with gear shifts, since the transmission is equipped with actuators that can move the gear lever. The 124L truck has no transmission control unit and therefore the gears are shifted manually. This truck is used for experiments for speed control with engine controlled damping of driveline resonances.



Figure 3.2 Scania 12 liter DSC12 engine.

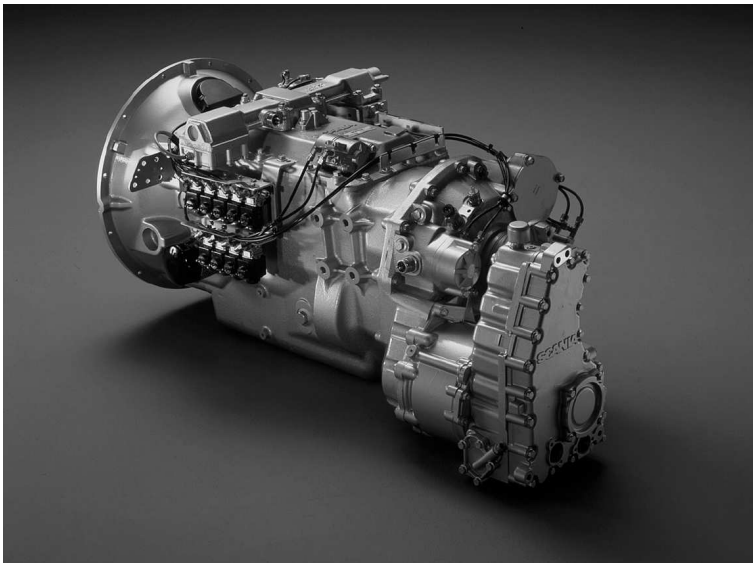


Figure 3.3 Scania GRS900R range-splitter transmission with retarder and Opti-Cruise automatic gear-shifting system.



Figure 3.4 Scania 144L truck.

3.1.1 Engine

The difference in engine type between the two trucks influences driveline modeling and control. The engines differ in size (i.e. engine moment of inertia), number of explosions per revolution, and in the way fuel is injected. The 124L 6 cylinder engine has the more recently introduced unit-pump injection system with one fuel pump for each cylinder. The V8 engine in the 144L truck, on the other hand, uses the more traditionally in-line pump system with one fuel pump supplying all eight cylinders with fuel.

Driveline modeling will be influenced by a number of subsystems of the engine that are common for both engine types. These are

Maximum torque delimiter The injected fuel amount is restricted by the physical character of the engine (i.e. engine size, number of cylinders, etc.), together with restrictions that the engine control system uses, for utilizing the engine in the best possible way. The maximum torque profiles for the two engines are seen in Figure 3.5.

Diesel smoke delimiter If the turbo pressure is low and a high engine torque is demanded, diesel smoke emissions will increase to an unacceptable level. This is prevented by restricting the fuel amount to a level with acceptable emissions at low turbo pressures.

Transfer function from fuel amount to engine torque The engine torque is the torque resulting from the explosions in the cylinders. A static function

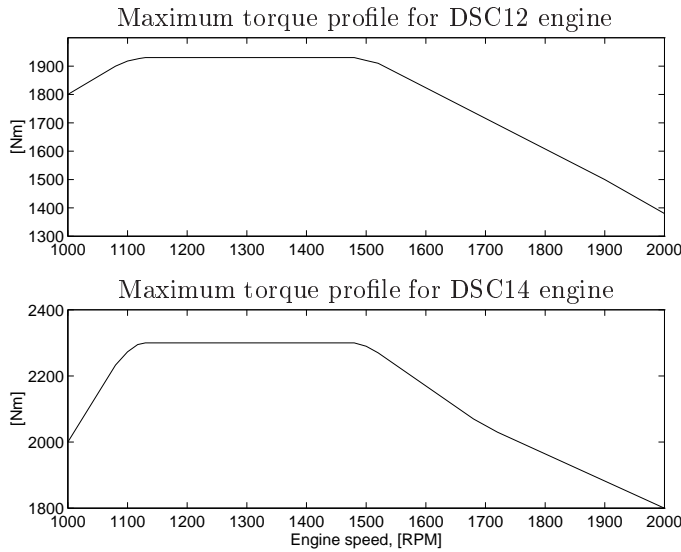


Figure 3.5 Maximum torque profiles for Scania DSC12 and DSC14 diesel engines.

relating the engine torque to injected fuel can be obtained in a dynamometer test. For a diesel engine this function is fairly static, and no dynamical models are used in this work.

Engine friction The engine output torque transferred to the clutch is equal to the engine torque (the torque resulting from the explosions) subtracted by the engine internal friction. Friction modeling is thus fundamental for driveline modeling and control.

3.1.2 Sensor System

The velocity of a rotating shaft is measured by using an inductive sensor [18], which detects the time when cogs from a rotating cogwheel are passing. This time sequence is then inverted to get the angle velocity. Hence, the bandwidth of the measured signal depends on the speed and the number of cogs the cogwheel is equipped with.

Three speed sensors are used to measure the speed of the flywheel of the engine ($\dot{\theta}_m$), the speed of the output shaft of the transmission ($\dot{\theta}_t$), and the speed of the driving wheel ($\dot{\theta}_w$). The transmission speed sensor has fewer cogs than the other two sensors, indicating that the bandwidth of this signal is lower.

By measuring the amount of fuel, m_f , that is fed to the engine, a measure of the driving torque, $M_m(m_f)$, is obtained from dynamometer tests, as mentioned before. The output torque of the engine is the driving torque subtracted by the engine friction, $M_{fr:m}$. This signal, $u = M_m(m_f) - M_{fr:m}$, is the torque acting

Measured Variables			
<i>Variable</i>	<i>Node</i>	<i>Resolution</i>	<i>Rate</i>
Engine speed, $\dot{\theta}_m$	Engine	0.013 rad/s	20 ms
Engine torque, M_m	Engine	1% of max torque	20 ms
Engine temp, T_m	Engine	1° C	1 s
Wheel speed, $\dot{\theta}_w$	ABS	0.033 rad/s	50 ms
Transmission speed, $\dot{\theta}_t$	Transmission	0.013 rad/s	50 ms

Table 3.1 Measured variables transmitted on the CAN-bus.

on the driveline, which is a pulsating signal with torque pulses from each cylinder explosion. However, the control signal $u = M_m(m_f) - M_{fr:m}$ is treated as a continuous signal, which is reasonable for the frequency range considered for control design. A motivation for this is that an eight-cylinder engine makes 80 strokes/s at an engine speed of 1200 rev/min. This means that a mean-value engine model is assumed (neglects variations during the engine cycle). This assumption will be validated by field trials in later implementation chapters.

The truck is equipped with a set of control units, each connected with a CAN-bus [4]. These CAN nodes are the engine control node, the transmission node, and the ABS brake system node. Each node measures a number of variables and transmits them via the bus.

3.2 Measurement and Control Platform

The measured signals are described in Table 3.1. The actuators available are the engine, which is controlled by injecting different amounts of fuel, and the transmission which by command can perform gear shifts. Driveline management consists of measuring the state of the driveline and the desire of the driver (i.e. desired speed and gear). The driveline is then controlled by injecting an appropriate fuel amount so that the speed is obtained and that gear shifts can be performed.

A PC with CAN communication is used to access the variables on the CAN-bus and transmit control signals. The situation is described in Figure 3.6. A PPCan CAN board [24] is attached to the parallel port of the PC and to the CAN-bus in the cab of the truck according to Figure 3.7. A real-time system [6] based on the RTKernel [25] real-time kernel is implemented together with the PPCan drivers.

As mentioned before, the 124L truck is not equipped with OptiCruise transmission control unit, and therefore the variables from the transmission node cannot be accessed. Hence, no transmission speed can be measured, and no gear shift can be commanded from the computer for this truck.

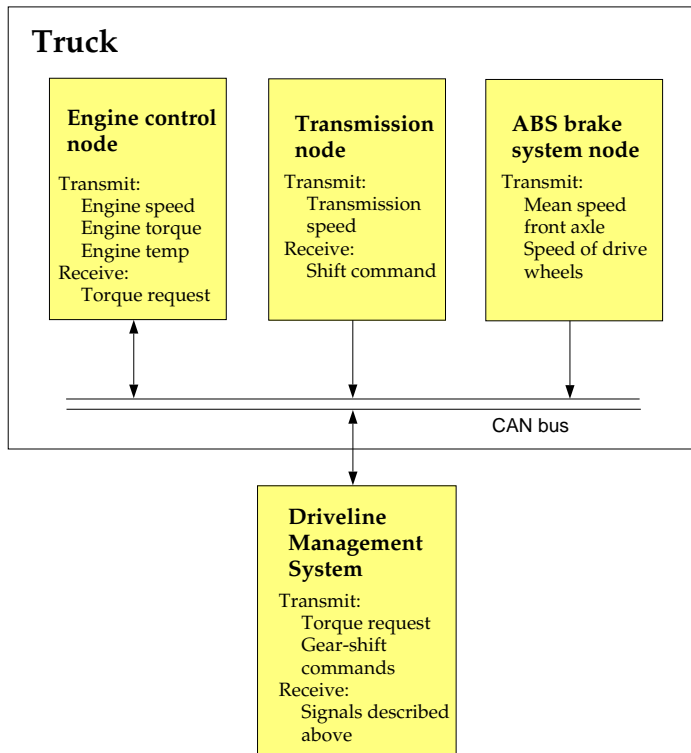


Figure 3.6 Description of the driveline management system interfacing with the truck. Variables from the engine node, the transmission node, and the ABS node are transmitted on the CAN-bus. The driveline management system is implemented on a PC, attached to the bus in the cab of the truck.

3.3 Experiments for Driveline Modeling

A number of test roads at Scania were used for testing. They have different known slopes. The variables in Table 3.1 are logged during tests that excite driveline resonances. In Figure 3.8 it is seen how impulse inputs in engine torque excite driveline resonances, giving oscillating wheel speed and engine speed on the 124L truck.

When using the 144L truck, also the transmission node can be accessed via the CAN-bus. Figure 3.9 shows a test with the 144L truck where step inputs in accelerator position excite driveline oscillations. The oscillations have different character depending on which truck that is being used. For example, the difference in engine inertia gives different oscillations. In Figure 3.9 it is seen that the main flexibility of the driveline is located between the output shaft of the transmission and the wheel, since the largest difference in speed is between the measured transmission speed and wheel speed.



Figure 3.7 Experiment situation. A PC with parallel-port CAN board attached to the CAN-bus in the cab of the truck.

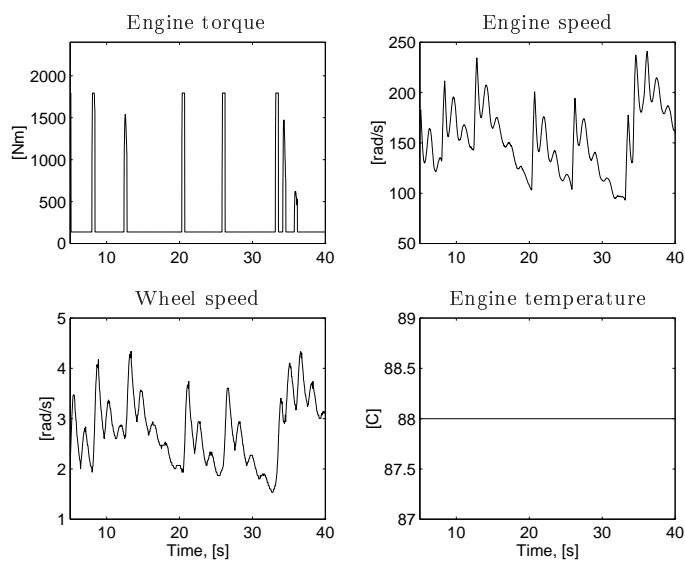


Figure 3.8 Logged data on the CAN-bus during engine torque impulse experiments with the 124L truck.

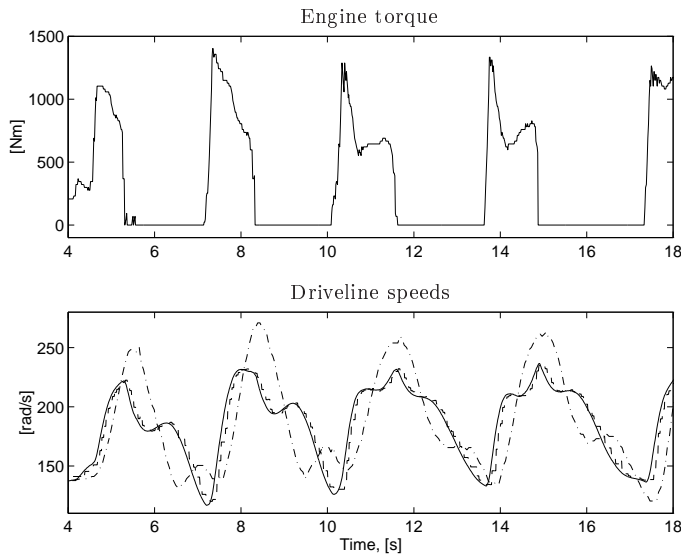


Figure 3.9 Logged data on the CAN-bus during step inputs in accelerator position with the 144L truck. The transmission speed (dashed) and the wheel speed (dash-dotted) are scaled to engine speed in solid. The main flexibility of the driveline is located between the output shaft of the transmission and the wheel, since the largest difference in speed is between the measured transmission speed and wheel speed.

Preprocessing Data

Since the sampling is not equidistant in time, the data sets are resampled. A new data set is obtained by interpolating the old data using linear interpolation. This introduces higher frequencies than those in the original data set. Therefore, the interpolated data is low-pass filtered with a frequency corresponding to half the sampling frequency in the original data. This is done off-line and without phase shifts in the signals.

Driveline Modeling

The driveline is a fundamental part of a vehicle and its dynamics has been modeled in different ways depending on the purpose. The frequency range treated in this work is the regime including the first resonance modes of the driveline [16,21]. Vibrations and noise contribute to a higher frequency range [8,28] which is not treated here.

The aim of the modeling is to find the most important physical effects explaining the oscillations in the measured engine speed, transmission speed, and wheel speed. The models are combinations of rotating inertias connected by damped shaft flexibilities. The generalized Newton's second law is used to derive the models.

A stationary torque map is assumed to be sufficient for describing the dynamic behavior of the diesel engine, together with a friction model as function of the engine speed and the engine temperature.

Measurements indicate that the main flexibility of the driveline is located between the output shaft of the transmission and the wheel, as pointed out in the previous chapter. This leads to a first model capturing the first main resonance of the driveline. The model assumes a stiff driveline up to the output shaft of the transmission, and a drive-shaft flexibility between the transmission and the wheel.

In order to explain the oscillations in the measured transmission speed, the drive-shaft model is extended with a clutch flexibility and a sensor filter. This model is able to capture the first two resonance modes of the driveline, and it will be used to explain the open question about the reason for the difference between the measured engine speed and transmission speed.

The main part of the experiments used for modeling considers low gears. The reason for this is that the lower the gear is, the higher the torque transferred in

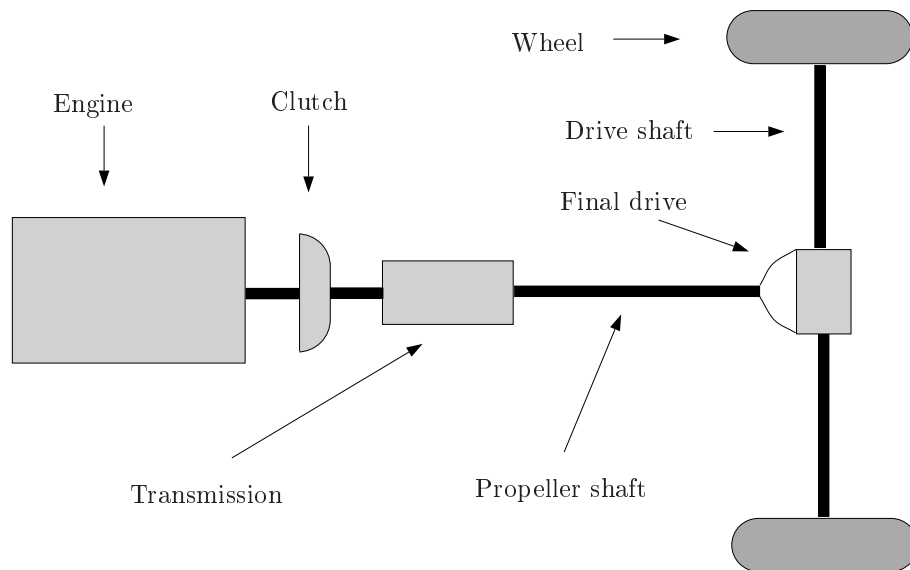


Figure 4.1 A rear-driven vehicular driveline.

the drive shaft is. This means that the shaft torsion is higher for lower gears, and hereby also the problems with oscillations. Furthermore, the amplitudes of the resonances in the wheel speed are higher for lower gears, since the load and vehicle mass appear reduced by the high conversion ratio.

Section 4.1 covers the derivation of basic equations describing a driveline. The engine friction is then modeled in Section 4.2, for both the 144L and the 124L trucks (described in the previous chapter). Specific modeling and parameter estimation for the 144L truck (Section 4.3) and the 124L truck (Section 4.4) are then covered. Finally, the modeling conclusions are summarized in Section 4.5.

4.1 Basic Driveline Equations

Figure 4.1 depicts a rear-driven heavy truck driveline. It consists of engine, clutch, transmission, propeller shaft, final drive, drive shafts, and wheels. Fundamental equations for the driveline will be derived by using the generalized Newton's second law of motion [15]. Some basic equations regarding the forces acting on the wheel are obtained, influenced by the complete dynamics of the vehicle. This means that effects from, for instance, vehicle mass and trailer will be included in the equations describing the wheels. Figure 4.2 shows the labels, the inputs, and the outputs of each subsystem of the driveline type considered in this work. Relations between inputs and outputs will in the following be described for each part.

Engine: The output torque of the engine is characterized by the driving torque (M_m) resulting from the combustion, the internal friction from the engine

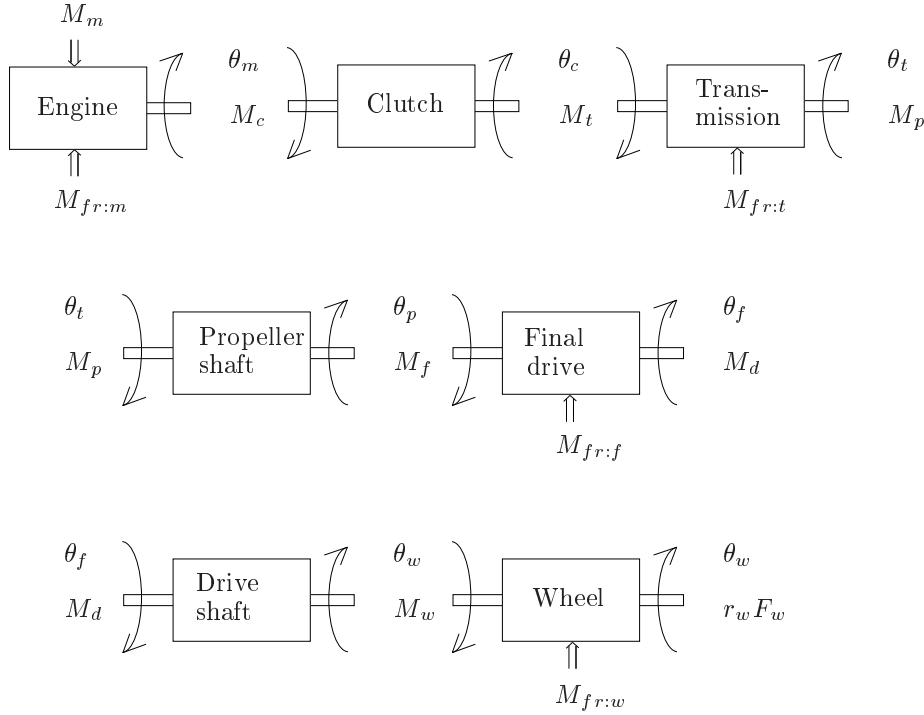


Figure 4.2 Subsystems of a vehicular driveline with their respective angle and torque labels.

($M_{fr:m}$), and the external load from the clutch (M_c). Newton's second law of motion gives the following model

$$J_m \ddot{\theta}_m = M_m - M_{fr:m} - M_c \quad (4.1)$$

where J_m is the mass moment of inertia of the engine and θ_m is the angle of the flywheel.

Clutch: A friction clutch found in vehicles equipped with a manual transmission consists of a clutch disk connecting the flywheel of the engine and the transmission's input shaft. When the clutch is engaged, and no internal friction is assumed, $M_c = M_t$ is obtained. The transmitted torque is a function of the angular difference ($\theta_m - \theta_c$) and the angular velocity difference ($\dot{\theta}_m - \dot{\theta}_c$) over the clutch

$$M_c = M_t = f_c(\theta_m - \theta_c, \dot{\theta}_m - \dot{\theta}_c) \quad (4.2)$$

Transmission: A transmission has a set of gears, each with a conversion ratio i_t . This gives the following relation between the input and output torque of the transmission

$$M_p = f_t(M_t, M_{fr:t}, \theta_c - \theta_t i_t, \dot{\theta}_c - \dot{\theta}_t i_t, i_t) \quad (4.3)$$

where the internal friction torque of the transmission is labeled $M_{fr:t}$. The reason for considering the angle difference $\theta_c - \theta_t i_t$ in (4.3) is the possibility of having torsional effects in the transmission.

Propeller shaft: The propeller shaft connects the transmission's output shaft with the final drive. No friction is assumed ($\Rightarrow M_p = M_f$), giving the following model of the torque input to the final drive

$$M_p = M_f = f_p(\theta_t - \theta_p, \dot{\theta}_t - \dot{\theta}_p) \quad (4.4)$$

Final drive: The final drive is characterized by a conversion ratio i_f in the same way as for the transmission. The following relation for the input and output torque holds

$$M_d = f_f(M_f, M_{fr:f}, \theta_p - \theta_f i_f, \dot{\theta}_p - \dot{\theta}_f i_f, i_f) \quad (4.5)$$

where the internal friction torque of the final drive is labeled $M_{fr:f}$.

Drive shafts: The drive shafts connect the wheels to the final drive. Here it is assumed that the wheel speed is the same for the two wheels. Therefore, the drive shafts are modeled as one shaft. When the vehicle is turning and the speed differs between the wheels, both drive shafts have to be modeled. No friction ($\Rightarrow M_w = M_d$) gives the model equation

$$M_w = M_d = f_d(\theta_f - \theta_w, \dot{\theta}_f - \dot{\theta}_w) \quad (4.6)$$

Wheel: Figure 4.3 shows the forces acting on a vehicle with mass m and speed v . Newton's second law in the longitudinal direction gives

$$F_w = m\dot{v} + F_a + F_r + mg \sin(\alpha) \quad (4.7)$$

The friction force (F_w) is described by the sum of the following quantities [8].

- F_a , the air drag, is approximated by

$$F_a = \frac{1}{2} c_w A_a \rho_a v^2 \quad (4.8)$$

where c_w is the drag coefficient, A_a the maximum vehicle cross section area, and ρ_a the air density. However, effects from, for instance, open or closed windows will make the force difficult to model.

- F_r , the rolling resistance, is approximated by

$$F_r = m(c_{r1} + c_{r2}v) \quad (4.9)$$

where c_{r1} and c_{r2} depend on, for instance, tires and tire pressure.

- $mg \sin(\alpha)$, the gravitational force, where α is the slope of the road.

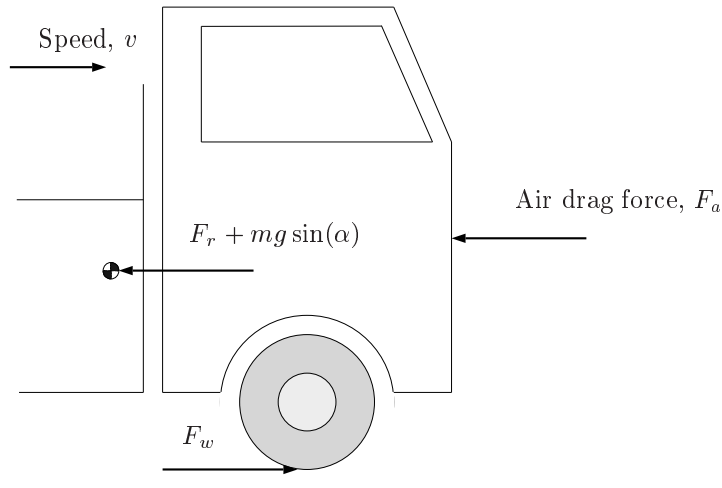


Figure 4.3 Longitudinal forces acting on a vehicle.

The coefficients of air drag and rolling resistance, (4.8) and (4.9), can be identified e.g. by an identification scheme [9].

The resulting torque due to F_w is equal to $F_w r_w$, where r_w is the wheel radius. Newton's second law gives

$$J_w \ddot{\theta}_w = M_w - F_w r_w - M_{fr:w} \quad (4.10)$$

where J_w is the mass moment of inertia of the wheel, M_w is given by (4.6), and $M_{fr:w}$ is the friction torque. Including (4.7) to (4.9) in (4.10) together with $v = r_w \dot{\theta}_w$ gives

$$\begin{aligned} (J_w + m r_w^2) \ddot{\theta}_w &= M_w - M_{fr:w} - \frac{1}{2} c_w A_a \rho_a r_w^3 \dot{\theta}_w^2 \\ &\quad - r_w m (c_{r1} + c_{r2} r_w \dot{\theta}_w) - r_w m g \sin(\alpha) \end{aligned} \quad (4.11)$$

The dynamical influence from the tire has been neglected in the equation describing the wheel.

A complete model of the driveline with the clutch engaged is described by Equations (4.1) to (4.11). So far the functions f_c , f_t , f_p , f_f , f_d , and the friction torques $M_{fr:t}$, $M_{fr:f}$, and $M_{fr:w}$ are unknown. In the following section assumptions will be made about these, resulting in a series of driveline models, with different complexities.

Parameter Estimation Software

To estimate the parameters of the linear models derived in this chapter the System Identification Toolbox [13] is used. The prediction error estimation method (PEM)

for parameterized state-space representations is used to estimate the unknown parameters and initial conditions.

In order to estimate the parameters and the initial condition of the nonlinear model derived, the continuous model is discretized. This is done by using Euler's method. For a continuous differential equation, the discrete version is

$$x_n = x_{n-1} + hf(x_{n-1}, u_{n-1}) \quad (4.12)$$

where h is the sampling time. The global truncation error with this method equals $O(h)$. Therefore it is necessary to keep h small. A too small h can give numerical problems and it also gives unnecessarily long iteration time. The data is resampled at a sampling frequency of 1 kHz. Furthermore, the differential equations describing the model, are scaled to be of the same magnitude.

For a given set of parameters, initial conditions, and control signal sequence u , the state vector is calculated at each sample. By comparing the model output (y_m , y_t , y_w) with the measured signals ($\dot{\theta}_m$, $\dot{\theta}_t$, $\dot{\theta}_w$) a cost function can be evaluated. After some comparison between different cost functions, the following is selected

$$\sum_{\forall i} \left((\dot{\theta}_m(i) - y_m(i))^2 + i_t^2 (\dot{\theta}_t(i) - y_t(i))^2 + i_t^2 i_f^2 (\dot{\theta}_w(i) - y_w(i))^2 \right) \quad (4.13)$$

where $\forall i$ means that the sum ranges over all samples in the estimation data. The optimal parameters and initial conditions are the ones minimizing (4.13). The data sets are divided into two parts, one to be used in the parameter estimation phase, and one used for validation purposes.

Each derived model is written in state-space form with the velocity of each inertia, and the torsion of each shaft flexibility as states. More details about the state-space representation can be found in Chapter 5.

4.2 Engine Friction Modeling

The engine friction $M_{fr:m}$ is modeled as a function of the engine speed and the engine temperature

$$M_{fr:m} = M_{fr:m}(\dot{\theta}_m, T_m) \quad (4.14)$$

The influence from the load is neglected. With neutral gear engaged, the engine speed is controlled to 20 levels between 600 and 2300 RPM, while measuring the engine torque and temperature. The resulting friction map is shown in Figure 4.4 for the 124L truck with unit-pump injection system. The corresponding friction map for the 144L truck with in-line injection pump system is shown in Figure 4.5.

The logged engine torque, $M_m(m_f)$, as a function of the fuel amount, is recalculated to control signal to the driveline by subtracting the engine friction from the engine torque as

$$u = M_m(m_f) - M_{fr:m}(\dot{\theta}_m, T_m) \quad (4.15)$$

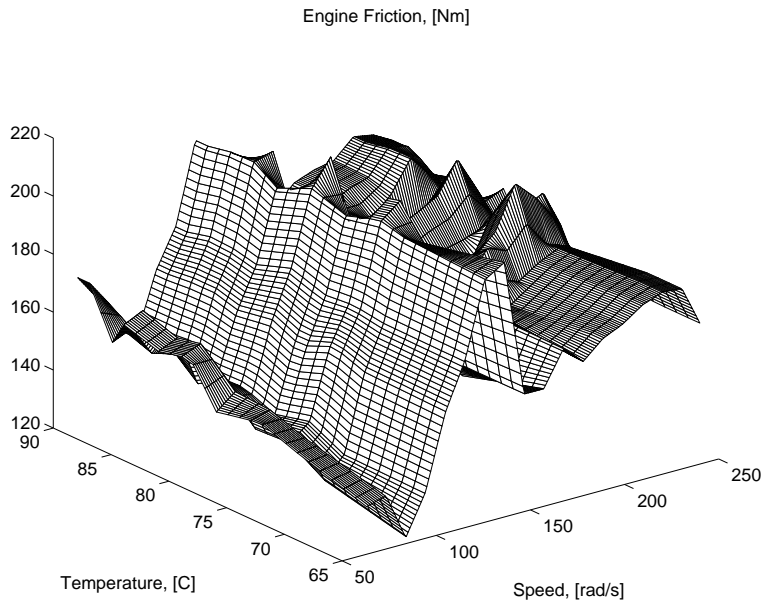


Figure 4.4 Engine friction for the 124L truck, modeled as a function of engine speed and engine temperature.

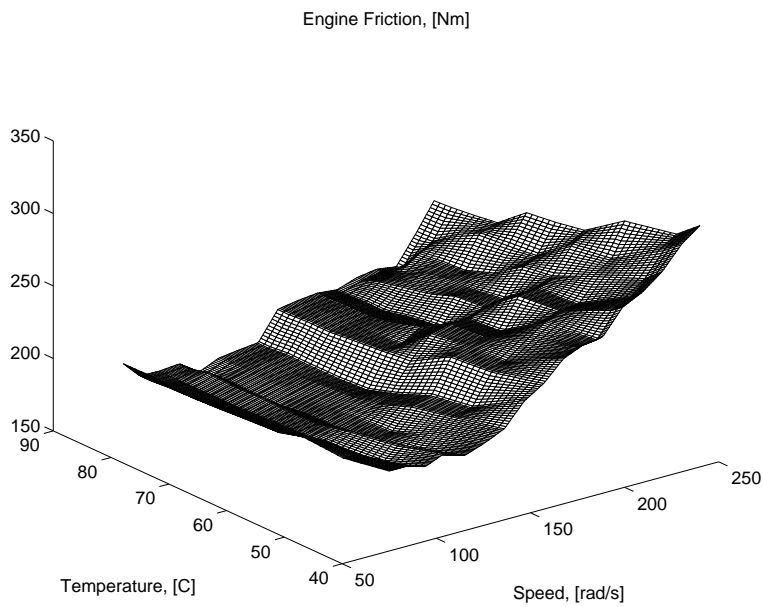


Figure 4.5 Engine friction for the 144L truck, modeled as a function of engine speed and engine temperature.

4.3 Modeling the Driveline of the 144L Truck

The measured engine speed, transmission speed, and wheel speed for the 144L truck is explained by deriving a set of models of increasing complexity. Figure 3.9 shows that the main difference in speed is between the measured transmission speed and wheel speed, indicating that the important flexibility of the driveline is located between the output shaft of the transmission and the wheel. This leads to a first model with a lumped engine and transmission inertia connected to the wheel inertia by a drive-shaft flexibility. The reason for this is that the drive shaft is subject to the relatively largest torsion. This is mainly due to the high torque difference that results from the amplification of the engine torque by the conversion ratio of the transmission (i_t) and the final drive (i_f). This number ($i_t i_f$) can be as high as 60 for the lowest gear. A total of three models will be derived for the 144L truck, all based on the basic driveline equations derived in Section 4.1. The 124L truck will be modeled in the section following.

4.3.1 Model with Drive-Shaft Flexibility

The simplest model with a drive-shaft flexibility is developed first. Assumptions about the fundamental equations in Section 4.1 are made in order to obtain a model with a lumped engine and transmission inertia and a drive-shaft flexibility. Labels are according to Figure 4.2. The clutch and the propeller shafts are assumed to be stiff, and the drive shaft is described as a damped torsional flexibility. The transmission and the final drive are assumed to multiply the torque by the conversion ratio, without losses.

Clutch: The clutch is assumed to be stiff, which gives the following equations for the torque and the angle

$$M_c = M_t, \quad \theta_m = \theta_c \quad (4.16)$$

Transmission: The transmission is described by one rotating inertia J_t . The friction torque is assumed to be described by a viscous damping coefficient b_t . The model of the transmission, corresponding to (4.3), is

$$\theta_c = \theta_t i_t \quad (4.17)$$

$$J_t \ddot{\theta}_t = M_t i_t - b_t \dot{\theta}_t - M_p \quad (4.18)$$

By using (4.16) and (4.17), the model can be rewritten as

$$J_t \ddot{\theta}_m = M_c i_t^2 - b_t \dot{\theta}_m - M_p i_t \quad (4.19)$$

Propeller shaft: The propeller shaft is also assumed to be stiff, which gives the following equations for the torque and the angle

$$M_p = M_f, \quad \theta_t = \theta_p \quad (4.20)$$

Final drive: In the same way as for the transmission, the final drive is modeled by one rotating inertia J_f . The friction torque is assumed to be described by a viscous damping coefficient b_f . The model of the final drive, corresponding to (4.5), is

$$\theta_p = \theta_f i_f \quad (4.21)$$

$$J_f \ddot{\theta}_f = M_f i_f - b_f \dot{\theta}_f - M_d \quad (4.22)$$

Equation (4.22) can be rewritten with (4.20) and (4.21) which gives

$$J_f \ddot{\theta}_t = M_p i_f^2 - b_f \dot{\theta}_t - M_d i_f \quad (4.23)$$

Converting (4.23) to a function of engine speed is done by using (4.16) and (4.17) resulting in

$$J_f \ddot{\theta}_m = M_p i_f^2 i_t - b_f \dot{\theta}_m - M_d i_f i_t \quad (4.24)$$

By replacing M_p in (4.24) with M_p in (4.19), a model for the lumped transmission, propeller shaft, and final drive is obtained

$$(J_t i_f^2 + J_f) \ddot{\theta}_m = M_c i_t^2 i_f^2 - b_t \dot{\theta}_m i_f^2 - b_f \dot{\theta}_m - M_d i_f i_t \quad (4.25)$$

Drive shaft: The drive shaft is modeled as a damped torsional flexibility, having stiffness k , and internal damping c . Hence, (4.6) becomes

$$\begin{aligned} M_w = M_d &= k(\theta_f - \theta_w) + c(\dot{\theta}_f - \dot{\theta}_w) = k(\theta_m/i_t i_f - \theta_w) \\ &+ c(\dot{\theta}_m/i_t i_f - \dot{\theta}_w) \end{aligned} \quad (4.26)$$

where (4.16), (4.17), (4.20), and (4.21) are used. By replacing M_d in (4.25) with (4.26) the equation describing the transmission, the propeller shaft, the final drive, and the drive shaft, becomes

$$\begin{aligned} (J_t i_f^2 + J_f) \ddot{\theta}_m &= M_c i_t^2 i_f^2 - b_t \dot{\theta}_m i_f^2 - b_f \dot{\theta}_m \\ &- k(\theta_m - \theta_w i_t i_f) - c(\dot{\theta}_m - \dot{\theta}_w i_t i_f) \end{aligned} \quad (4.27)$$

Wheel: If (4.11) is combined with (4.26), the following equation for the wheel is obtained:

$$\begin{aligned} (J_w + m r_w^2) \ddot{\theta}_w &= k(\theta_m/i_t i_f - \theta_w) + c(\dot{\theta}_m/i_t i_f - \dot{\theta}_w) \\ &- b_w \dot{\theta}_w - \frac{1}{2} c_w A_a \rho_a r_w^3 \dot{\theta}_w^2 - m c_{r2} r_w^2 \dot{\theta}_w - r_w m (c_{r1} + g \sin(\alpha)) \end{aligned} \quad (4.28)$$

where the friction torque is described as viscous damping, with label b_w .

The complete model, named the Drive-shaft model, is obtained by inserting M_c from (4.27) into (4.1), together with (4.28), which gives the following equations. An illustration of the model can be seen in Figure 4.6.

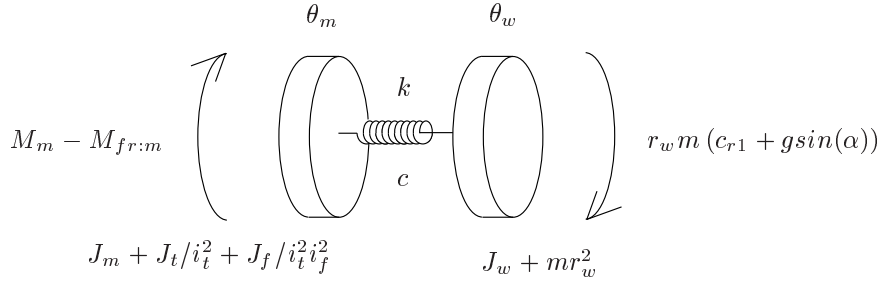


Figure 4.6 The Drive-shaft model consists of a lumped engine and transmission inertia connected to the wheel inertia by a damped torsional flexibility.

The Drive-Shaft Model

$$(J_m + J_t/i_t^2 + J_f/i_t^2 i_f^2) \ddot{\theta}_m = M_m - M_{f r:m} - (b_t/i_t^2 + b_f/i_t^2 i_f^2) \dot{\theta}_m - k(\theta_m/i_t i_f - \theta_w) - c(\dot{\theta}_m/i_t i_f - \dot{\theta}_w) \quad (4.29)$$

$$(J_w + m r_w^2) \ddot{\theta}_w = k(\theta_m/i_t i_f - \theta_w) + c(\dot{\theta}_m/i_t i_f - \dot{\theta}_w) - (b_w + m c_{r2} r_w^2) \dot{\theta}_w - \frac{1}{2} c_w A_a \rho_a r_w^3 \dot{\theta}_w^2 - r_w m (c_{r1} + g \sin(\alpha)) \quad (4.30)$$

The Drive-shaft model is the simplest model of three considered. The drive-shaft torsion, the engine speed, and the wheel speed are used as states according to

$$x_1 = \theta_m/i_t i_f - \theta_w, \quad x_2 = \dot{\theta}_m, \quad x_3 = \dot{\theta}_w \quad (4.31)$$

More details of state-space descriptions are given in Chapter 5. For low gears, the influence from the air drag is low and by neglecting $\frac{1}{2} c_w A_a \rho_a r_w^3 \dot{\theta}_w^2$ in (4.30), the model is linear in the states, but nonlinear in the parameters.

Parameter estimation of the Drive-shaft model

A data set containing engine torque, engine speed, and wheel speed measurements are used to estimate the parameters and the initial conditions of the Drive-shaft model. The estimated parameters are

$$\begin{aligned} i &= i_t i_f, & l &= r_w m (c_{r1} + g \sin(\alpha)) \\ J_1 &= J_m + J_t/i_t^2 + J_f/i_t^2 i_f^2, & J_2 &= J_w + m r_w^2 \\ b_1 &= b_t/i_t^2 + b_f/i_t^2 i_f^2, & b_2 &= b_w + m c_{r2} r_w^2 \end{aligned} \quad (4.32)$$

together with the stiffness, k , and the internal damping, c , of the drive shaft. The estimated initial conditions of the states are labeled x_{10} , x_{20} , and x_{30} , according to (4.31). More details about the parameter estimation software is found in Section 4.1.

Figure 4.7 shows an example of how the model fits the measured data. The measured driveline speed are shown together with the model output, x_1 , x_2 , and x_3 . According to the model, the clutch is stiff, and therefore, the transmission speed is equal to the engine speed scaled with the conversion ratio of the transmission (i_t). In the figure, this signal is shown together with the measured transmission speed. The plots are typical examples that show that a major part of the driveline dynamics is captured with a linear mass-spring model with the drive shafts as the main flexibility.

Results of parameter estimation

- The main contribution to driveline dynamics from driving torque to engine speed and wheel speed is the drive shaft, explaining the first main resonance of the driveline.
- The true drive-shaft torsion (x_1) is unknown, but the value estimated by the model has physically reasonable values. These values will be further validated in Chapter 10.
- The model output transmission speed (x_2/i_t) fits the measured transmission speed data reasonably well, but there is still a systematic dynamics lag between model outputs and measurements.

4.3.2 Influence from Propeller-Shaft Flexibility

The Drive-shaft model assumes stiff driveline from the engine to the final drive. The propeller shaft and the drive shaft are separated by the final drive, which has a small inertia compared to other inertias, e.g. the engine inertia. This section covers an investigation of how the model parameters of the Drive-shaft model are influenced by a flexible propeller shaft.

A model is derived with a stiff driveline from the engine to the output shaft of the transmission. The propeller shaft and the drive shafts are modeled as damped torsional flexibilities. As in the derivation of the Drive-shaft model, the transmission and the final drive are assumed to multiply the torque with the conversion ratio, without losses.

The derivation of the Drive-shaft model is repeated here with the difference that the model for the propeller shaft (4.20) is replaced by a model of a flexibility with stiffness k_p and internal damping c_p

$$M_p = M_f = k_p(\theta_t - \theta_p) + c_p(\dot{\theta}_t - \dot{\theta}_p) = k_p(\theta_m/i_t - \theta_p) + c_p(\dot{\theta}_m/i_t - \dot{\theta}_p) \quad (4.33)$$

where (4.16) and (4.17) are used in the last equality. This formulation means that there are two torsional flexibilities, the propeller shaft and the drive shaft. Inserting

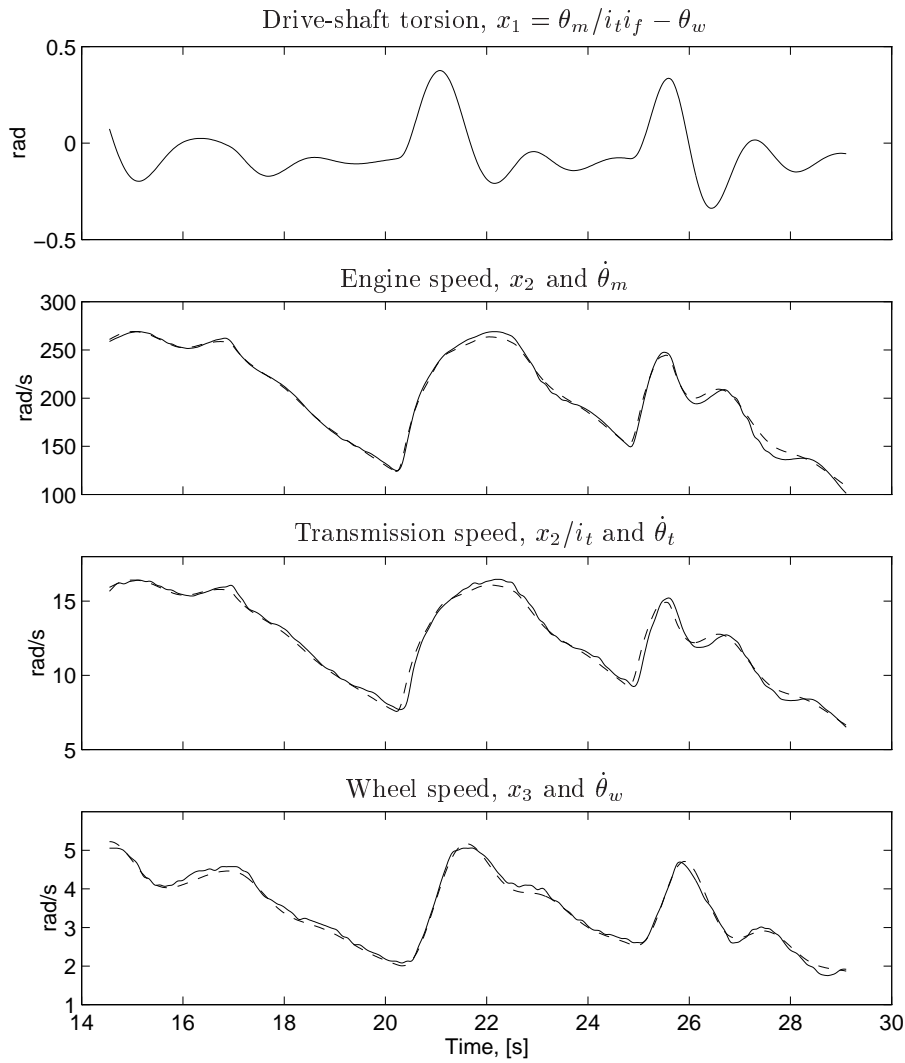


Figure 4.7 The parameters of the *Drive-shaft model* estimated on data with step inputs in accelerator position using gear 1. The top figure shows the estimated drive-shaft torsion, and the bottom figures show the model outputs (x_2 , x_3) in dashed lines, together with the measured driveline speeds in solid. The plots are typical examples of that a major part of the dynamics is captured by a linear model with a drive-shaft flexibility.

(4.33) into (4.19) gives

$$J_t \ddot{\theta}_m = M_c i_t^2 - b_t \dot{\theta}_m - \left(k_p (\theta_m / i_t - \theta_p) + c_p (\dot{\theta}_m / i_t - \dot{\theta}_p) \right) i_t \quad (4.34)$$

By combining this with (4.1) the following differential equation describing the lumped engine and transmission results

$$\begin{aligned} (J_m + J_t / i_t^2) \ddot{\theta}_m &= M_m - M_{fr:m} - b_t / i_t^2 \dot{\theta}_m \\ &\quad - \frac{1}{i_t} \left(k_p (\theta_m / i_t - \theta_p) + c_p (\dot{\theta}_m / i_t - \dot{\theta}_p) \right) \end{aligned} \quad (4.35)$$

The final drive is described by inserting (4.33) in (4.22) and using (4.21)

$$\theta_p = \theta_f i_f \quad (4.36)$$

$$J_f \ddot{\theta}_f = i_f \left(k_p (\theta_m / i_t - \theta_p) + c_p (\dot{\theta}_m / i_t - \dot{\theta}_p) \right) - b_f \dot{\theta}_f - M_d \quad (4.37)$$

Including (4.36) in (4.37) gives

$$J_f \ddot{\theta}_p = i_f^2 \left(k_p (\theta_m / i_t - \theta_p) + c_p (\dot{\theta}_m / i_t - \dot{\theta}_p) \right) - b_f \dot{\theta}_p - i_f M_d \quad (4.38)$$

The equation for the drive shaft (4.26) is repeated with new labels

$$M_w = M_d = k_d (\theta_f - \theta_w) + c_d (\dot{\theta}_f - \dot{\theta}_w) = k_d (\theta_p / i_f - \theta_w) + c_d (\dot{\theta}_p / i_f - \dot{\theta}_w) \quad (4.39)$$

where (4.36) is used in the last equality.

The equation for the final drive (4.38) now becomes

$$\begin{aligned} J_f \ddot{\theta}_p &= i_f^2 \left(k_p (\theta_m / i_t - \theta_p) + c_p (\dot{\theta}_m / i_t - \dot{\theta}_p) \right) - b_f \dot{\theta}_p \\ &\quad - i_f \left(k_d (\theta_p / i_f - \theta_w) + c_d (\dot{\theta}_p / i_f - \dot{\theta}_w) \right) \end{aligned} \quad (4.40)$$

The equation for the wheel is derived by combining (4.11) with (4.39). The equation describing the wheel becomes

$$\begin{aligned} (J_w + m r_w^2) \ddot{\theta}_w &= k_d (\theta_p / i_f - \theta_w) + c_d (\dot{\theta}_p / i_f - \dot{\theta}_w) \\ &\quad - b_w \dot{\theta}_w - \frac{1}{2} c_w A_a \rho_a r_w^3 \dot{\theta}_w^2 - m c_{r2} r_w^2 \dot{\theta}_w - r_w m (c_{r1} + g \sin(\alpha)) \end{aligned} \quad (4.41)$$

where again the friction torque is assumed to be described by a viscous damping coefficient b_w . The complete model with drive shaft and propeller shaft flexibilities is the following, which can be seen in Figure 4.8.

$$\begin{aligned} (J_m + J_t / i_t^2) \ddot{\theta}_m &= M_m - M_{fr:m} - b_t / i_t^2 \dot{\theta}_m \\ &\quad - \frac{1}{i_t} \left(k_p (\theta_m / i_t - \theta_p) + c_p (\dot{\theta}_m / i_t - \dot{\theta}_p) \right) \end{aligned} \quad (4.42)$$

$$J_f \ddot{\theta}_p = i_f^2 \left(k_p (\theta_m / i_t - \theta_p) + c_p (\dot{\theta}_m / i_t - \dot{\theta}_p) \right) - b_f \dot{\theta}_p \quad (4.43)$$

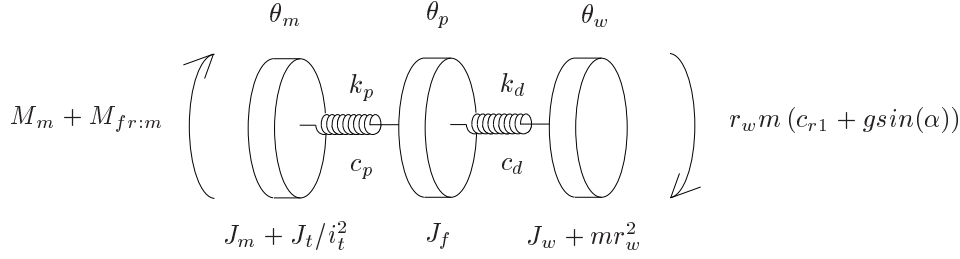


Figure 4.8 Model with flexible propeller shaft and drive shaft.

$$\begin{aligned}
 & -i_f \left(k_d(\theta_p/i_f - \theta_w) + c_d(\dot{\theta}_p/i_f - \dot{\theta}_w) \right) \\
 (J_w + mr_w^2)\ddot{\theta}_w &= k_d(\theta_p/i_f - \theta_w) + c_d(\dot{\theta}_p/i_f - \dot{\theta}_w) \quad (4.44) \\
 & - (b_w + mc_{r2}r_w^2)\dot{\theta}_w - \frac{1}{2}c_w A_a \rho_a r_w^3 \dot{\theta}_w^2 - r_w m (c_{r1} + g \sin(\alpha))
 \end{aligned}$$

The model equations (4.42) to (4.44) describe the Drive-shaft model extended with the propeller shaft with stiffness k_p and damping c_p . The three inertias in the model are

$$\begin{aligned}
 J_1 &= J_m + J_t/i_t^2 \\
 J_2 &= J_f \\
 J_3 &= J_w + mr_w^2
 \end{aligned} \quad (4.45)$$

If the magnitude of the three inertias are compared, the inertia of the final drive (J_f) is considerably less than J_1 and J_2 in (4.45). Therefore, the model will act as if there are two damped springs in series. The total stiffness of two undamped springs in series is

$$k = \frac{k_p i_f^2 k_d}{k_p i_f^2 + k_d} \quad (4.46)$$

whereas the total damping of two dampers in series is

$$c = \frac{c_p i_f^2 c_d}{c_p i_f^2 + c_d} \quad (4.47)$$

The damping and the stiffness of the drive shaft in the previous section will thus typically be underestimated due to the flexibility of the propeller shaft. This effect will increase with lower conversion ratio in the final drive, i_f . The individual stiffness values obtained from parameter estimation are somewhat lower than the values obtained from material data.

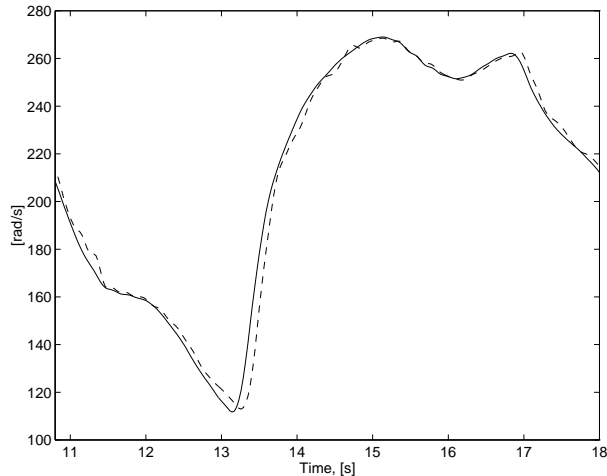


Figure 4.9 Measured engine speed (solid) and transmission speed (dashed). The transmission speed is multiplied with the conversion ratio of the transmission, i_t .

4.3.3 Deviations between Engine Speed and Transmission Speed

As mentioned above, there is good agreement between model output and experimental data for $u = M_m - M_{fr:m}$, θ_m , and $\dot{\theta}_w$, but there is a slight deviation between measured and estimated transmission speed. With the Drive-shaft model, stiff dynamics between the engine and the transmission is assumed, and hence the only difference between the model outputs engine speed and transmission speed is the gain i_t (conversion ratio of the transmission). However, a comparison between the measured engine speed and transmission speed shows that there is not only a gain difference according to Figure 4.9. This deviation has a character of a phase shift and some smoothing (signal levels and shapes agree). This indicates that there is some additional dynamics between engine speed, θ_m , and transmission speed, $\dot{\theta}_t$. Two natural candidates are additional mass-spring dynamics in the driveline, or sensor dynamics. The explanation is that there is a combined effect, with the major difference explained by the sensor dynamics. The motivation for this is that the high stiffness of the clutch flexibility (given from material data) cannot result in a phase shift form of the magnitude shown in Figure 4.9. Neither can backlash in the transmission explain the difference, because then the engine and transmission speeds would be equal when the backlash is at its endpoints.

As mentioned before, the bandwidth of the measured transmission speed is lower than the measured engine and wheel speeds, due to fewer cogs in the sensor. It is assumed that the engine speed and the wheel speed sensor dynamics are not influencing the data for the frequencies considered. The speed dependence of the transmission sensor dynamics is neglected. The following sensor dynamics are

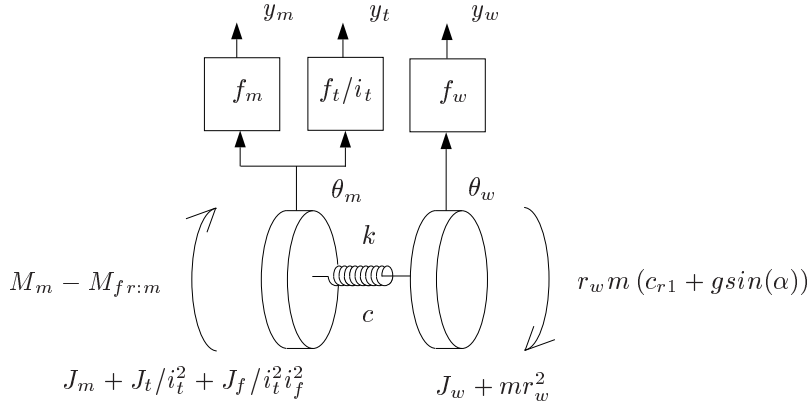


Figure 4.10 The Drive-shaft model with sensor dynamics.

assumed, after some comparison between sensor filters of different order,

$$\begin{aligned} f_m &= 1 \\ f_t &= \frac{1}{1 + \gamma s} \\ f_w &= 1 \end{aligned} \quad (4.48)$$

where a first order filter with an unknown parameter γ models the transmission sensor. Figure 4.10 shows the configuration with the Drive-shaft model and sensor filter f_m , f_t , and f_w . The outputs of the filters are y_m , y_t , and y_w .

Now the parameters, the initial condition, and the unknown filter constant γ can be estimated such that the model outputs (y_m, y_t, y_w) fit the measured data. The result of this is seen in Figure 4.11 for gear 1. The conclusion is that the main part of the deviation between engine speed and transmission speed is due to sensor dynamics. Figure 4.12 shows an enlarged plot of the transmission speed, with the model output from the Drive-shaft model with and without sensor filtering.

Results of parameter estimation

- If the Drive-shaft model is extended with a first order sensor filter for the transmission speed, all three velocities $(\dot{\theta}_m, \dot{\theta}_t, \dot{\theta}_w)$ are estimated by the model. The model outputs fit the data except for some time intervals where there are deviations between model and measured data (see Figure 4.12). However, these deviations will in the following be related to nonlinearities at low clutch torques.

4.3.4 Model with Flexible Clutch and Drive Shaft

The clutch has so far been assumed stiff and the main contribution to low-frequency oscillations is the drive-shaft flexibility. However, measured data suggests that

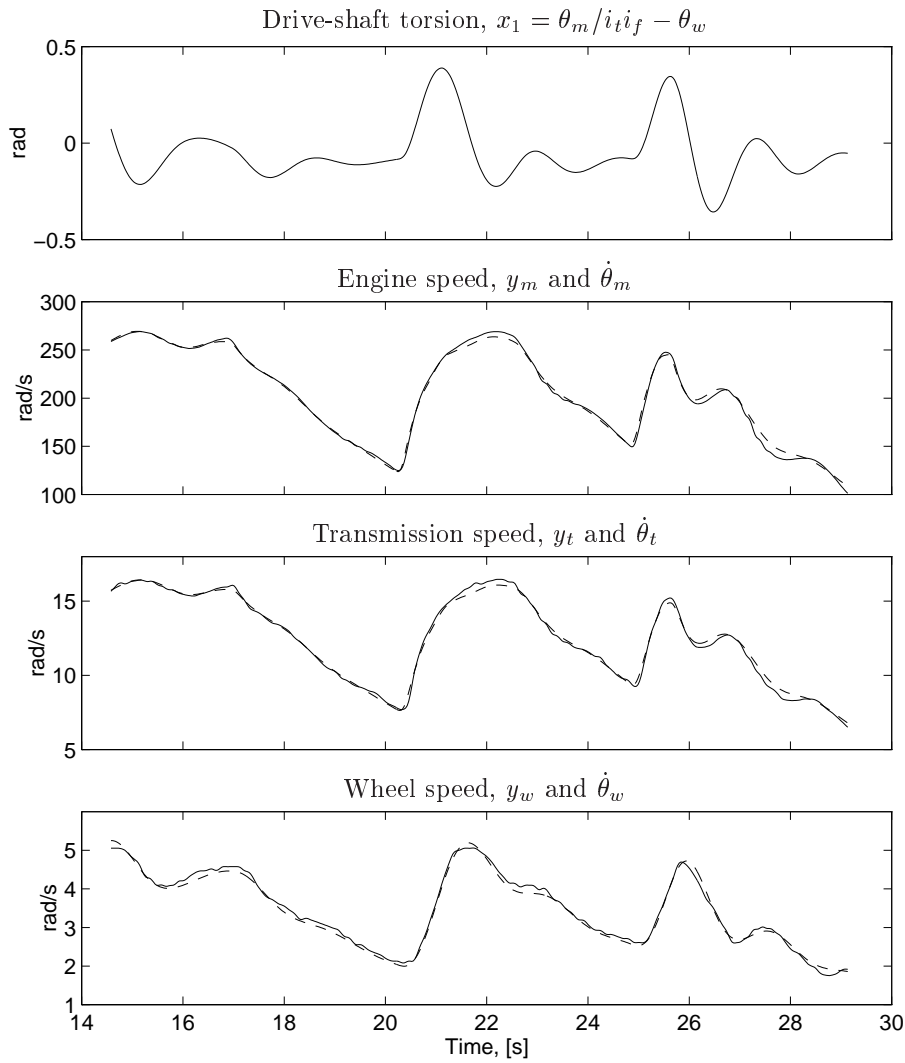


Figure 4.11 Parameter estimation of the Drive-shaft model as in Figure 4.7, but with sensor dynamics included. The top figure shows the estimated drive-shaft torsion, and the bottom figures show the model outputs (y_m , y_t , y_w) in dashed, together with the measured data in solid. The main part of the deviation between engine speed and transmission speed is due to sensor dynamics. See also Figure 4.12.

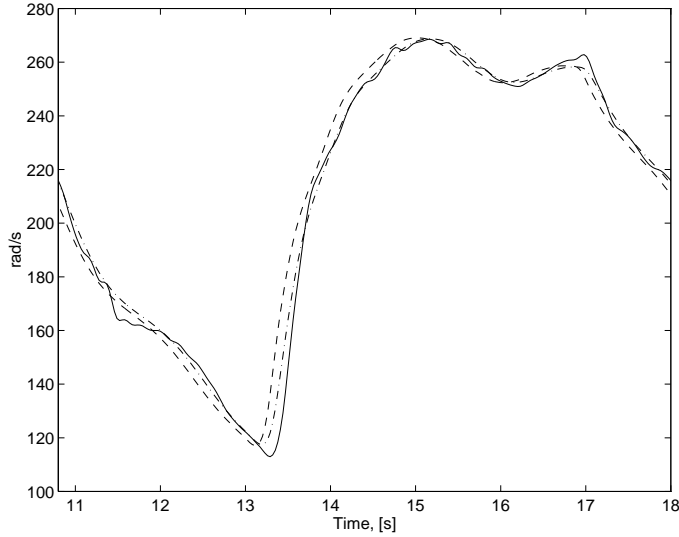


Figure 4.12 Enlargement of part of Figure 4.11. Measured transmission speed (solid), output from the *Drive-shaft model* without sensor filtering (dashed), and output from the *Drive-shaft model* with sensor filtering (dash-dotted). The parameters are estimated based on experiments with gear 1.

there is some additional dynamics between the engine and the transmission. The candidate which is most flexible is the clutch. Hence, the model will include two torsional flexibilities, the drive shaft, and the clutch. With this model structure, the first and second resonance modes of the driveline are explained. The reason to this ordering in frequency is the relatively higher stiffness in the clutch, because the relative stiffness of the drive shaft is reduced by the conversion ratio.

A model with a linear clutch flexibility and one torsional flexibility (the drive shaft) is derived by repeating the procedure for the *Drive-shaft model* with the difference that the model for the clutch is a flexibility with stiffness k_c and internal damping c_c

$$M_c = M_t = k_c(\theta_m - \theta_c) + c_c(\dot{\theta}_m - \dot{\theta}_c) = k_c(\theta_m - \theta_t i_t) + c_c(\dot{\theta}_m - \dot{\theta}_t i_t) \quad (4.49)$$

where (4.17) is used in the last equality. By inserting this into (4.1) the equation describing the engine inertia is given by

$$J_m \ddot{\theta}_m = M_m - M_{fr:m} - \left(k_c(\theta_m - \theta_t i_t) + c_c(\dot{\theta}_m - \dot{\theta}_t i_t) \right) \quad (4.50)$$

Also by inserting (4.49) into (4.18), the equation describing the transmission is

$$J_t \ddot{\theta}_t = i_t \left(k_c(\theta_m - \theta_t i_t) + c_c(\dot{\theta}_m - \dot{\theta}_t i_t) \right) - b_t \dot{\theta}_t - M_p \quad (4.51)$$

M_p is derived from (4.23) giving

$$(J_t + J_f/i_f^2)\ddot{\theta}_t = i_t \left(k_c(\theta_m - \theta_t i_t) + c_c(\dot{\theta}_m - \dot{\theta}_t i_t) \right) - (b_t + b_f/i_f^2)\dot{\theta}_t - M_d/i_f \quad (4.52)$$

which is the equation describing the lumped transmission, propeller shaft, and final drive inertia.

The drive shaft is modeled according to (4.26) as

$$M_w = M_d = k_d(\theta_f - \theta_w) + c_d(\dot{\theta}_f - \dot{\theta}_w) = k_d(\theta_t/i_f - \theta_w) + c_d(\dot{\theta}_t/i_f - \dot{\theta}_w) \quad (4.53)$$

where (4.20) and (4.21) are used in the last equality.

The complete model, named the Clutch and drive-shaft model, is obtained by inserting (4.53) into (4.52) and (4.11). An illustration of the model can be seen in Figure 4.13.

The Clutch and Drive-Shaft Model

$$J_m \ddot{\theta}_m = M_m - M_{fr:m} - \left(k_c(\theta_m - \theta_t i_t) + c_c(\dot{\theta}_m - \dot{\theta}_t i_t) \right) \quad (4.54)$$

$$(J_t + J_f/i_f^2)\ddot{\theta}_t = i_t \left(k_c(\theta_m - \theta_t i_t) + c_c(\dot{\theta}_m - \dot{\theta}_t i_t) \right) - (b_t + b_f/i_f^2)\dot{\theta}_t - \frac{1}{i_f} \left(k_d(\theta_t/i_f - \theta_w) + c_d(\dot{\theta}_t/i_f - \dot{\theta}_w) \right) \quad (4.55)$$

$$(J_w + mr_w^2)\ddot{\theta}_w = k_d(\theta_t/i_f - \theta_w) + c_d(\dot{\theta}_t/i_f - \dot{\theta}_w) - (b_w + c_{r2}r_w)\dot{\theta}_w - \frac{1}{2}c_w A_a \rho_a r_w^3 \dot{\theta}_w^2 - r_w m (c_{r1} + g \sin(\alpha)) \quad (4.56)$$

The clutch torsion, the drive-shaft torsion, and the driveline speeds are used as states according to

$$x_1 = \theta_m - \theta_t i_t, \quad x_2 = \theta_t/i_f - \theta_w, \quad x_3 = \dot{\theta}_m, \quad x_4 = \dot{\theta}_t, \quad x_5 = \dot{\theta}_w \quad (4.57)$$

More details about state-space representations and parameters are covered in Chapter 5. For low gears, the influence from the air drag is low and by neglecting $\frac{1}{2}c_w A_a \rho_a r_w^3 \dot{\theta}_w^2$ in (4.56), the model is linear in the states, but nonlinear in the parameters. The model equipped with the sensor filter in (4.48) gives the true sensor outputs (y_m, y_t, y_w).

Parameter estimation of the Clutch and drive-shaft model

The parameters and the initial conditions of the Clutch and drive-shaft model are estimated with the sensor dynamics described above, in the same way as the Drive-shaft model in this section. A problem when estimating the parameters of the Clutch and drive-shaft model is that the bandwidth of the measured signals is not enough to estimate the stiffness k_c in the clutch. Therefore, the value of the stiffness given from material data is used and fixed, and the rest of the parameters are estimated.

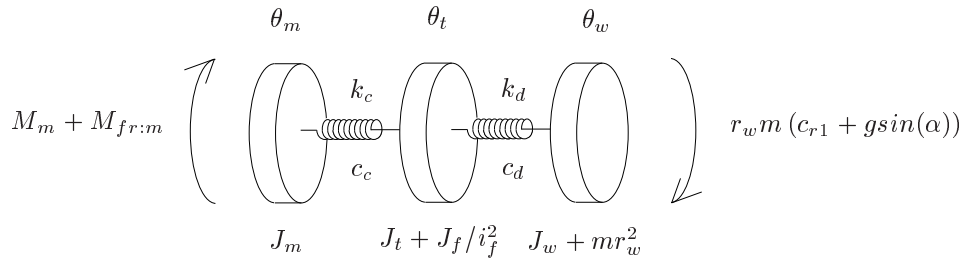


Figure 4.13 The Clutch and drive-shaft model: Linear clutch and drive-shaft torsional flexibility.

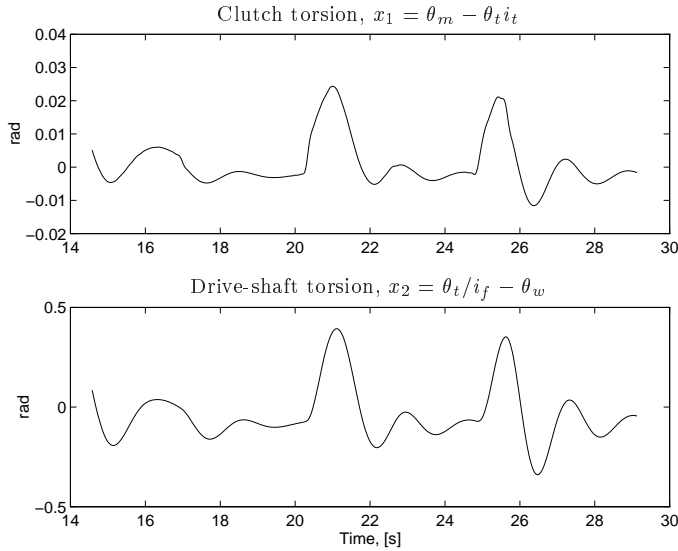


Figure 4.14 Clutch torsion (top figure) and drive-shaft torsion (bottom figure) resulting from parameter estimation of the Clutch and drive-shaft model with sensor filtering, on data with gear 1. The true values of these torsions are not known, but the plots show that the drive-shaft torsion has realistic values.

The resulting clutch torsion (x_1) and the drive-shaft torsion (x_2) are shown in Figure 4.14. The true values of these torsions are not known, but the figure shows that the amplitude of the drive-shaft torsion has realistic values that agree with material data. However, the clutch torsion does not have realistic values (explained later), which can be seen when comparing with the static nonlinearity in Figure 4.15.

The model output velocities ($\dot{\theta}_m$, $\dot{\theta}_t$, $\dot{\theta}_w$) show no improvement compared to those generated by the Drive-shaft model with sensor dynamics, displayed in Figure 4.11.

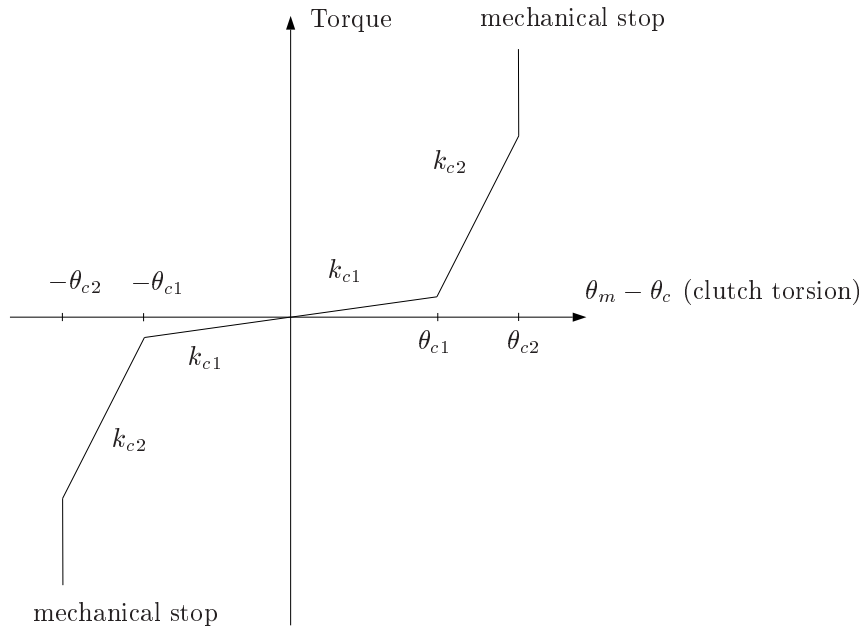


Figure 4.15 Nonlinear clutch characteristics.

Results of parameter estimation

- The model including a linear clutch does not improve the data fit. The interpretation of this is that the clutch model does not add information for frequencies in the measured data.

4.3.5 Nonlinear Clutch and Drive-Shaft Flexibility

When studying a clutch in more detail it is seen that the torsional flexibility is a result of an arrangement with smaller springs in series with springs with much higher stiffness. The reason for this arrangement is vibration insulation. When the angle difference over the clutch starts from zero and increases, the smaller springs, with stiffness k_{c1} , are being compressed. This ends when they are fully compressed at θ_{c1} radians. If the angle is increased further, the stiffer springs, with stiffness k_{c2} , are beginning to be compressed. When θ_{c2} is reached, the clutch hits a mechanical stop. This clutch characteristics can be modeled as in Figure 4.15. The resulting stiffness $k_c(\theta_m - \theta_c)$ of the clutch is given by

$$k_c(x) = \begin{cases} k_{c1} & \text{if } |x| \leq \theta_{c1} \\ k_{c2} & \text{if } \theta_{c1} < |x| \leq \theta_{c2} \\ \infty & \text{otherwise} \end{cases} \quad (4.58)$$

The torque $M_{kc}(\theta_m - \theta_c)$ from the clutch nonlinearity is

$$M_{kc}(x) = \begin{cases} k_{c1}x & \text{if } |x| \leq \theta_{c1} \\ k_{c1}\theta_{c1} + k_{c2}(x - \theta_{c1}) & \text{if } \theta_{c1} < x \leq \theta_{c2} \\ -k_{c1}\theta_{c1} + k_{c2}(x + \theta_{c1}) & \text{if } -\theta_{c2} < x \leq -\theta_{c1} \\ \infty & \text{otherwise} \end{cases} \quad (4.59)$$

If the linear clutch in the Clutch and drive-shaft model is replaced by the clutch nonlinearity according to Figure 4.15, the following model, called the Nonlinear clutch and drive-shaft model, is derived.

The Nonlinear Clutch and Drive-Shaft Model

$$J_m \ddot{\theta}_m = M_m - M_{fr:m} - M_{kc}(\theta_m - \theta_t i_t) - c_c(\dot{\theta}_m - \dot{\theta}_t i_t) \quad (4.60)$$

$$(J_t + J_f/i_f^2) \ddot{\theta}_t = i_t \left(M_{kc}(\theta_m - \theta_t i_t) + c_c(\dot{\theta}_m - \dot{\theta}_t i_t) \right) - (b_t + b_f/i_f^2) \dot{\theta}_t - \frac{1}{i_f} \left(k_d(\theta_t/i_f - \theta_w) + c_d(\dot{\theta}_t/i_f - \dot{\theta}_w) \right) \quad (4.61)$$

$$(J_w + m r_w^2) \ddot{\theta}_w = k_d(\theta_t/i_f - \theta_w) + c_d(\dot{\theta}_t/i_f - \dot{\theta}_w) - (b_w + m c_{r2} r_w) \dot{\theta}_w - \frac{1}{2} c_w A_a \rho_a r_w^3 \dot{\theta}_w^2 - r_w m (c_{r1} + g \sin(\alpha)) \quad (4.62)$$

Nonlinear driveline model with five states. (The same state-space representation as for the Clutch and drive-shaft model can be used.) The function $M_{kc}(\cdot)$ is given by (4.59). The model equipped with the sensor filter in (4.48) gives the true sensor outputs (y_m, y_t, y_w) .

Parameter estimation of the Nonlinear clutch and drive-shaft model

When estimating the parameters and the initial conditions of the Nonlinear clutch and drive-shaft model, the clutch static nonlinearity is fixed with known physical values and the rest of the parameters are estimated, except for the sensor filter which is the same as in the previous model estimations.

The resulting clutch torsion ($x_1 = \theta_m - \theta_t i_t$) and drive-shaft torsion ($x_2 = \theta_t/i_f - \theta_w$) after minimizing (4.13) are shown in Figure 4.16. The true values of these torsions are not known as mentioned before. However, the figure shows that both angles have realistic values that agree with other experience. The model output velocities ($\dot{\theta}_m, \dot{\theta}_t, \dot{\theta}_w$) show no improvement compared to those generated by the Drive-shaft model with sensor dynamics, displayed in Figure 4.11.

In Figure 4.12 it was seen that the model with the sensor filtering fitted the signal except for a number of time intervals with deviations. The question is if this is a result of some nonlinearity. Figure 4.17 shows the transmission speed plotted together with the model output and the clutch torsion. It is clear from this figure that the deviation between model and experiments occurs when the clutch angle passes the area with the low stiffness in the static nonlinearity (see Figure 4.15).

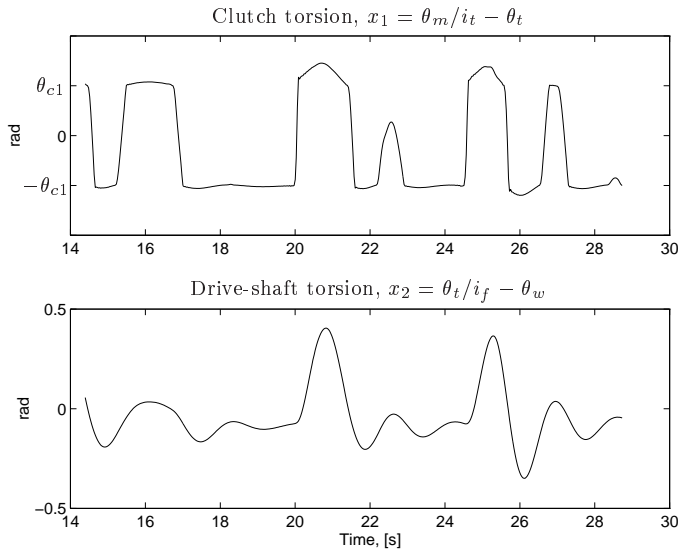


Figure 4.16 Clutch torsion (top figure) and drive-shaft torsion (bottom figure) resulting from parameter estimation of the *Nonlinear clutch and drive-shaft model with sensor filtering*, on data with gear 1. The true values of these torsions are not known, but the plots show that they have realistic values.

Results of parameter estimation

- The model including the nonlinear clutch does not improve the overall data fit for frequencies in the measured data.
- The model is able to estimate a clutch torsion with realistic values.
- The estimated clutch torsion shows that when the clutch passes the area with low stiffness in the nonlinearity, the model deviates from the data. The reason is unmodeled dynamics at low clutch torques [3].

4.3.6 Model Validity

As mentioned before, the data sets are divided into two parts. The parameters are estimated on the estimation data. The results are then evaluated on the validation data, and these are the results shown in this chapter.

In the parameter estimation, the unknown load, l , which vary between the trials, is estimated. The load can be recalculated to estimate road slope, and the calculated values agree well with the known values of the road slopes at Scania. Furthermore, the estimation of the states describing the torsion of the clutch and the drive shaft shows realistic values. This gives further support to model structure and parameters.

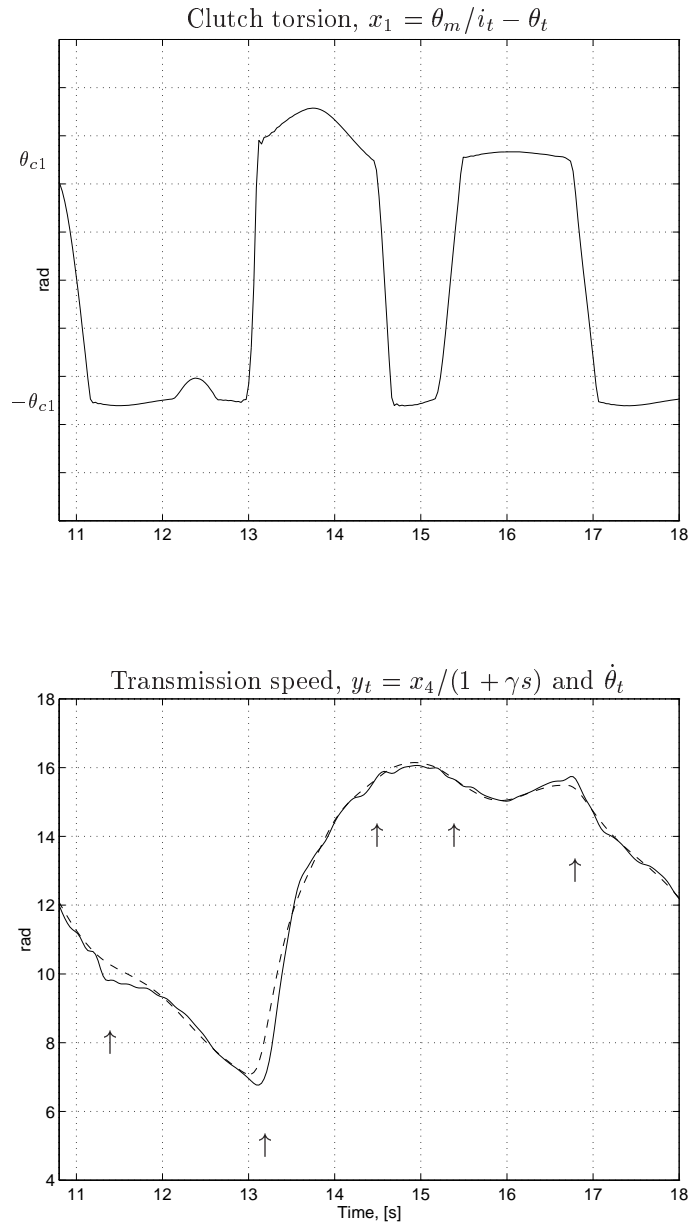


Figure 4.17 Clutch torsion (top figure) and measured and estimated transmission speeds (bottom figure) from the *Nonlinear clutch and drive-shaft model with sensor dynamics with gear 1*. The result is that the main differences between model (dashed) and experiments (solid) occur when the clutch torsion passes the area with the low stiffness ($|\theta| < \theta_{c1}$) in the static clutch nonlinearity.

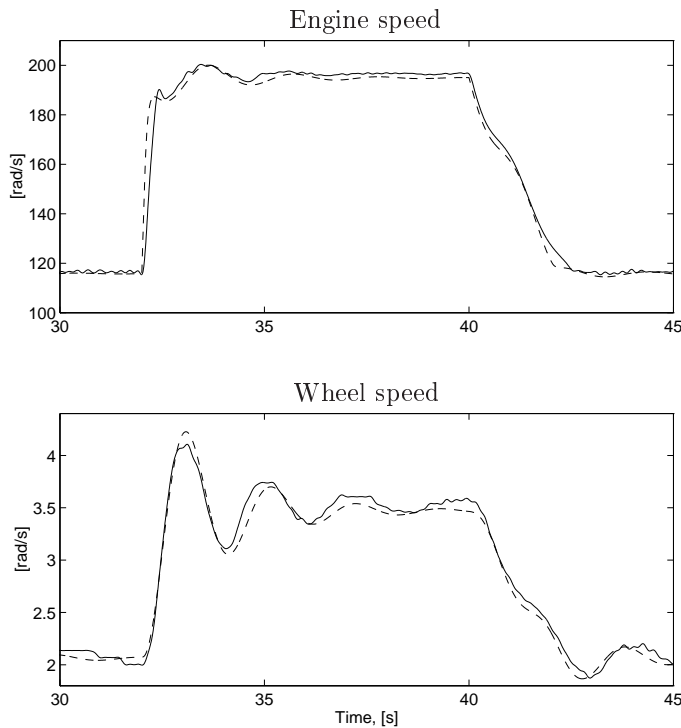


Figure 4.18 Measured step response from 1100 RPM to 1900 RPM at $t=32$ s, with an RQV controller for speed control in solid. Simulations with the same controller and the Drive-shaft model is shown in dashed lines. The Drive-shaft model captures the main resonance in the measured engine speed and wheel speed.

The assumption about sensor dynamics in the transmission speed influencing the experiments, agrees well with the fact that the engine speed sensor and the wheel speed sensor have considerably higher bandwidth (more cogs) than the transmission speed sensor.

When estimating the parameters of the Drive-shaft model, there is a problem when identifying the viscous friction components b_1 and b_2 . The sensitivity in the model to variations in the friction parameters is low, and the same model fit can be obtained for a range of friction parameters. However the sum $b_1 i^2 + b_2$ is constant during these tests. The problem with estimating viscous parameters will be further discussed in later design chapters.

4.4 Modeling the Driveline of the 124L Truck

The driveline of the 144L V8 truck has successfully been modeled in the previous section. The 124L truck has a 6 cylinder engine with a smaller engine inertia.

Furthermore, the fuel injection system is different, and there is no transmission node to access via the CAN-bus. This means that the modeling of the driveline is limited to models having the engine speed and the wheel speed as outputs. The Drive-shaft model considers these two outputs.

The parameters and the initial conditions of the model are estimated on data described in Chapter 3 in the same way as for the 144L truck in Section 4.3, and with similar results. Figure 4.18 shows validation of model structure and parameters in a closed-loop test. Field trials are performed with the 124L truck with an RQV fuel-injection controller (see Chapter 2) controlling the engine speed from 1100 RPM to 1900 RPM at $t = 32$ s. The same controller is used in simulations with the Drive-shaft model with parameters estimated for the 124L truck. There is good agreement between model outputs and experiments, which shows that the model captures the main resonance in the engine speed and the wheel speed, also for the unit-pump injection system.

4.5 Summary

Parameter estimation shows that a model with one torsional flexibility and two inertias is able to fit the measured engine speed and wheel speed in a frequency regime including the first main resonance of the driveline. This result is valid for both in-line and unit pump fuel-injection systems. By considering the difference between measured transmission speed and wheel speed it is reasonable to deduce that the main flexibility is the drive shafts.

In order for the model to also fit the measured transmission speed, a first order sensor filter is added to the model, in accordance with properties of the sensor system. It is shown that all three velocities are fitted accurately enough. Parameter estimation of a model with a nonlinear clutch explains that the difference between the measured data and the model outputs occurs when the clutch transfers zero torque.

Further supporting facts of the validity of the models are that they give values to the non-measured variables, drive shaft and clutch torsion, that agree with experience from other sources. Furthermore, the known road slopes are well estimated.

The result is a series of models that describe the driveline in increasing detail by, in each extension, adding the effect that seems to be the major cause for the deviation still left.

The result, from a user perspective, is that, within the frequency regime interesting for control design, the Drive-shaft model with some sensor dynamics gives good agreement with experiments. It is thus suitable for control design. The major deviations left are captured by the nonlinear effects in the Nonlinear clutch and drive-shaft model, which makes this model suitable for verifying simulation studies in control design.

Architectural Issues for Driveline Control

As seen in the previous chapters, there are significant torsional resonances in a driveline. Active control of these resonances is the topic of the rest of this thesis. Besides formulating the control problem in this chapter, there is one architectural issue that will be given special attention. There are different possible choices in driveline control between using different sensor locations, since the driveline normally is equipped with at least two sensors for rotational speed, but sometimes more. If the driveline was rigid, the choice of sensor would not matter, since the sensor outputs would differ only by a scaling factor. However, it will be demonstrated that the presence of torsional flexibilities implies that sensor choice gives different control problems. The difference can be formulated in control theoretic terms e.g. by saying that the poles are the same, but the zeros differ both in number and values. The issue of sensor location seems to be a little studied topic [11, 12], even though its relevance for control characteristics. This principle study should not be understood as a study on where to put a single sensor. Instead, it aims at an understanding of where to invest in increased sensor performance in future driveline management systems. This issue will also be investigated in later design chapters.

The driveline model equations in Chapter 4 are written in state-space form in Section 5.1. The formulation of performance output and controller structures used in the rest of the thesis is given in Section 5.2. Control of resonant systems with simple controllers is known to have structural properties e.g. with respect to sensor location [27], as mentioned before. In Section 5.3, these differences are illustrated for driveline models. In Section 5.4, forming the main contribution of this chapter, an investigation is made about how these properties transfer when

using more complicated controller structures like LQG/LTR. This part is based on the material in [21].

5.1 State-Space Formulation

The input to the open-loop driveline system is $u = M_m - M_{fr:m}$, i.e. the difference between the driving torque and the friction torque. Possible physical state variables in the models of Chapter 4 are torques, angle differences, and angle velocity of any inertia. In this work, the angle difference of each torsional flexibility and the angle velocity of each inertia are used as state variables, as already mentioned in Chapter 4. The state space representation is

$$\dot{x} = Ax + Bu + Hl \quad (5.1)$$

where A , B , H , x , and l are defined next for the Drive-shaft model and for the Clutch and drive-shaft model defined in Chapter 4.

State-space formulation of the linear Drive-shaft model:

$$\begin{aligned} x_1 &= \theta_m/i_t i_f - \theta_w \\ x_2 &= \dot{\theta}_m \\ x_3 &= \dot{\theta}_w \\ l &= r_w m (c_{r1} + g \sin(\alpha)) \end{aligned} \quad (5.2)$$

giving

$$A = \begin{pmatrix} 0 & 1/i & -1 \\ -k/iJ_1 & -(b_1 + c/i^2)/J_1 & c/iJ_1 \\ k/J_2 & c/iJ_2 & -(c + b_2)/J_2 \end{pmatrix}, \quad (5.3)$$

$$B = \begin{pmatrix} 0 \\ 1/J_1 \\ 0 \end{pmatrix}, \quad H = \begin{pmatrix} 0 \\ 0 \\ -1/J_2 \end{pmatrix} \quad (5.4)$$

where

$$\begin{aligned} i &= i_t i_f \\ J_1 &= J_m + J_t/i_t^2 + J_f/i_t^2 i_f^2 \\ J_2 &= J_w + m r_w^2 \\ b_1 &= b_t/i_t^2 + b_f/i_t^2 i_f^2 \\ b_2 &= b_w + m c_{r2} r_w^2 \end{aligned} \quad (5.5)$$

State-space formulation of the linear Clutch and drive-shaft model:

$$\begin{aligned} x_1 &= \theta_m - \theta_t i_t \\ x_2 &= \theta_t/i_f - \theta_w \end{aligned}$$

$$\begin{aligned}
x_3 &= \dot{\theta}_m \\
x_4 &= \dot{\theta}_t \\
x_5 &= \dot{\theta}_w
\end{aligned} \tag{5.6}$$

A is given by the matrix

$$\begin{pmatrix}
0 & 0 & 1 & -i_t & 0 \\
0 & 0 & 0 & 1/i_f & -1 \\
-k_c/J_1 & 0 & -c_c/J_1 & c_c i_t/J_1 & 0 \\
k_c i_t/J_2 & -k_d/i_f J_2 & c_c i_t/J_2 & -(c_c i_t^2 + b_2 + c_d/i_f^2)/J_2 & c_d/i_f J_2 \\
0 & k_d/J_3 & 0 & c_d/i_f J_3 & -(b_3 + c_d)/J_3
\end{pmatrix}$$

and

$$B = \begin{pmatrix} 0 \\ 0 \\ 1/J_1 \\ 0 \\ 0 \end{pmatrix}, \quad H = \begin{pmatrix} 0 \\ 0 \\ 0 \\ 0 \\ -1/J_2 \end{pmatrix} \tag{5.7}$$

where

$$\begin{aligned}
J_1 &= J_m \\
J_2 &= J_t + J_f/i_f^2 \\
J_2 &= J_w + mr_w^2 \\
b_2 &= b_t + b_f/i_f^2 \\
b_3 &= b_w + c_{r2}r_w
\end{aligned} \tag{5.8}$$

The model equipped with the sensor filter derived in (4.48) gives the true sensor outputs (y_m, y_t, y_w) , according to Chapter 4.

5.1.1 Disturbance Description

The influence from the road is assumed to be described by the slow-varying load l and an additive disturbance v . A second disturbance n is a disturbance acting on the input of the system. This disturbance is considered because the firing pulses in the driving torque can be seen as an additive disturbance acting on the input. The state-space description then becomes

$$\dot{x} = Ax + Bu + Bn + Hl + Hv \tag{5.9}$$

with x , A , B , H , and l defined in (5.2) to (5.5) or in (5.6) to (5.8), depending on model choice.

5.1.2 Measurement Description

For controller synthesis it is of fundamental interest which physical variables of the process that can be measured. In the case of a vehicular driveline the normal sensor

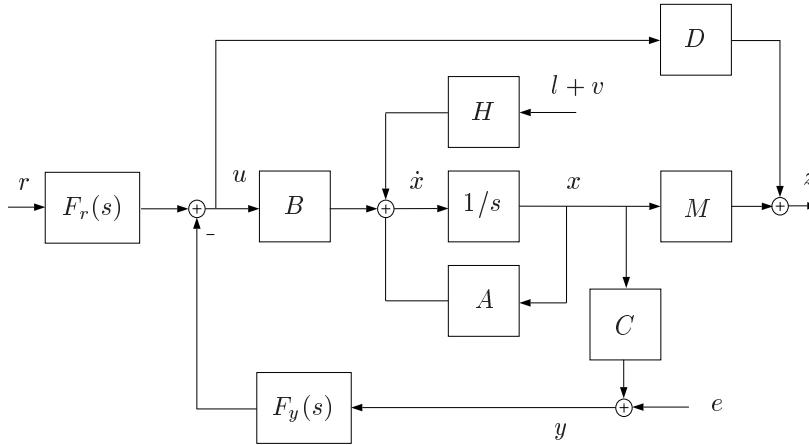


Figure 5.1 Plant and controllers F_r and F_y .

alternative is an inductive sensor mounted on a cogwheel measuring the angle, as mentioned before. Sensors that measure torque are expensive, and are seldom used in production vehicular applications.

The output of the process is defined as a combination of the states given by the matrix C in

$$y = Cx + e \quad (5.10)$$

where e is a measurement disturbance.

In this work, only angle velocity sensors are considered, and therefore, the output of the process is one/some of the state variables defining an angle velocity. Especially, the following C -matrices are defined (corresponding to a sensor on $\dot{\theta}_m$ and $\dot{\theta}_w$ for the Drive-shaft model).

$$C_m = (0 \ 1 \ 0) \quad (5.11)$$

$$C_w = (0 \ 0 \ 1) \quad (5.12)$$

5.2 Controller Formulation

The performance output z is the combination of states that has requirements to behave in a certain way. This combination is described by the matrices M and D in the following way

$$z = Mx + Du \quad (5.13)$$

The resulting control problem can be seen in Figure 5.1. The unknown controllers F_r and F_y are to be designed so that the performance output (5.13) meets its requirements (defined later).

If state-feedback controllers are used, the control signal u is a linear function of the states (if they are all measured) or else the state estimates, \hat{x} , which are obtained from a Kalman filter [14]. The control signal is described by

$$u = l_0 r - K_c \hat{x} \quad (5.14)$$

where r represents the commanded signal with the gain l_0 , and K_c is the state-feedback matrix. The equations describing the Kalman filter is

$$\dot{\hat{x}} = A\hat{x} + Bu + K_f(y - C\hat{x}) \quad (5.15)$$

where K_f is the Kalman gain.

Identifying the matrices $F_r(s)$ and $F_y(s)$ in Figure 5.1 gives

$$F_y(s) = K_c(sI - A + BK_c + K_f C)^{-1} K_f \quad (5.16)$$

$$F_r(s) = l_0 (1 - K_c(sI - A + BK_c + K_f C)^{-1} B)$$

The closed-loop transfer functions from r , v , and e to the control signal u are given by

$$G_{ru} = (I - K_c(sI - A + BK_c)^{-1} B) l_0 r \quad (5.17)$$

$$G_{vu} = K_c(sI - A + K_f C)^{-1} N - K_c(sI - A + BK_c)^{-1} N - K_c(sI - A + BK_c)^{-1} BK_c(sI - A + K_f C)^{-1} N \quad (5.18)$$

$$G_{eu} = K_c((sI - A + BK_c)^{-1} BK_c - I)(sI - A + K_f C)^{-1} K_f \quad (5.19)$$

The transfer functions to the performance output z are given by

$$G_{rz} = (M(sI - A)^{-1} B + D) G_{ru} \quad (5.20)$$

$$G_{vz} = M(sI - A + BK_c)^{-1} BK_c(sI - A + K_f C)^{-1} N + M(sI - A + BK_c)^{-1} N + D G_{vu} \quad (5.21)$$

$$G_{ez} = (M(sI - A)^{-1} B + D) G_{vu} \quad (5.22)$$

Two return ratios (loop gains) result, which characterize the closed-loop behavior at the plant output and input respectively

$$G F_y = C(sI - A)^{-1} B F_y \quad (5.23)$$

$$F_y G = F_y C(sI - A)^{-1} B \quad (5.24)$$

When only one sensor is used, these return ratios are scalar and thus equal.

LQG/LTR is not directly applicable to driveline control with more than one sensor as input to the observer. This is because there are unequal number of sensors and control signals. This gives further motivation for the type of investigation about sensor location made in this chapter, before extending to more sensors.

5.3 Some Feedback Properties

The performance output when controlling the driveline to a certain speed is the velocity of the wheel, defined as

$$z = \dot{\theta}_w = C_w x \quad (5.25)$$

When studying the closed-loop control problem with a sensor on $\dot{\theta}_m$ or $\dot{\theta}_w$, two different control problems result. Figure 5.2 shows a root locus with respect to a P-controller gain for two gears using velocity sensor $\dot{\theta}_m$ and $\dot{\theta}_w$ respectively. The open-loop transfer functions from control signal to engine speed G_{um} has three poles and two zeros, as can be seen in Figure 5.2. G_{uw} on the other hand has one zero and the same poles. Hence, the relative degree [10] of G_{um} is one and G_{uw} has a relative degree of two. This means that when $\dot{\theta}_w$ -feedback is used, and the gain is increased, two poles must go to infinity which makes the system unstable. When the velocity sensor $\dot{\theta}_m$ is used, the relative degree is one, and the closed-loop system is stable for all gains. (Remember that $\dot{\theta}_w$ is the performance output and thus desirable to use.)

The same effect can be seen in step response tests when the P-controller is used. Figure 5.3 demonstrates the problem with resonances that occur with increasing gain for the two cases of feedback. When the engine-speed sensor is used, the engine speed is well damped when the gain is increased, but the resonance in the drive shaft makes the wheel speed oscillate. When using $\dot{\theta}_w$ -feedback it is difficult to increase the bandwidth, since the poles moves closer to the imaginary axis, and give a resonant system.

The characteristic results in Figures 5.2 and 5.3 only depend on the relative degree, and are thus parameter independent. However, this observation may depend on feedback structure, and therefore a more detailed analysis is performed in the following section.

5.4 Driveline Control with LQG/LTR

Different sensor locations result in different control problems with different inherent characteristics, as illustrated in the previous section. The topic of this section is to show how this influences control design when using LQG/LTR with design of the return ratio at the output of the plant [14]. The design in the rest of this thesis will be with the dual method with design of the return ratio at the plant input. The reason for using LQG/LTR, in this principle study, is that it offers a control design method resulting in a controller and observer of the same order as the plant model, and it is also an easy method for obtaining robust controllers.

5.4.1 Transfer Functions

When comparing the control problem of using $\dot{\theta}_m$ or $\dot{\theta}_w$ as sensor, the open-loop transfer functions G_{um} and G_{uw} results. These have the same number of poles but

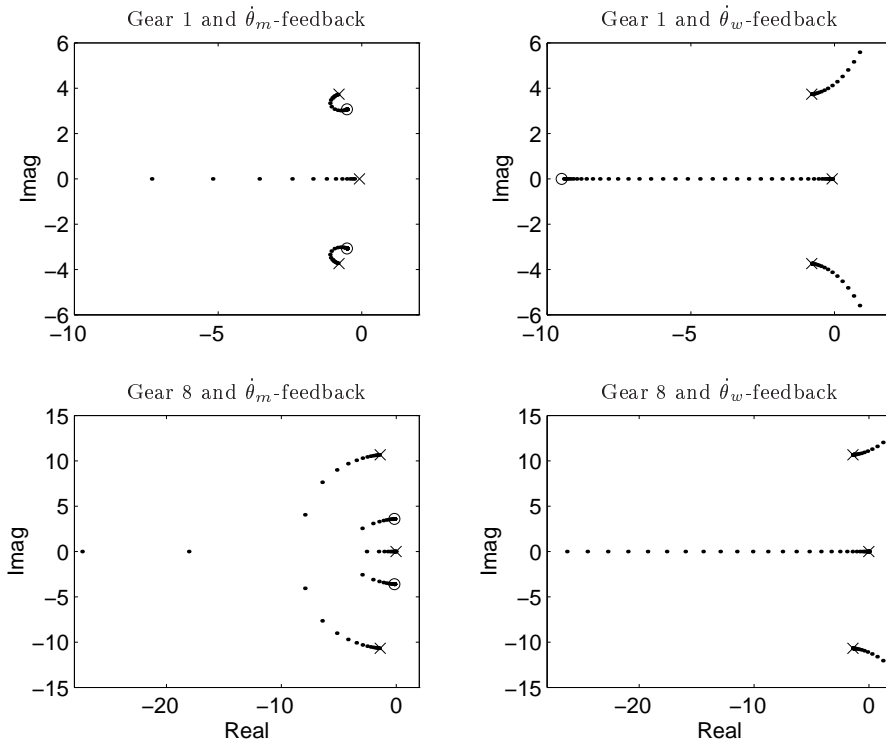


Figure 5.2 Root locus with respect to a P -controller gain, for gear 1 (top figures) and gear 8 (bottom figures), with sensor on $\dot{\theta}_m$ (left figures), or $\dot{\theta}_w$ (right figures). The cross represent the open-loop poles, while the rings represent the open-loop zeros. The system goes unstable when the $\dot{\theta}_w$ -gain is increased, but is stable for all $\dot{\theta}_m$ -gains.

different number of zeros, as mentioned before. Two different closed-loop systems are obtained depending on which sensor that is being used.

Feedback from $\dot{\theta}_w$

A natural feedback configuration is to use the performance output, $\dot{\theta}_w$. Then among others the following transfer functions result

$$G_{rz} = \frac{G_{uw}F_yF_r}{1 + G_{uw}F_y} = T_wF_r \quad (5.26)$$

$$G_{nu} = \frac{1}{1 + G_{uw}F_y} = S_w \quad (5.27)$$

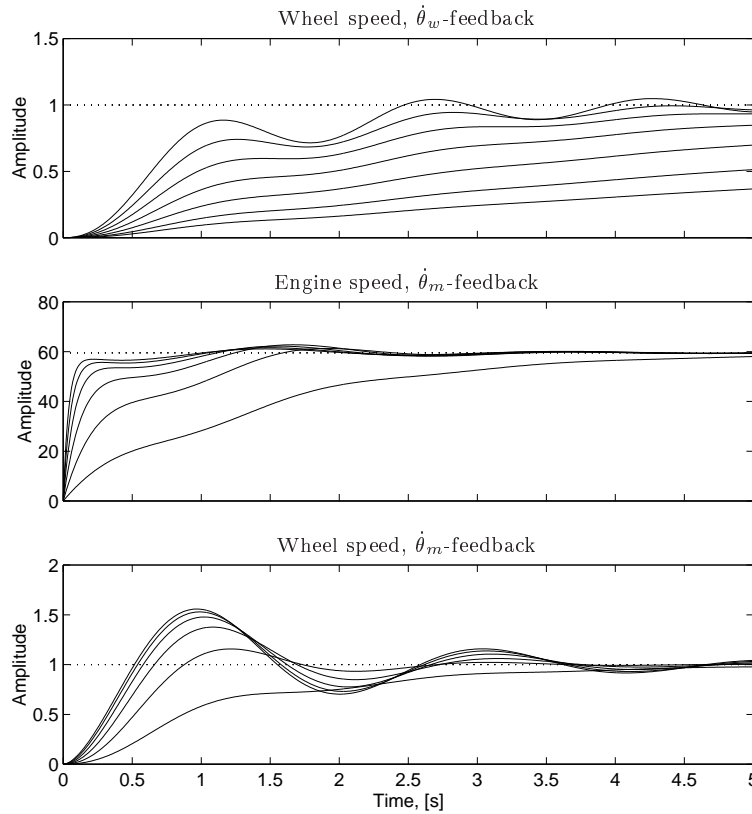


Figure 5.3 Step responses when using a P -controller with different gains on the Drive-shaft model with gear 1. With $\dot{\theta}_w$ -feedback (top figure), increased gain results in instability. With $\dot{\theta}_m$ -feedback (bottom figures), increased gain results in a well damped engine speed, but an oscillating wheel speed.

where (5.17) to (5.22) are used together with the matrix inversion lemma [10], and n is the input disturbance. The transfer functions S_w and T_w are the *sensitivity* function and the *complementary sensitivity* function [14]. The relation between these transfer function is, as usual,

$$S_w + T_w = 1 \quad (5.28)$$

Feedback from $\dot{\theta}_m$

The following transfer functions result if the $\dot{\theta}_m$ -sensor is used.

$$G_{rz} = \frac{G_{uw}F_yF_r}{1 + G_{um}F_y} \quad (5.29)$$

$$G_{nu} = \frac{1}{1 + G_{um}F_y} \quad (5.30)$$

The difference between the two feedback configurations is that the return difference is $1 + G_{uw}F_y$ or $1 + G_{um}F_y$.

It is desirable to have sensitivity functions that corresponds to $y = \dot{\theta}_m$ and $z = \dot{\theta}_w$. The following transfer functions are defined

$$S_m = \frac{1}{1 + G_{um}F_y}, \quad T_m = \frac{G_{um}F_y}{1 + G_{um}F_y} \quad (5.31)$$

These transfer functions correspond to a configuration where $\dot{\theta}_m$ is the output (i.e. $y = z = \dot{\theta}_m$). Using (5.29) it is natural to define \bar{T}_m by

$$\bar{T}_m = \frac{G_{uw}F_y}{1 + G_{um}F_y} = T_m \frac{G_{uw}}{G_{um}} \quad (5.32)$$

The functions S_m and \bar{T}_m describe the design problem when feedback from θ_m is used.

When combining (5.31) and (5.32), the corresponding relation to (5.28) is

$$S_m + \bar{T}_m \frac{G_{um}}{G_{uw}} = 1 \quad (5.33)$$

If S_m is made zero for some frequencies in (5.33), then \bar{T}_m will not be equal to one, as in (5.28). Instead, $\bar{T}_m = G_{uw}/G_{um}$ for these frequency domains.

Limitations on Performance

The relations (5.28) and (5.33) will be the fundamental relations for discussing design considerations. The impact of the ratio G_{uw}/G_{um} will be analyzed in the following sections.

Definition 5.1 \bar{T}_m in (5.32) is the modified complementary sensitivity function, and $G_{w/m} = G_{uw}/G_{um}$ is the dynamic output ratio.

5.4.2 Design Example with a Simple Mass-Spring Model

Linear Quadratic Design with Loop-Transfer Recovery will be treated in four cases, being combinations of two sensor locations, $\dot{\theta}_m$ or $\dot{\theta}_w$, and two models with the same structure, but with different parameters. Design without pre-filter ($F_r = 1$) is considered.

The section covers a general plant with n inertias connected by $k - 1$ torsional flexibilities, without damping and load, and with unit conversion ratio. There are $(2n - 1)$ poles, and the location of the poles is the same for the different sensor locations. The number of zeros depends on which sensor that is used, and when using $\dot{\theta}_w$ there are no zeros. When using feedback from $\dot{\theta}_m$ there are $(2n - 2)$ zeros. Thus, the transfer functions G_{um} and G_{uw} , have the same denominators, and a relative degree of 1 and $(2n - 1)$ respectively.

Structural Properties of Sensor Location

The controller (5.16) has a relative degree of one. The relative degree of $G_{um}F_y$ is thus 2, and the relative degree of $G_{uw}F_y$ is $2n$. When considering design, a good alternative is to have relative degree one in GF_y , implying infinite gain margin and high phase margin.

When using $G_{um}F_y$, one pole has to be moved to infinity, and when using $G_{uw}F_y$, $2n - 1$ poles have to be moved to infinity, in order for the ratio to resemble a first order system at high frequencies.

When the return ratio behaves like a first order system, also the closed-loop transfer function behaves like a first order system. This conflicts with the design goal of having a steep roll-off rate for the closed-loop system in order to attenuate measurement noise. Hence, there is a trade-off when using $\dot{\theta}_w$ -feedback.

When using $\dot{\theta}_m$ -feedback, there is no trade-off, since the relative degree of G_{um} is one.

Structure of $G_{w/m}$

We have in the previous simple examples seen that the relative degree and the zeros are important. The dynamic output ratio contains exactly this information and nothing else.

For low frequencies the dynamic output ratio has gain equal to one,

$$|G_{w/m}(0)| = 1$$

(if the conversion ratio is equal to one). Furthermore, $G_{w/m}$ has a relative degree of $2n - 2$ and thus, a high frequency gain roll-off rate of $20(2n - 2)$ dB/decade. Hence, the dynamic output ratio gives the closed-loop transfer function \bar{T}_m a high frequency gain roll-off rate of $q_m + 20(2n - 2)$ dB/decade, where q_m is the roll-off rate of $G_{um}F_y$. When using $\dot{\theta}_w$ -feedback, T_w will have the same roll-off rate as $G_{uw}F_y$.

Parametric properties of $G_{w/m}$

Typical parametric properties of $G_{w/m}$ can be seen in the following example.

Example 5.1 Two different plants of the form (5.2) to (5.5) are considered with the following values:

a) $J_1 = 0.0974$, $J_2 = 0.0280$, $k = 2.80$, $c = 0$, $b_1 = 0.0244$, $b_2 = 0.566$, $l = 0$.

b) $J_1 = 0.0974$, $J_2 = 0.220$, $k = 5.50$, $c = 0$, $b_1 = 1.70$, $b_2 = 0.660$, $l = 0$.

with labels according to the state-space formulation in Section 5.1. The shape of $G_{w/m}$ can be seen in Figure 5.4. The rest of the chapter will focus on control design of these two plant models.

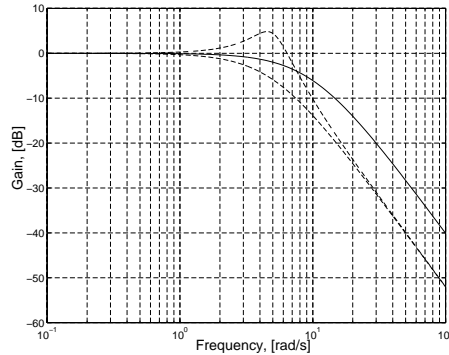


Figure 5.4 Dynamic output ratio $G_{w/m}$ for Example 5.1a (solid line) and Example 5.1b (dashed line).

LQG Designs

Integral action is included by augmenting the state to attenuate step disturbances in v [14]. The state-space realization A_a , B_a , M_a , C_{wa} , and C_{ma} results. The Kalman-filter gain, K_f , is derived by solving the Riccati equation [14]

$$P_f A^T + A P_f - P_f C^T V^{-1} C P_f + B W B^T = 0 \quad (5.34)$$

The covariances W and V , for disturbances v and e respectively, are adjusted until the return ratio

$$C(sI - A)^{-1} K_f, \quad K_f = P_f C^T V^{-1} \quad (5.35)$$

and the closed-loop transfer functions S and T show satisfactory performance. The Nyquist locus remains outside the unit circle centered at -1 . This means that there is infinite gain margin, and a phase margin of at least 60° . Furthermore, the relative degree is one, and $|S| \leq 1$.

Design for $\dot{\theta}_w$ -feedback. W is adjusted (and thus $F_y(s)$) such that S_w and T_w show satisfactory performance, and that the desired bandwidth is obtained. The design of the driveline models in Example 5.1 is shown in Figure 5.5. Note that the roll-off rate of T_w is 20 dB/decade.

Design for $\dot{\theta}_m$ -feedback. W is adjusted (and thus $F_y(s)$) so that S_m and T_m (and thus $\dot{\theta}_m$) show satisfactory performance. Depending on the shape of $G_{w/m}$ for middle high frequencies, corrections in W must be taken so that \bar{T}_m achieves the desired bandwidth. If there is a resonance peak in $G_{w/m}$, the bandwidth in \bar{T}_m is chosen such that the peak is suppressed. Figure 5.5 shows such an example (the plant in Example 5.1b with $\dot{\theta}_m$ -feedback), where the bandwidth is lower in order to suppress the peak in $G_{w/m}$. Note also the difference between S_w and S_m .

The parameters of the dynamic output ratio are thus important in the LQG step of the design.

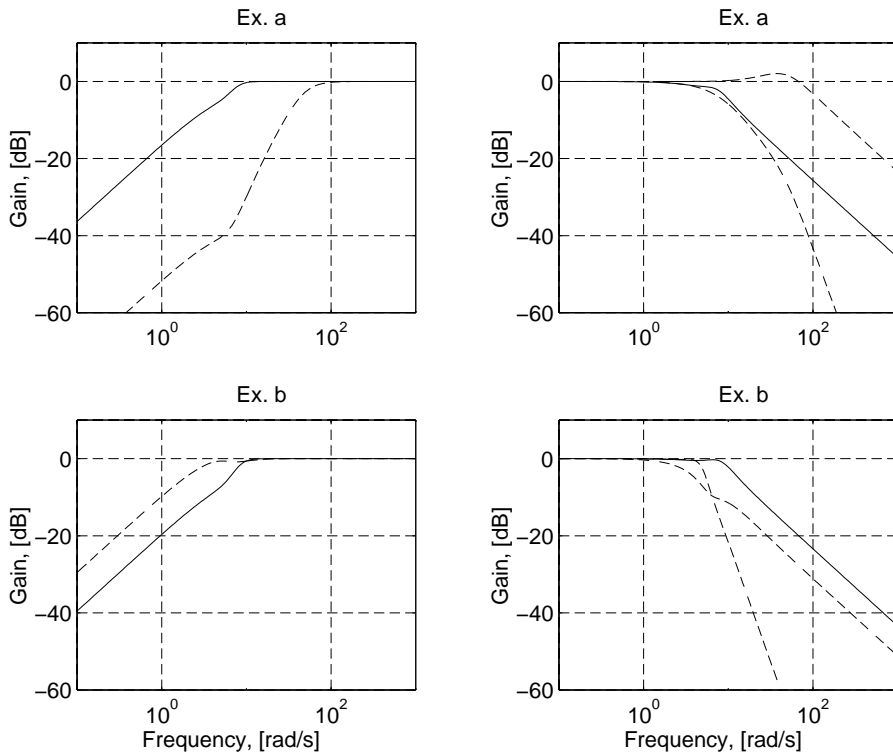


Figure 5.5 Closed-loop transfer functions S (left figures), and T (right figures). Feedback from $\dot{\theta}_w$ is seen in solid lines, and feedback from $\dot{\theta}_m$ in dashed lines. \bar{T}_m is seen in the right figures in dash-dotted lines. For the $\dot{\theta}_m$ -design, $W = 5 \cdot 10^4$ (Ex. 5.1a) and $W = 50$ (Ex. 5.1b) are used, and for the $\dot{\theta}_w$ -design, $W = 15$ (Ex. 5.1a) and $W = 5 \cdot 10^2$ (Ex. 5.1b) are used.

Loop-Transfer Recovery, LTR

The next step in the design process is to include K_c , and recover the satisfactory return ratio obtain previously. When using the combined state feedback and Kalman filter, the return ratio is $GF_y = C(sI - A)^{-1}BK_c(sI - A + BK_c + K_fC)^{-1}K_f$. A simplistic LTR can be obtained by using $K_c = \rho C$ and increasing ρ . As ρ is increased, $2n - 1$ poles move towards the open system zeros. The remaining poles move towards infinity (compare to Section 5.1). If the Riccati equation

$$A^T P_c + P_c A - P_c B R^{-1} B^T P_c + C^T Q C = 0 \quad (5.36)$$

is solved with $Q = \rho$, and $R = 1$, $K_c = \sqrt{\rho}C$ is obtained in the limit, and to guarantee stability, this K_c is used for recovery.

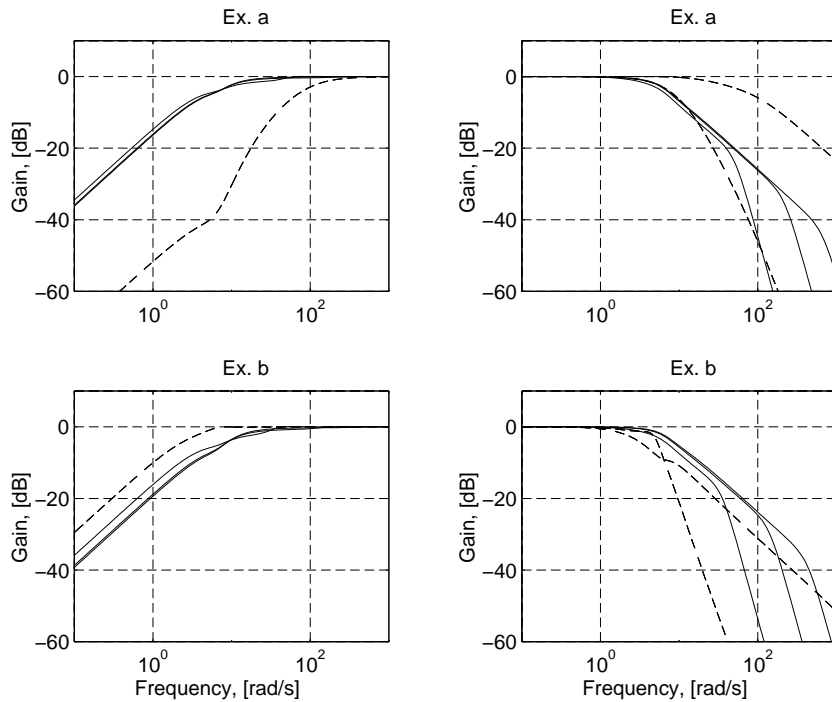


Figure 5.6 Closed-loop transfer functions S (left figures), and T (right figures) after recovery. Feedback from $\dot{\theta}_w$ is seen in solid lines, and feedback from $\dot{\theta}_m$ in dashed lines. \bar{T}_m is seen in the right figures in dash-dotted lines. For the $\dot{\theta}_m$ -design, $\rho = 10^6$ (Ex. 5.1a) and $\rho = 10^5$ (Ex. 5.1b) are used, and for the $\dot{\theta}_w$ -design, $\rho = 10^4$, 10^8 , and 10^{11} are used in both Ex. 5.1a and b.

Figure 5.6 shows the recovered closed-loop transfer functions for Example 5.1. Nyquist locus and control signal transfer function, $G_{ru} = F_y / (1 + G_{uw} F_y)$, are shown in Figure 5.7.

Recovery for $\dot{\theta}_w$ -feedback. There is a trade-off when choosing an appropriate ρ . A low ρ gives good attenuation of measurement noise and a low control signal, but in order to have good stability margins, a high ρ must be chosen. This gives an increased control signal, and a 20 dB/decade roll-off rate in T_w for a wider frequency range.

Recovery for $\dot{\theta}_m$ -feedback. There is no trade-off when choosing ρ . It is possible to achieve good recovery with reasonable stability margins and control signal, together with a steep roll-off rate.

The structural properties, i.e. the relative degrees are thus dominant in determining the LTR step of the design.

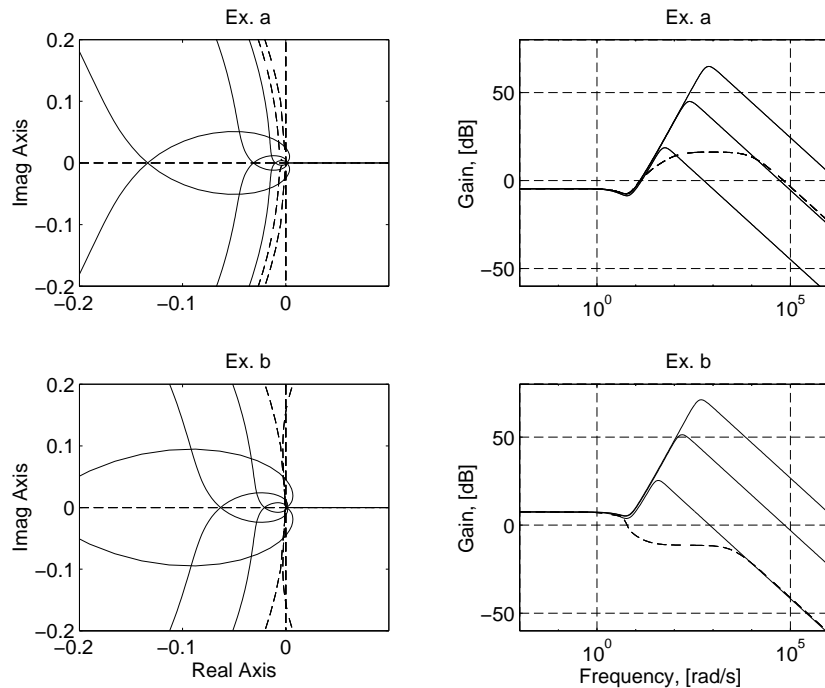


Figure 5.7 Nyquist plot of return ratio (left figures) and control signal transfer function $F_y/(1 + G_{uw}F_y)$ (right figures). Feedback from $\dot{\theta}_w$ is seen in solid lines, and feedback from $\dot{\theta}_m$ in dashed lines. For the $\dot{\theta}_m$ -design, $\rho = 10^6$ (Ex. 5.1a) and $\rho = 10^5$ (Ex. 5.1b) are used, and for the $\dot{\theta}_w$ -design, $\rho = 10^4$, 10^8 , and 10^{11} are used in both Ex. 5.1a and b. A dash-dotted circle with radius one, centered at -1, is also shown in the Nyquist plots.

5.5 Summary

Control and damping of torsional oscillations in vehicular drivelines are important problems. Different sensor locations give different transfer functions, G_{um} or G_{uw} . These functions have the same poles, but have different relative degrees and different zeros. The *dynamic output ratio*, $G_{w/m}$, exactly captures these differences and nothing else. The problem that the performance output signal is not the same as the measured output signal is handled by introducing a *modified complementary sensitivity* function, being modified with $G_{w/m}$. Both structural and parameter dependent aspects of sensor location have been characterized. In LQG/LTR, parameter dependent properties dominate in the LQG step of the design, whereas structural properties, i.e. sensor location, dominate in the LTR step.

6

Speed Controller Design and Simulations

The background and problems with traditional diesel engine speed control (RQV) were covered in Chapter 2. Speed control is here defined as the extension of RQV control with engine controlled active damping of driveline resonances. Active damping is obtained by using a feedback law that calculates the fuel amount so that the engine inertia works in the opposite direction of the oscillations, at the same time as the desired speed is obtained. The calculated fuel amount is a function of the engine speed, the wheel speed, and the drive-shaft torsion, which are states of the Drive-shaft model, derived in Chapter 4. These variables are estimated by a Kalman filter with either the engine speed or the wheel speed as input. The feedback law is designed by deriving a criterion in which the control problem is given mathematical formulation.

Two different observer problems result depending on if the engine speed or the wheel speed is used as input to the observer. The difference in disturbance rejection between the two sensor locations will be demonstrated. The RQV control scheme gives a specific character to the driving feeling e.g. when going uphill and downhill. This driving character is important to maintain when extending RQV control with active damping. Traditional RQV control is further explained in Section 6.1. Thereafter, the speed control problem keeping RQV characteristics is formulated in Section 6.2. The problem formulation is then studied in the following sections using available computationally powerful methods like LQG/LTR. Finally, the design based on the Drive-shaft model is simulated together with the more complicated Nonlinear clutch and drive-shaft model as vehicle model. Some important disturbances are simulated that are difficult to generate in systematic ways in real experiments.

6.1 RQV Control

RQV control is the traditional diesel engine control scheme covered in Chapter 2. The controller is essentially a proportional controller with the accelerator as reference value and a sensor measuring the engine speed. The RQV controller has no information about the load, and a nonzero load, e.g. when going uphill or downhill, gives a stationary error. The RQV controller is described by

$$u = u_0 + K_p(ri - \dot{\theta}_m) \quad (6.1)$$

where $i = i_{ti_f}$ is the conversion ratio of the driveline, K_p is the controller gain, and r is the reference velocity. The constant u_0 is a function of the speed, but not the load since this is not known. The problem with vehicle shuffle when increasing the controller gain, in order to increase the bandwidth, is demonstrated in the following example.

Example 6.1 Consider the 144L truck modeled in Chapters 4 traveling at a speed of 2 rad/s (3.6 km/h) with gear 1 and a total load of 3000 Nm ($\approx 2\%$ road slope). Let the new desired velocity be $r = 2.3$ rad/s. Figure 6.1 shows the RQV control law (6.1) applied to the Drive-shaft model with three gains, K_p . In the plots, u_0 from (6.1) is calculated so that the stationary level is the same for the three gains. (Otherwise there would be a gain dependent stationary error.)

When the controller gain is increased, the rise time decreases and the overshoot in the wheel speed increases. Hence, there is a trade-off between short rise time and little overshoot. The engine speed is well damped, but the flexibility of the driveline causes the wheel speed to oscillate with higher amplitude the more the gain is increased.

The same behavior is seen in Figure 6.2, which shows the transfer functions from load and measurement disturbances, v and e , to the performance output, when the RQV controller is used. The value of the resonance peak in the transfer functions increases when the controller gain is increased.

6.2 Problem Formulation

The goals of the speed control concept were outlined in Chapter 2. These are here given a mathematical formulation, which is solved for a controller using established techniques and software.

The performance output for the speed controller is the wheel speed, $z = \dot{\theta}_w$, as defined in Chapter 5, since the wheel speed rather than the engine speed determines vehicle behavior. Figure 6.3 shows the transfer functions from control signal (u) and load (l) to the wheel speed (z) for both the Drive-shaft model and the Clutch and drive-shaft model. The Clutch and drive-shaft model adds a second resonance peak originating from the clutch. Furthermore, the high frequency roll-off rate is steeper for the Clutch and drive-shaft model than for the Drive-shaft model. Note that the transfer function from the load to the performance output is the same for the two

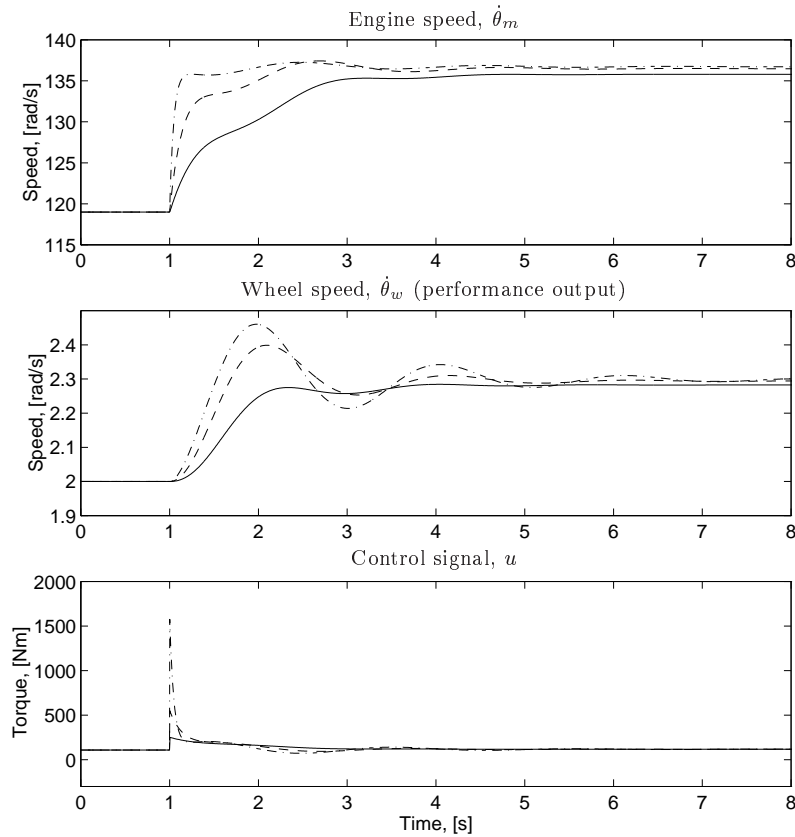


Figure 6.1 Response of step in accelerator position at $t=1$ s, with RQV control (6.1) controlling the Drive-shaft model. Controller gains $K_p=8$, $K_p=25$, and $K_p=85$ are shown in solid, dashed, and dash-dotted lines respectively. Increased gain results in a well damped engine speed and an oscillating wheel speed.

models. This chapter deals with the development of a controller based on the Drive-shaft model, neglecting the influence from the clutch for higher frequencies.

A first possible attempt for speed control is a scheme of applying the engine torque to the driveline such that the following cost function is minimized

$$\lim_{T \rightarrow \infty} \int_0^T (z - r)^2 \quad (6.2)$$

where r is the reference velocity given by the driver. The cost function (6.2) can be made arbitrarily small if there are no restrictions on the control signal u , since the plant model is linear. However, a diesel engine can only produce torque in a certain range, and therefore, (6.2) is extended such that a large control signal is penalized in the cost function.

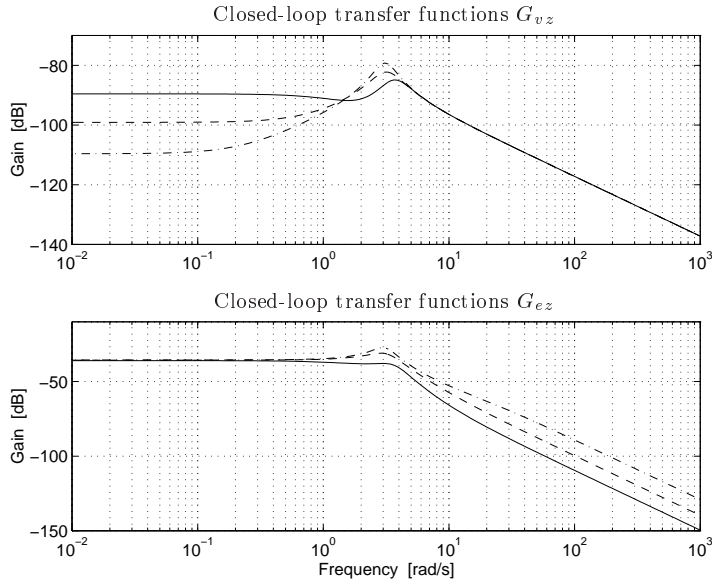


Figure 6.2 Closed-loop transfer functions G_{vz} and G_{ez} when using the RQV control law (6.1) for the controller gains $K_p=8$ (solid), $K_p=25$ (dashed), and $K_p=85$ (dash-dotted). The resonance peaks increase with increasing gain.

The stationary point $z = r$ is reached if a stationary control signal, u_0 , is used. This torque is a function of the reference value, r , and the load, l . For a given wheel speed, $\dot{\theta}_w$, and load, the driveline has the following stationary point

$$x_0(\dot{\theta}_w, l) = \begin{pmatrix} b_2/k & 1/k \\ i & 0 \\ 1 & 0 \end{pmatrix} \begin{pmatrix} \dot{\theta}_w \\ l \end{pmatrix} = \delta_x \dot{\theta}_w + \delta_l l \quad (6.3)$$

$$u_0(\dot{\theta}_w, l) = \begin{pmatrix} (b_1 i^2 + b_2)/i & 1/i \end{pmatrix} \begin{pmatrix} \dot{\theta}_w \\ l \end{pmatrix} = \lambda_x \dot{\theta}_w + \lambda_l l \quad (6.4)$$

The stationary point is obtained by solving

$$Ax + Bu + Hl = 0 \quad (6.5)$$

for x and u , where A , B , and H are given by (5.2) to (5.5).

The cost function is modified by using (6.3) and (6.4), such that a control signal that deviates from the stationary value $u_0(r, l)$ adds to the cost function. The extended cost function is given by

$$\lim_{T \rightarrow \infty} \int_0^T (z - r)^2 + \eta(u - u_0(r, l))^2 \quad (6.6)$$

where η is used to control the trade-off between short rise time and control signal amplitude.

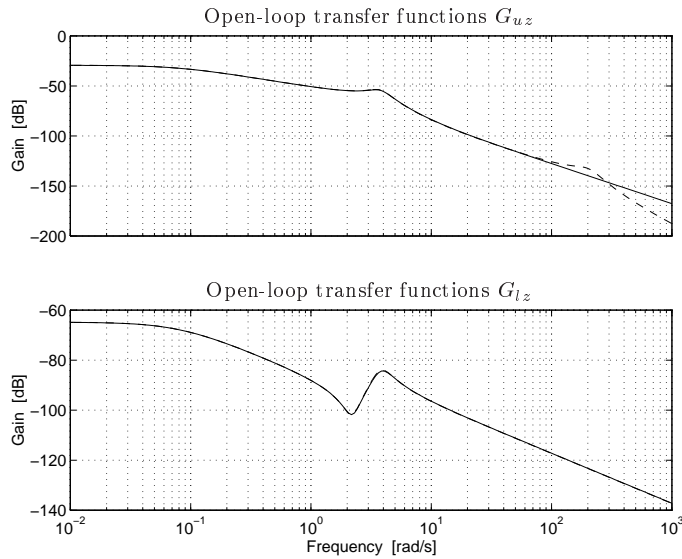


Figure 6.3 Transfer functions from control signal, u , and load, l , to performance output, z . The Drive-shaft model is shown in solid and the Clutch and drive-shaft model is shown in dashed. The modeled clutch gives a second resonance peak and a steeper roll-off rate.

The controller that minimizes (6.6), called the speed controller, has no stationary error, since the load, l , is included and thus compensated for. However, it is desirable that the stationary error characteristic for the RQV controller is maintained in the speed controller, as mentioned before. A stationary error comparable with that of the RQV controller can be achieved by using only a part of the load in the criterion (6.6), as will be demonstrated in Section 6.3.1.

6.3 Speed Control with Active Damping and RQV Behavior

The problem formulation (6.6) will be treated in two steps. First without RQV behavior i.e. using the complete load in the criterion, and then extending to RQV behavior. The problem formulation (6.6) is in this section solved with LQG technique. This is done by linearizing the driveline model and rewriting (6.6) in terms of the linearized variables. A state-feedback matrix is derived that minimizes (6.6) by solving a Riccati equation. The derived feedback law is a function of η which is chosen such that high bandwidth together with a feasible control signal is obtained.

The model (5.1)

$$\dot{x} = Ax + Bu + Hl \quad (6.7)$$

is affine since it includes a constant term, l . The model is linearized in the neighborhood of the stationary point (x_0, u_0) . The linear model is described by

$$\Delta \dot{x} = A\Delta x + B\Delta u \quad (6.8)$$

where

$$\begin{aligned} \Delta x &= x - x_0 \\ \Delta u &= u - u_0 \\ x_0 &= x_0(x_{30}, l) \\ u_0 &= u_0(x_{30}, l) \end{aligned} \quad (6.9)$$

where the stationary point (x_0, u_0) is given by (6.3) and (6.4) (x_{30} is the initial value of x_3). Note that the linear model is the same for all stationary points.

The problem is to devise a feedback control law that minimizes the cost function (6.6). The cost function is expressed in terms of Δx and Δu by using (6.9)

$$\lim_{T \rightarrow \infty} \int_0^T (M(x_0 + \Delta x) - r)^2 + \eta(u_0 + \Delta u - u_0(r, l))^2 \quad (6.10)$$

$$= \lim_{T \rightarrow \infty} \int_0^T (M\Delta x + r_1)^2 + \eta(\Delta u + r_2)^2 \quad (6.11)$$

with

$$r_1 = Mx_0 - r \quad (6.12)$$

$$r_2 = u_0 - u_0(r, l)$$

In order to minimize (6.10) a Riccati equation is used. Then the constants r_1 and r_2 must be expressed in terms of state variables. This can be done by augmenting the plant model (A, B) with models of the constants r_1 and r_2 . Since these models will not be controllable, they must be stable in order to solve the Riccati equation [14]. Therefore the model $\dot{r}_1 = \dot{r}_2 = 0$ is not used because the poles are located on the imaginary axis. Instead the following models are used

$$\dot{r}_1 = -\sigma r_1 \quad (6.13)$$

$$\dot{r}_2 = -\sigma r_2 \quad (6.14)$$

which with a low σ indicates that r is a slow-varying constant.

The augmented model is given by

$$A_r = \begin{pmatrix} & & 0 & 0 \\ & A & 0 & 0 \\ & & 0 & 0 \\ 0 & 0 & 0 & -\sigma & 0 \\ 0 & 0 & 0 & 0 & -\sigma \end{pmatrix}, \quad (6.15)$$

$$B_r = \begin{pmatrix} B \\ 0 \\ 0 \end{pmatrix}, \quad x_r = (\Delta x^T \ r_1 \ r_2)^T \quad (6.16)$$

By using these equations, the cost function (6.10) can be written in the form

$$\lim_{T \rightarrow \infty} \int_0^T x_r^T Q x_r + R \Delta u^2 + 2x_r^T N \Delta u \quad (6.17)$$

with

$$\begin{aligned} Q &= (M \ 1 \ 0)^T (M \ 1 \ 0) + \eta (0 \ 0 \ 0 \ 0 \ 1)^T (0 \ 0 \ 0 \ 0 \ 1) \\ N &= \eta (0 \ 0 \ 0 \ 0 \ 1)^T \\ R &= \eta \end{aligned} \quad (6.18)$$

The cost function (6.10) is minimized by using

$$\Delta u = -K_c x_r \quad (6.19)$$

with

$$K_c = Q^{-1} (B_r^T P_c + N^T) \quad (6.20)$$

where P_c is the stabilizing solution to the Riccati equation

$$A_r^T P_c + P_c A_r + R - (P_c B_r + N) Q^{-1} (P_c B_r + N)^T = 0 \quad (6.21)$$

The control law (6.19) becomes

$$\Delta u = -K_c x_r = - \begin{pmatrix} K_{c1} & K_{c2} & K_{c3} \end{pmatrix} \Delta x - K_{c4} r_1 - K_{c5} r_2 \quad (6.22)$$

By using (6.9) and (6.12) the control law for the speed controller is written as

$$u = K_0 x_{30} + K_l l + K_r r - \begin{pmatrix} K_{c1} & K_{c2} & K_{c3} \end{pmatrix} x \quad (6.23)$$

with

$$\begin{aligned} K_0 &= \begin{pmatrix} K_{c1} & K_{c2} & K_{c3} \end{pmatrix} \delta_x - K_{c4} M \delta_x + \lambda_x - K_{c5} \lambda_x \\ K_r &= K_{c4} + K_{c5} \lambda_x \\ K_l &= \begin{pmatrix} K_{c1} & K_{c2} & K_{c3} \end{pmatrix} \delta_l - K_{c4} M \delta_l + \lambda_l \end{aligned} \quad (6.24)$$

where δ_x , δ_l , λ_x , and λ_l are described in (6.3) and (6.4).

When this control law is applied to Example 6.1 the controller gain becomes

$$u = 0.230 x_{30} + 4470 r + 0.125 l - \begin{pmatrix} 7620 & 0.0347 & 2.36 \end{pmatrix} x \quad (6.25)$$

where $\eta = 5 \cdot 10^{-8}$ and $\sigma = 0.0001$ are used. With this controller the phase margin is guaranteed to be at least 60° with infinite amplitude margin [14]. A step-response simulation with the speed controller (6.25) is shown in Figure 6.4.

The rise time of the speed controller is shorter than for the RQV controller. Also the overshoot is less when using speed control. The driving torque is controlled such that the oscillations in the wheel speed are actively damped. This means that the controller applies the engine torque in a way that the engine inertia works in the opposite direction of the oscillation. Then the engine speed oscillates, but the important wheel speed is well behaved as seen in Figure 6.4.

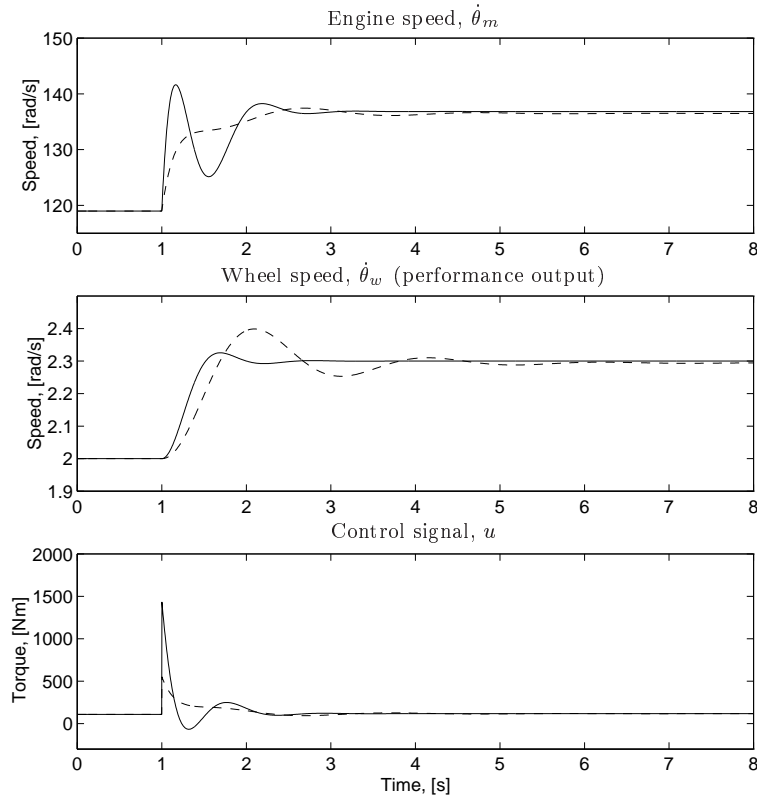


Figure 6.4 Response of step in accelerator position at $t=1$ s. The Drive-shaft model is controlled with the speed control law (6.25) in solid lines. RQV control (6.1) with $K_p=25$ is seen in dashed lines. With active damping, the engine speed oscillates, resulting in a well damped wheel speed.

6.3.1 Extending with RQV Behavior

The RQV controller has no information about the load, l , and therefore a stationary error will be present when the load is different from zero. The speed controller (6.23) is a function of the load, and the stationary error is zero if the load is estimated and compensated for. There is however a demand from the driver that the load should give a stationary error, and only when using a cruise controller the stationary error should be zero.

The speed controller can be modified such that a load different from zero gives a stationary error. This is done by using βl instead of the complete load l in (6.23). The constant β ranges from $\beta = 0$ which means no compensation for the load, to $\beta = 1$ which means fully compensation of the load and no stationary error. The

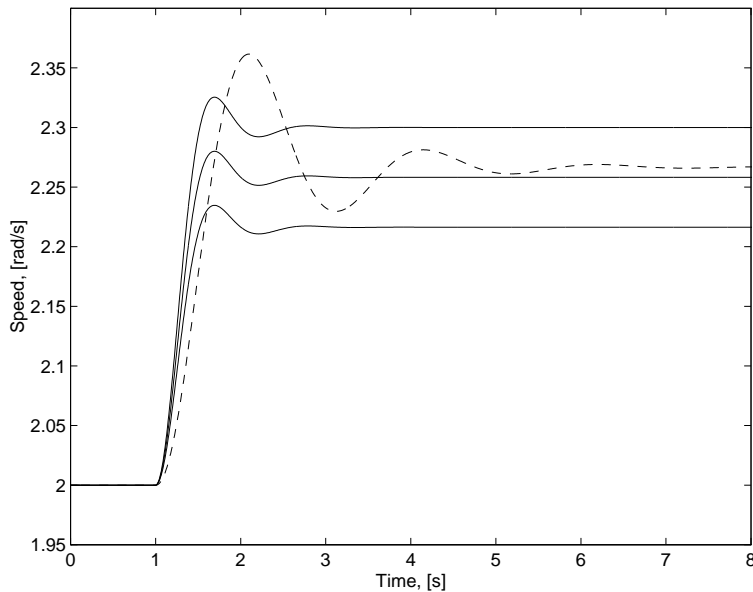


Figure 6.5 Wheel-speed response of step in accelerator position at $t=1$ s. The Drive-shaft model is controlled with the RQV controller (6.1) in dashed line, and the speed controller with stationary error (6.26) with $\beta = 0, 0.5, 1$ in solid lines. The speed controller achieves the same stationary level as the RQV controller by tuning β .

compensated speed control law becomes

$$u = K_0 x_{30} + K_l \beta l + K_r r - \begin{pmatrix} K_{c1} & K_{c2} & K_{c3} \end{pmatrix} x \quad (6.26)$$

In Figure 6.5, the RQV controller with its stationary error (remember the reference value $r = 2.3$ rad/s) is compared to the compensated speed controller (6.26) applied to Example 6.1 for three values of β . By adjusting β , the speed controller with active damping is extended with a stationary error comparable with that of the RQV controller.

6.4 Influence from Sensor Location

The speed controller investigated in the previous section uses feedback from all states ($x_1 = \theta_m / i_l i_f - \theta_w$, $x_2 = \dot{\theta}_m$, and $x_3 = \dot{\theta}_w$). A sensor measuring shaft torsion (e.g. x_1) is normally not used, and therefore an observer is needed to estimate the unknown states. In this work, either the engine speed or the wheel speed is used as input to the observer. This results in different control problems depending on sensor location. Especially the difference in disturbance rejection is investigated.

The observer gain is calculated using Loop-Transfer Recovery (LTR) [14]. The speed control law (6.23) then becomes

$$u = K_0 x_{30} + K_r r + K_l l - \begin{pmatrix} K_{c1} & K_{c2} & K_{c3} \end{pmatrix} \hat{x} \quad (6.27)$$

with K_0 , K_r , and K_l given by (6.24). The estimated states \hat{x} are given by the Kalman filter

$$\Delta \dot{\hat{x}} = A \Delta \hat{x} + B \Delta u + K_f (\Delta y - C \Delta \hat{x}) \quad (6.28)$$

$$K_f = P_f C^T V^{-1} \quad (6.29)$$

where P_f is derived by solving the Riccati equation

$$P_f A^T + A P_f - P_f C^T V^{-1} C P_f + W = 0 \quad (6.30)$$

The covariance matrices W and V correspond to disturbances v and e respectively. The output matrix C is either equal to C_m (5.11) when measuring the engine speed, or C_w (5.12) when measuring the wheel speed.

To recover the properties (phase margin and amplitude margin) achieved in the previous design step when all states are measured, the following values are selected [14]

$$\begin{aligned} V &= 1 \\ W &= \rho B B^T \\ C &= C_m \text{ or } C_w \\ \rho &= \rho_m \text{ or } \rho_w \end{aligned} \quad (6.31)$$

Equations (6.29) and (6.30) are then solved for K_f .

When using LQG with feedback from all states, the phase margin, φ , is at least 60° and the amplitude margin, a , is infinity as stated before. This is obtained also when using the observer by increasing ρ towards infinity. For Example 6.1 the following values are used

$$\begin{aligned} \rho_m &= 5 \cdot 10^5 \Rightarrow \varphi_m = 60.5^\circ, \quad a_m = \infty \\ \rho_w &= 10^{14} \Rightarrow \varphi_w = 59.9^\circ, \quad a_w = 35.0 \end{aligned} \quad (6.32)$$

where the aim has been to have at least 60° phase margin. The large difference between ρ_m and ρ_w in (6.32) is due to the structural difference between the two sensor locations, according to Chapter 5.

The observer dynamics is cancelled in the transfer functions from reference value to performance output ($z = \dot{\theta}_w$) and to control signal (u). Hence, these transfer functions are not affected by sensor location. However, the observer dynamics will be included in the transfer functions from disturbances v and e to both z and u .

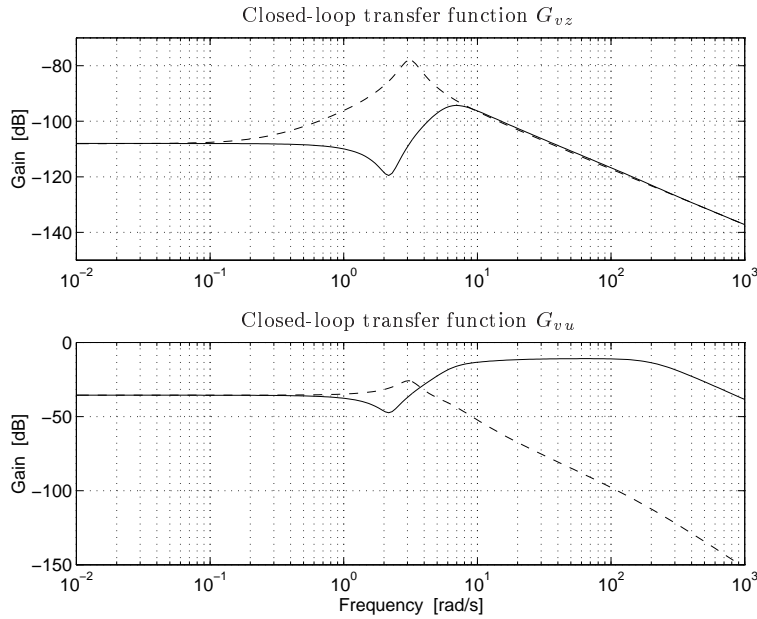


Figure 6.6 Closed-loop transfer functions from load disturbance, v , to performance output, z , and to control signal, u . Feedback from $\dot{\theta}_w$ is shown in solid and feedback from $\dot{\theta}_m$ is shown in dashed lines. With $\dot{\theta}_m$ -feedback the transfer functions have a resonance peak, resulting from the open-loop zeros.

6.4.1 Influence from Load Disturbances

Figure 6.6 shows how the performance output and the control signal are affected by the load disturbance v . There is a resonance peak in G_{vz} when using feedback from the engine-speed sensor, which is not present when feedback from the wheel-speed sensor is used. The reason for this can be seen when studying the transfer function G_{vz} in (5.21). By using the matrix inversion lemma [10] (5.21) is rewritten as

$$(G_{vz})_{cl} = \frac{G_{vz} + F_y(G_{uy}G_{vz} - G_{uz}G_{vy})}{1 + G_{uy}F_y} \quad (6.33)$$

where G_{ab} denotes the transfer function from signal a to b , and cl stands for closed loop. The subscript y in (6.33) represents the output of the system, i.e. either $\dot{\theta}_w$ or $\dot{\theta}_m$. The controller F_y is given by (5.16) as

$$F_y(s) = K_c(sI - A + BK_c + K_fC)^{-1}K_f \quad (6.34)$$

with C either being C_m for engine-speed feedback, or C_w for wheel-speed feedback. For the speed controller ($z = \theta_w$), Equation (6.33) becomes

$$(G_{vz})_{cl} = \frac{G_{vw}}{1 + G_{uw}F_y} \quad (6.35)$$

when the sensor measures the wheel speed. Equation (6.35) is obtained by replacing the subscript y in (6.33) by the subscript w . Then the parenthesis in (6.33) equals zero. In the same way, the resulting equation for the $\dot{\theta}_m$ -feedback case is

$$(G_{vz})_{cl} = \frac{G_{vw} + F_y(G_{um}G_{vw} - G_{uw}G_{vm})}{1 + G_{um}F_y} \quad (6.36)$$

Hence, when using the wheel-speed sensor, the controller is cancelled in the numerator, and when the engine-speed sensor is used, the controller is not cancelled.

The optimal return ratio in the LQG step is

$$K_c(sI - A)^{-1}B \quad (6.37)$$

Hence, the poles from A is kept, but there are new zeros that are placed such that the relative degree of (6.37) is one, assuring a phase margin of at least 60° ($\varphi > 60^\circ$), and an infinite gain margin. In the LTR step the return ratio is

$$F_y G_{uy} = K_c(sI - A - BK_c - K_f C)^{-1} K_f C (sI - A)^{-1} B \quad (6.38)$$

When ρ in (6.31) is increased towards infinity, (6.37) equals (6.38). This means that the zeros in the open-loop system $C(sI - A)^{-1}B$ are cancelled by the controller. Hence, the open-loop zeros will become poles in the controller F_y . This means that the closed-loop system will have the open-loop zeros as poles when using the engine-speed sensor. The closed-loop poles become $-0.5187 \pm 3.0753j$, which causes the resonance peak in Figure 6.6.

6.4.2 Influence from Measurement Disturbances

The influence from measurement disturbances e is shown in Figure 6.7. The transfer functions from measurement noise to output, (5.22), can be rewritten via the matrix inversion lemma as

$$(G_{ez})_{cl} = -\frac{G_{uz}F_y}{1 + G_{uy}F_y} \quad (6.39)$$

The complementary sensitivity function is defined for the two sensor alternatives as

$$T_w = \frac{G_{uw}F_y}{1 + G_{uw}F_y}, \quad T_m = \frac{G_{um}F_y}{1 + G_{um}F_y} \quad (6.40)$$

Then by replacing the subscript y in (6.39) with m or w (for $\dot{\theta}_m$ -feedback or $\dot{\theta}_w$ -feedback), and comparing with (6.40), the following relations hold

$$(G_{ez})_{cl} = -T_w \quad \text{with } \dot{\theta}_w\text{-feedback} \quad (6.41)$$

$$(G_{ez})_{cl} = -T_m \frac{G_{uw}}{G_{um}} = T_m G_{w/m} \quad \text{with } \dot{\theta}_m\text{-feedback} \quad (6.42)$$

where the dynamic output ratio $G_{w/m}$ was defined in Definition 5.1. For the Drive-shaft model the dynamic output ratio is

$$G_{w/m} = \frac{cs + k}{i(J_2 s^2 + (c + b_2)s + k)} \quad (6.43)$$

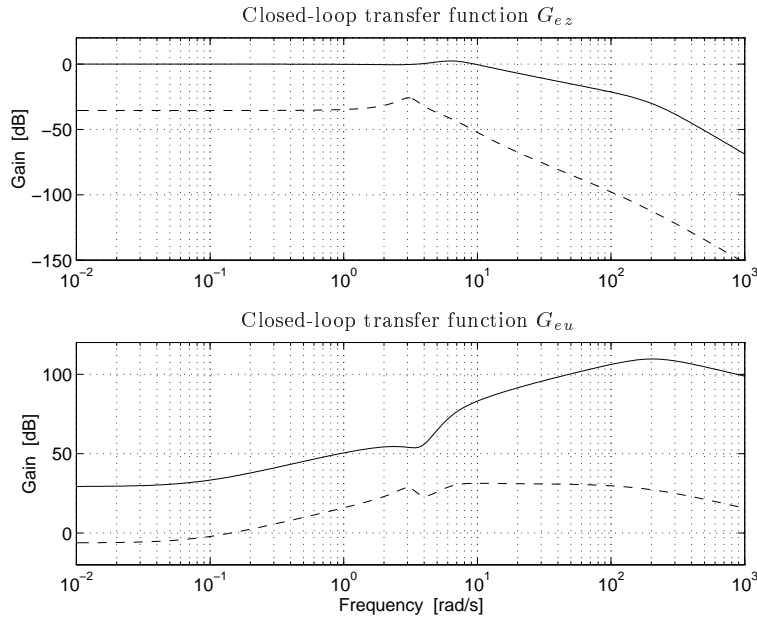


Figure 6.7 Closed-loop transfer functions from measurement noise, e , to performance output, z , and to control signal, u . Feedback from $\dot{\theta}_w$ is shown in solid and feedback from $\dot{\theta}_m$ is shown in dashed lines. The difference between the two feedback principles is described by the dynamic output ratio. The effect increases with lower gears.

where the state-space description in Chapter 5 is used. Especially for low frequencies, $G_{w/m}(0) = 1/i = 1/i_t i_f$. The dynamic output ratio can be seen in Figure 6.8 for three different gears.

When ρ in (6.31) is increased towards infinity, (6.37) equals (6.38), which means that $T_m = T_w$. Then (6.41) and (6.42) gives

$$(G_{ez})_{cl,m} = (G_{ez})_{cl,w} G_{w/m} \quad (6.44)$$

where cl, m and cl, w means closed loop with feedback from $\dot{\theta}_m$ and $\dot{\theta}_w$ respectively.

The frequency range in which $T_m = T_w$ is valid depends on how large ρ in (6.31) is made. Figure 6.9 shows the sensitivity functions

$$S_w = \frac{1}{1 + G_{uw}F_y}, \quad S_m = \frac{1}{1 + G_{um}F_y} \quad (6.45)$$

and the complementary sensitivity functions T_w and T_m (6.40) for the two cases of feedback. It is seen that $T_m = T_w$ is valid up to about 100 rad/s (≈ 16 Hz). The roll-off rate at higher frequencies differ between the two feedback principles. This is due to that the open-loop transfer functions G_{uw} and G_{um} have different

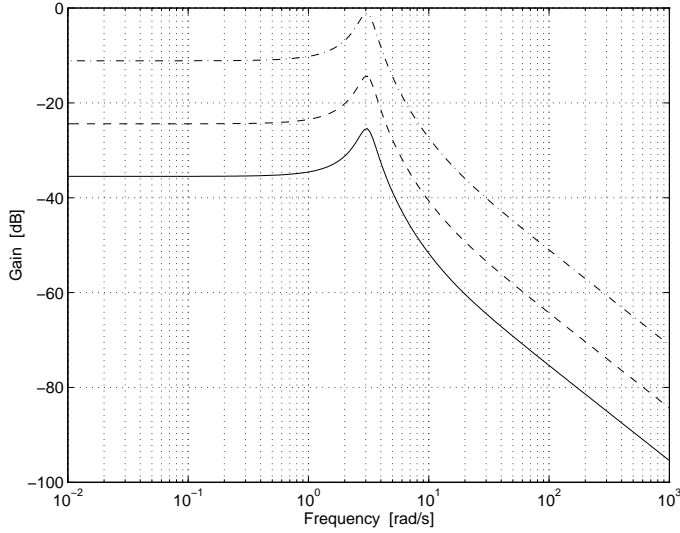


Figure 6.8 The dynamic output ratio $G_{w/m}$ for gear 1 (solid), gear 7 (dashed), and gear 14 (dash-dotted).

relative degrees. G_{uw} has a relative degree of two, and G_{um} has a relative degree of one. Therefore, T_w has a steeper roll-off rate than T_m .

Hence, the difference in G_{ez} depending on sensor location is described by the dynamic output ratio $G_{w/m}$. The difference in low-frequency level is equal to the conversion ratio of the driveline. Therefore, this effect increases with lower gears.

6.4.3 Load Estimation

The feedback law with unknown load is

$$u = K_0 x_{30} + K_r r + K_l \hat{l} - \begin{pmatrix} K_{c1} & K_{c2} & K_{c3} \end{pmatrix} \hat{x} \quad (6.46)$$

where \hat{l} is the estimated load. In order to estimate the load, the model used in the Kalman filter is augmented with a model of the load. The load is hard to model correctly since it is a function of road slope. However it can be treated as a slow-varying constant. A reasonable augmented model is

$$x_4 = \hat{l}, \quad \text{with} \quad \dot{x}_4 = 0 \quad (6.47)$$

This gives

$$\dot{\hat{x}} = A_l \hat{x}_l + B_l u + K_f (y - C_l \hat{x}_l) \quad (6.48)$$

with

$$\hat{x}_l = \begin{pmatrix} \hat{x} & \hat{l} \end{pmatrix}^T, \quad (6.49)$$

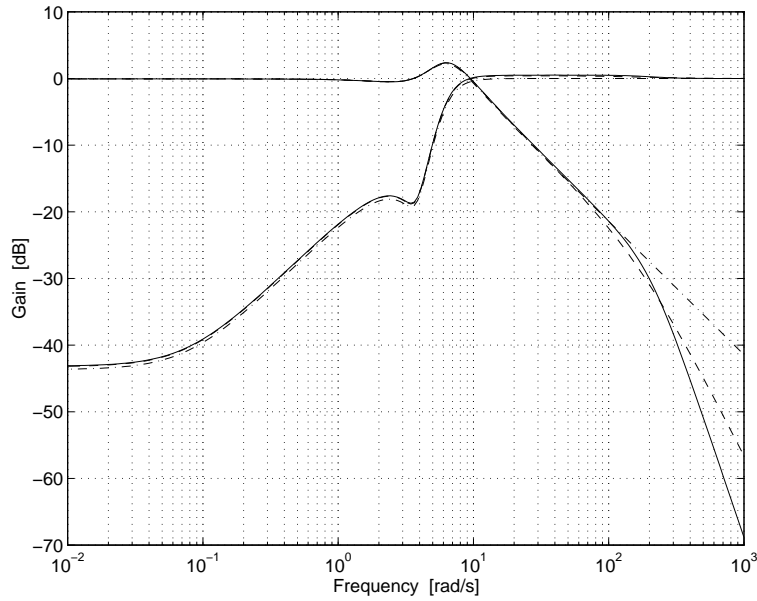


Figure 6.9 Sensitivity function S and complementary sensitivity function T . The dash-dotted lines correspond to the case with all states known. When only one velocity is measured, the solid lines correspond to $\hat{\theta}_w$ -feedback, and the dashed lines correspond to $\hat{\theta}_m$ -feedback.

$$A_l = \begin{pmatrix} & & & 0 \\ & A & & 0 \\ & & & -1/J_2 \\ 0 & 0 & 0 & 0 \end{pmatrix}, \quad (6.50)$$

$$B_l = \begin{pmatrix} B \\ 0 \end{pmatrix}, \quad C_l = (C \quad 0) \quad (6.51)$$

The feedback law is

$$u = K_0 x_{30} + K_r r - (K_{c1} \quad K_{c2} \quad K_{c3} \quad -K_l) \hat{x}_l \quad (6.52)$$

6.5 Simulations

An important step in demonstrating feasibility for real implementation is that a controller behaves well when simulated on a more complicated vehicle model than it was designed for. Even more important in a principle study is that such disturbances can be introduced that hardly can be generated in systematic ways in real experiments. One such example is impulse disturbances from a towed trailer.

The control law based on the reduced driveline model is simulated with a more complete nonlinear model, derived in Chapter 4. The purpose is also to study

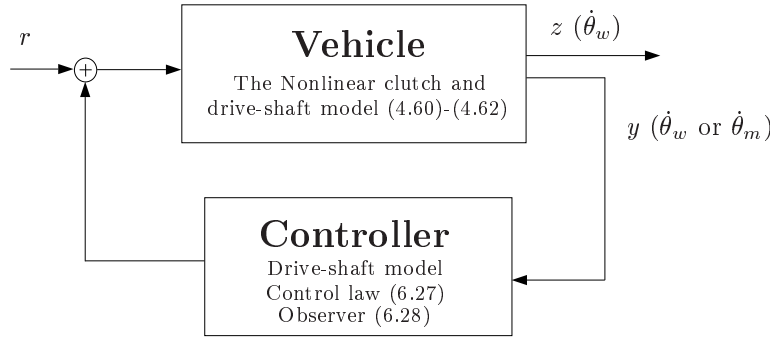


Figure 6.10 Simulation configuration. As a step for demonstrating feasibility for real implementation, the Nonlinear clutch and drive-shaft model is simulated with the controller based on the Drive-shaft model.

effects from different sensor locations as discussed in Section 6.4. The simulation situation is seen in Figure 6.10. The Nonlinear clutch and drive-shaft model, given by (4.60) to (4.62), is used as vehicle model. The steady-state level for the Nonlinear clutch and drive-shaft model is calculated by solving the model equations for the equilibrium point when the load and speed are known.

The controller used is based on the Drive-shaft model, as was derived in the previous sections. The wheel speed or the engine speed is the input to the observer (6.28), and the control law (6.27) with $\beta = 0$ generates the control signal.

The simulation case presented here is the same as in Example 6.1, i.e. a velocity step response, but a load disturbance is also included. The stationary point is given by

$$\dot{\theta}_w = 2, l = 3000 \Rightarrow x_0 = (0.0482 \quad 119 \quad 2.00)^T, u_0 = 109 \quad (6.53)$$

where (6.3) and (6.4) are used, and the desired new speed is $\dot{\theta}_w = 2.3$ rad/s. At steady state, the clutch transfers the torque $u_0 = 109$ Nm. This means that the clutch angle is in the area with higher stiffness ($\theta_{c1} < \theta_c \leq \theta_{c2}$) in the clutch nonlinearity, seen in Figure 4.15. This is a typical driving situation when speed control is used. However, at low clutch torques ($\theta_c < \theta_{c1}$) the clutch nonlinearity can produce limit cycle oscillations [3]. This situation occurs when the truck is traveling downhill with a load of the same size as the friction in the driveline, resulting in a low clutch torque. This is however not treated here. At $t = 6$ s, a load impulse disturbance is simulated. The disturbance is generated as a square pulse with 0.1 s width and 1200 Nm height, added to the load according to (5.9).

In order to simulate the nonlinear model, the differential equations (4.60) to (4.62) are scaled such that the five differential equations (one for each state) have about the same magnitude. The model is simulated using the Runge Kutta (45) method [26] with a low step size to catch the effect of the nonlinearity.

Figures 6.11 to 6.13 show the result of the simulation. These figures should be compared to Figure 6.4, where the same control law is applied to the Drive-shaft

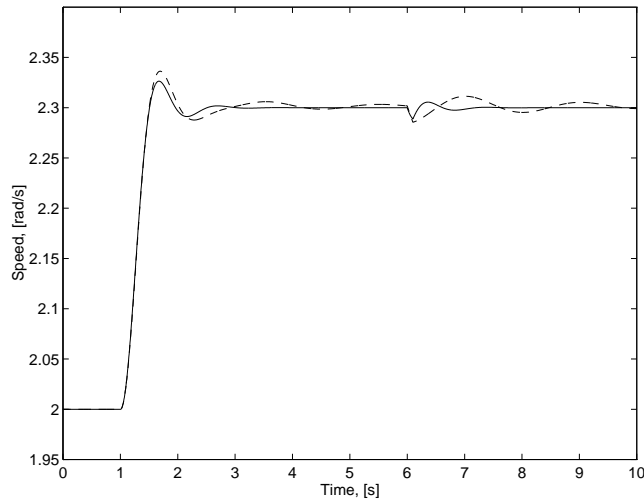


Figure 6.11 Wheel-speed response of step in accelerator position at $t=1$ s with the speed controller (6.27) derived from the *Drive-shaft model*, controlling the *Nonlinear clutch and drive-shaft model*. The solid line corresponds to $\dot{\theta}_w$ -feedback and feedback from $\dot{\theta}_m$ is seen in dashed line. At $t=6$ s, an impulse disturbance v acts on the load. The design still works when simulated with extra clutch dynamics.

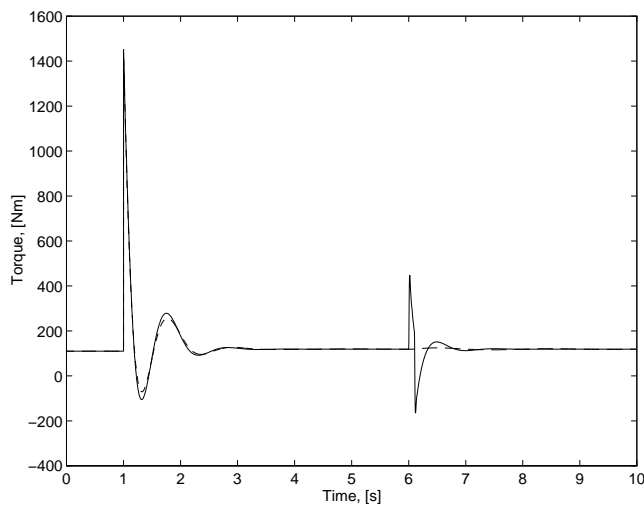


Figure 6.12 Control signal corresponding to Figure 6.11. There is only little difference between the two sensor alternatives in the step response at $t=1$ s. However, the load impulse (at $t=6$ s) generates a control signal that damps the impulse disturbance when feedback from the wheel-speed sensor is used, but not with engine-speed feedback.

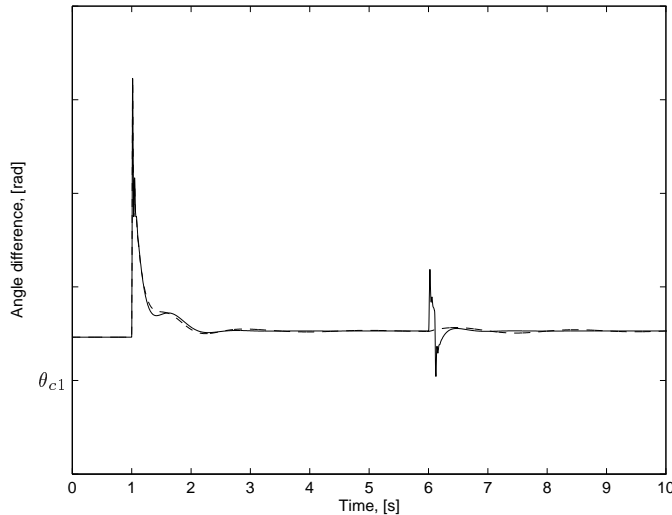


Figure 6.13 Clutch-angle difference corresponding to Figure 6.11. The influence from the clutch nonlinearity can be neglected, because the area with low stiffness ($\theta_c < \theta_{c1}$) is never entered.

model. From these plots it is demonstrated that the performance does not critically depend on the simplified model structure. The design still works if the extra dynamics is added. Further evidence supporting this is seen in Figure 6.13. The area with low stiffness in the clutch nonlinearity ($\theta_c < \theta_{c1}$) is never entered. The load impulse disturbance is better attenuated with feedback from the wheel-speed sensor, which is a verification of the behavior that was discussed in Section 6.4.

6.6 Summary

Speed control with engine controlled damping of driveline resonances has been proposed in this chapter. RQV control is the traditional way speed control is performed in diesel engines, which gives a certain driving character with a load dependent stationary error when going uphill or downhill. With RQV, there is no active damping of wheel-speed oscillations, resulting in vehicle shuffle. An increased controller gain results in increased wheel-speed oscillations while the engine speed is well damped.

A major contribution of this chapter is a formulation of a criterion for speed control with active damping of wheel-speed oscillations and a stationary error giving RQV behavior. To solve the criterion, a linear driveline model with drive-shaft flexibility, and with parameters estimated from experiments is used. Simulations show that the performance of the design, based on the simplified model, works well for a more complicated model, with a nonlinear clutch characteristics.

An investigation of the influence from different sensor locations on the control design shows that when using LQG/LTR the open-loop zeros are cancelled by the controller. With engine-speed feedback this is critical, because the open-loop transfer function has a resonant zero couple. It is shown that this zero couple becomes poles of the transfer functions from load disturbances to wheel speed. This results in undamped load disturbances when engine-speed feedback is used. When feedback from the wheel-speed sensor is used, no resonant open-loop poles are cancelled. Load disturbances are thus better attenuated with this feedback configuration.

Measurement disturbances are better attenuated when the engine-speed sensor is used, than when using the wheel-speed sensor. This effect increases with lower gears. Two different closed-loop transfer functions result, depending on feedback configuration. The difference between these two is described by the dynamic output ratio. As mentioned before, both sensors are normally available on a driveline, but the principle study can be used as a guideline on where to invest in improved sensor quality.

In conclusion, the use of active damping significantly improves the behavior for both sensor cases. Furthermore, the formulation is natural, it allows efficient solution, and there is a simple tuning of the amount of RQV feeling.

Speed Controller Experiments

A speed control strategy with engine controlled damping of driveline resonances was derived in the previous chapter. The topic of this chapter is to demonstrate that the method is applicable for real implementations in a heavy truck. The goal is further to demonstrate that the simplified treatment of the diesel engine (smooth torque, dynamical behavior, etc, according to Chapter 2) holds in field trials.

The speed control strategy is implemented by discretizing the feedback law and the observer. The controller parameters are tuned for the practical constraints given by the measured signals. Step response tests in engine speed are performed with the strategy and the results are compared to the traditionally used RQV controller for speed control. In order to have as small restrictions on the control signal as possible, tests are first performed without a diesel smoke delimiter, limiting the engine torque for low turbo pressures. It is then demonstrated how this nonlinear torque limitation can be handled.

Section 7.1 covers controller discretization and parameter tuning. The main contribution of the chapter is the demonstration of active damping in field trials in the sections following.

7.1 Controller Implementation

The speed controller is implemented in a real-time system on a PC, as described in Chapter 3. The controller, developed in Chapter 6, consists of an observer and a feedback law, which are implemented in the C programming language. The

observer is described by (6.28) as

$$\Delta \dot{\hat{x}} = A\Delta \hat{x} + B\Delta u + K_f(\Delta y - C\Delta \hat{x}) \quad (7.1)$$

and the feedback law is described by (6.26) as

$$u = K_0 x_{30} + K_l \beta l + K_r r - \begin{pmatrix} K_{c1} & K_{c2} & K_{c3} \end{pmatrix} \hat{x} \quad (7.2)$$

7.1.1 Controller Discretization

The observer is discretized by Tustin's method [7]. This method results in a discrete version of the observer equation (7.1) of the form

$$x_{k+1} = E x_k + F(u_k + u_{k-1}) + G(y_k + y_{k-1}) \quad (7.3)$$

where x_k is the state vector, u_k is the control signal, and y_k is the output (either the wheel speed or the engine speed) at iteration k and

$$\begin{aligned} E &= H \left(2I + T(A - K_f C) \right) \\ F &= H B T \\ G &= H K_f T \\ H &= \left(2I - T(A - K_f C) \right)^{-1} \end{aligned} \quad (7.4)$$

where A , B , and C describes the model, T is the sampling time, and K_f is the observer gain.

Equation (7.4) is calculated off-line prior to execution in order to save on-line execution time. This means that a total of 15 multiplications and 8 additions are needed every iteration to implement the observer (7.3).

After computing the states by using (7.3), the control signal is obtained by the state-feedback law (7.2). The complete algorithm computed every iteration is as follows.

Control algorithm

1. Read engine speed ($\dot{\theta}_m$) and engine temperature (T_m).
2. Calculate engine friction torque, $M_{fr}(\dot{\theta}_m, T_m)$, as function of the engine speed and the engine temperature. The friction values are obtained from a map, described in Section 4.2, by an interpolation routine.
3. Read the engine torque (M_m) and the variable used as input to the observer (engine speed, θ_m , or wheel speed, θ_w).
4. Calculate the control signal $u_k = (M_m - M_{fr}(\dot{\theta}_m, T_m))$, and update the observer equations (7.3).
5. Read the reference value (r_k), and use the feedback law (7.2) to calculate the new control signal, u_{k+1} .

-
6. The new control signal is transferred to requested engine torque by adding the engine friction torque to the control signal ($u_{k+1} + M_{fr}(\dot{\theta}_m, T_m)$). The requested engine torque is then sent to the engine control unit.
-

The repetition-rate of the algorithm is chosen the same as the sampling rate of the input variable to the observer. This means that the sampling-rate is 50 Hz when using feedback from the engine-speed sensor, and 20 Hz with feedback from the wheel-speed sensor. More information about the measured variables are found in Table 3.1.

The parameters of the implemented algorithm are in the following sections tuned for the practical constraints given by the sensor characteristics.

7.1.2 Tuning the Controller Parameters σ and β

The controller parameter σ , introduced in (6.13), is used for describing the reference signal in the cost function (6.10) as states, and thus be able to solve the criterion. The parameter has little influence on control performance as long as it has a value close to zero. As in the simulations described in Section 6.5, $\sigma = 0.0001$ is used.

The controller parameter β , introduced in (6.26), is used to obtain the stationary error characteristic for RQV control, as described in Section 6.3.1. The stationary error is not considered further in this chapter, and therefore, $\beta = 1$ is used, giving no stationary error.

7.1.3 Tuning the Controller Parameter η

A third controller parameter η is introduced in (6.6) in Section 6.3, which is used to control the trade-off between control signal amplitude and closed-loop bandwidth. It is desired to have as low η as possible (giving high bandwidth), but if the control signal reaches its limitations, no active damping is obtained, which must be avoided. This is of specific interest in this application due to varying restrictions on the control signal as a function of engine speed and turbo pressure, as described in Chapter 3.

Figure 7.1 shows the closed-loop transfer functions from reference value (r) to performance output (z) and to control signal (u) for $\eta = 5 \cdot 10^{-8}$. A bandwidth of about 7 rad/s (≈ 1 Hz) is obtained. However, this bandwidth is only achieved for small changes in reference value, since this η leads to control signals reaching the limits for larger changes in the reference value. The large control signals are mainly a result of the high gain in G_{ru} for high frequencies, according to Figure 7.1. The gain at high frequency in G_{rz} is low and decreasing, and therefore, the main effect from high frequencies in the reference value is seen in high control signal amplitudes. By pre-filtering the reference value with a low-pass filter, the result will be a reduced control signal amplitude with little effect on the bandwidth of the performance output (wheel speed).

Figure 7.2 shows closed-loop control with reference value without filtering compared to one that is filtered with a first order filter with a bandwidth of 25 Hz.

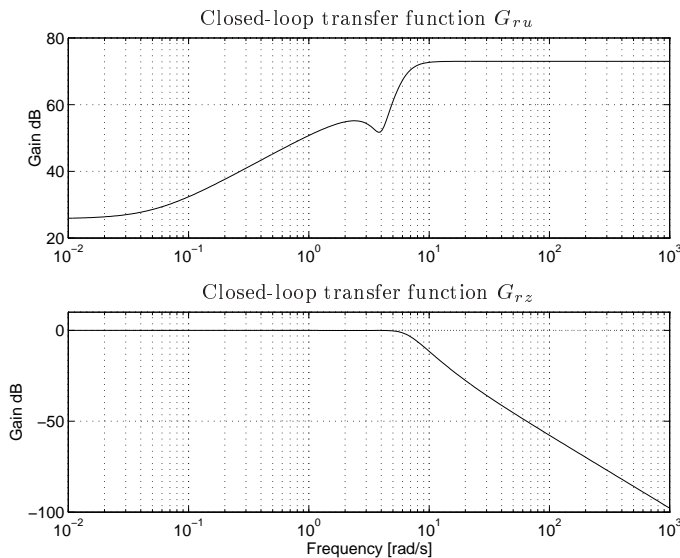


Figure 7.1 Closed-loop transfer functions from reference value, r , to performance output ($z = \text{wheel speed}$) and to control signal, u . The main reason to large control signal amplitudes at fast changes in reference value is the high gain in G_{ru} at high frequencies.

The control signal becomes

$$u = K_0 x_{30} + K_l \beta l + K_r \frac{1}{0.04s + 1} r - K_c \hat{x} \quad (7.5)$$

It is demonstrated that the control signal is reduced to half its peak value, and that the rise-time of the wheel speed is little affected.

7.1.4 Tuning the Controller Parameter ρ

The parameter ρ , introduced in the LTR step (6.31) of the design in Section 6.4, parameterizes the observer such that the optimal feedback properties (when all states are measured) can be obtained also when an observer is used to estimate some states. If ρ is increased towards infinity, the optimal properties are obtained, as discussed before. Increasing ρ means that the algorithm is 'told' that an increasing proportion of the variance in the plant output is due to state variations, and a decreasing proportion to measurement errors. A large ρ together with measurement disturbances will result in an observer tracking the measured signal with its errors, giving a poor estimation of the other states. Hence, there is a trade-off between having good robustness properties and estimation quality when using LTR technique, and having measured outputs with poor quality.

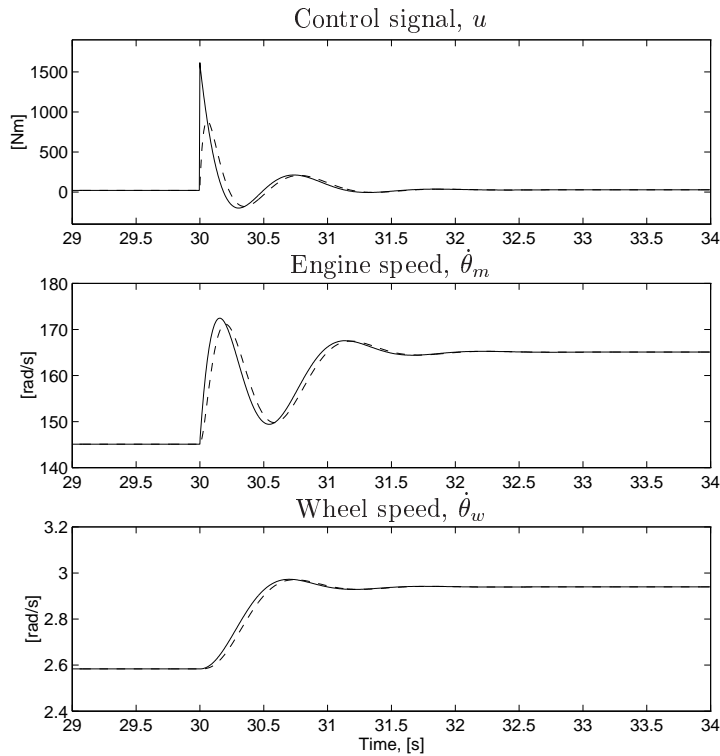


Figure 7.2 Speed controller simulated with and without pre-filtering the reference value, according to (7.5) and (7.2). The dashed lines show a case where the reference value is filtered with a first order low-pass filter with cut-off frequency 25 Hz. Pre-filtering can reduce control signal peaks with only a small decrease in bandwidth of the wheel speed.

Estimator performance

In the simulation study in Section 6.5, there were no measurement errors in the measured outputs, and high values of ρ ($\rho_m = 5 \cdot 10^5$ and $\rho_w = 10^{14}$) were possible to use. With these values, about the same phase margin (60°) in the closed-loop system was obtained. In real implementations, where the measured signals are distorted by measurement noise and quantification errors, ρ is tuned to a lower value. After tests with observers with different ρ , the following values were used throughout the experiments, $\rho_m = \rho_w = 10^5$.

Figure 7.3 shows a test with an observer estimating the states using $\rho_m = \rho_w = 10^5$. In the first experiment (when the engine speed is used as input to the observer) the quality of the measurements is such that ρ can be increased to almost the level used in the simulation study. This means that there is little difference between the measured and estimated engine speed.

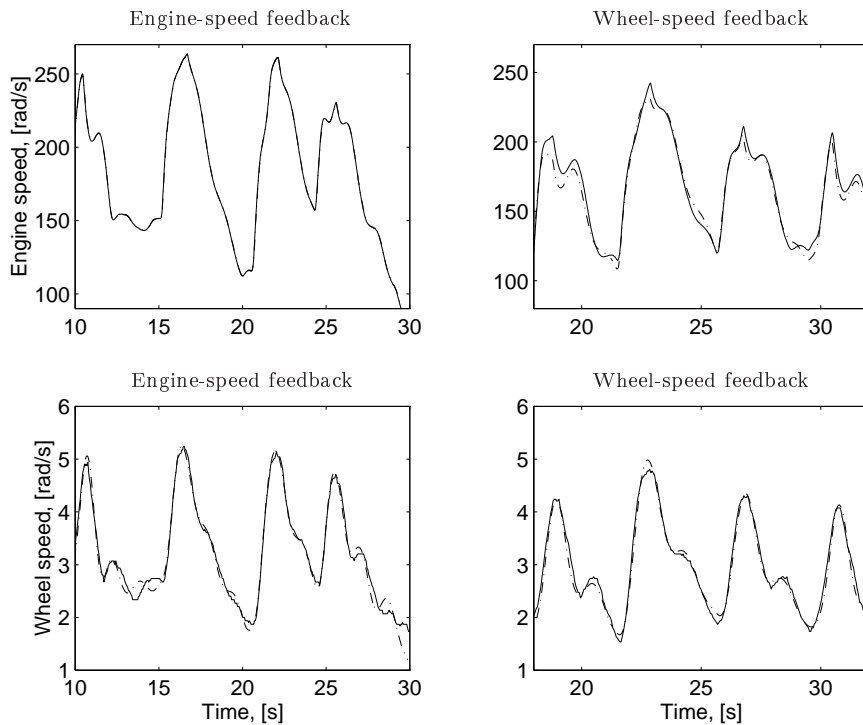


Figure 7.3 Experiments with two observers estimating the engine speed (top figures) and wheel speed (bottom figures). The observer with feedback from engine speed is seen in left figures, and wheel-speed feedback to the right. Measured signals are seen in solid lines and the estimated signals are seen in dashed lines. The wheel-speed sensor is of lower quality than the engine-speed sensor.

In the second experiment (when the wheel speed is used as input to the observer), ρ cannot be increased to the value used in the simulations, due to the quantification errors in the measurement signal (the relative size of the quantification error is higher for the wheel speed than for the engine speed, according to Table 3.1). This results in an observer that filters the measured wheel speed, without following the measurement errors.

After tuning ρ for both feedback principles, the estimated states have only small deviations from the measured signals, for low-frequency driveline oscillations. However, the closed-loop performance will not only depend on the quality of the estimations, but also the value of ρ , which will be investigated next.

Closed-loop performance

The robustness properties of a closed-loop design can be studied by investigating the sensitivity function, S , and the complementary sensitivity function, T . These

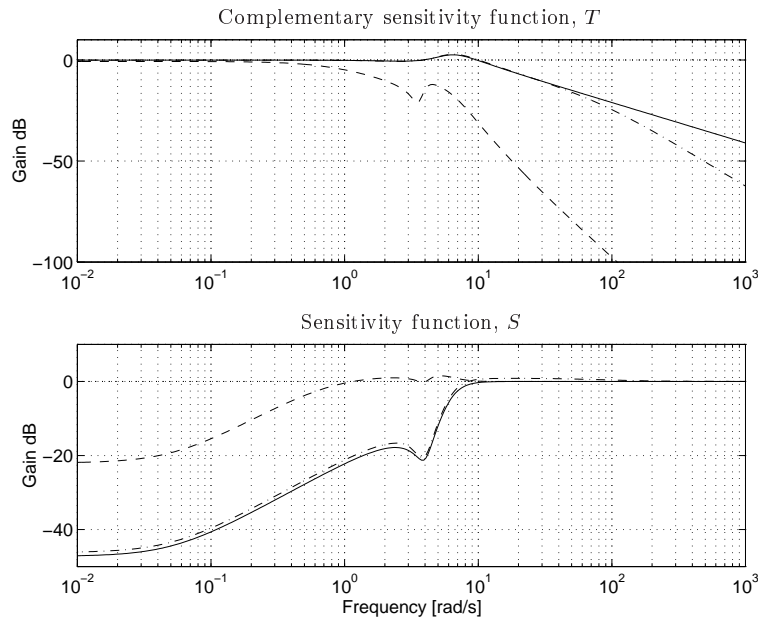


Figure 7.4 Complementary sensitivity function, T , and sensitivity function, S . In solid lines the optimal case (all states are measurable) is shown, and in dashed lines the case with feedback from the wheel speed is shown. Feedback from engine speed is seen in dash-dotted lines, and the observer gain is calculated with the values $\rho_m = \rho_w = 10^5$. The difference is mainly due to a difference in sensor quality.

transfer functions describe sensitivity to state disturbances (S) and measurement disturbances (T). Note, that the differences in sensitivity depending on sensor location discussed in this section are mainly a result of sensor signals with different quality, and not the structural difference depending on sensor location, covered in Section 6.4.

Figure 7.4 shows the sensitivity functions, S and T , for the two cases of feedback, together with the optimal case (i.e. when all states are measured).

The parameter ρ_m (for engine-speed feedback) has a value such that the sensitivity is close to the optimal sensitivity functions. The difference in T at high frequencies is desirable in order to have good attenuation of high-frequency measurement noise (hence, ρ should not be increased higher than necessary).

The sensitivity when using feedback from the wheel speed have larger deviations from the optimal functions. This is due to the low ρ_w forced by the lower quality sensor. This is seen to result in lower sensitivity to measurement disturbances (T), compared to when using feedback from the engine speed. The sensitivity to state disturbances and modeling errors (S) is hereby higher for this feedback configuration. The sensitivity is even higher than one for some frequencies, which can be serious if they are excited.

7.1.5 Influence from Sampling Time and Bus Delay

Before performing field trials with the speed controller, it is necessary to investigate how sampling and bus delay will affect the closed-loop performance. This is done by using a driveline real-time simulator. This simulator consists of the PC where the real-time system and controller is implemented. This PC is connected via a CAN-bus to another PC where the driveline model is simulated in real-time. The interface between the two computers is the same as between the PC and the truck. By this arrangement, hardware and software can be tested, together with the effects that discretization, sampling, and bus delay have on the performance of the controller.

Figure 7.5 shows such a simulation where the speed controller design is simulated in Simulink [26], together with the real-time simulator, when using feedback from both the engine speed and the wheel speed. In the simulations in Simulink, only the linear model and feedback law are used, and no sensor models or quantification effects are included. Remember that the sampling frequency is 50 Hz with engine-speed feedback and 20 Hz with wheel-speed feedback.

The simulations differ in the time interval $t=30-32$ s. When simulating with sampling and bus delay, the control signal oscillates more than when using Simulink. The discrepancies are larger when using feedback from the wheel speed. The overshoot is also larger when using wheel-speed feedback.

The reasons for the deviation between the simulations are the time delay (resulting from sampling and bus delay), differences between the continuous and the discrete models, and estimation quality. In the real implementation also effects from unmodeled dynamics will add to the source of errors. The main reason for the oscillations in the control signal, seen in Figure 7.5, is the time delay which adds negative phase in the loop. This can be compensated for by using State-Feedback Redesign [1]. This approach has been tested, but the result from a wheel-speed perspective is that little is gained. The effect that is most tricky to handle is the combination of slow sampling and relatively high quantification errors in the wheel-speed measurements. The situation in Figure 7.5 works well, but if a higher bandwidth is wanted (i.e. lower η according to (6.6)) the situation will be worse with a larger overshoot that is difficult to suppress.

7.2 Experiments without Smoke Delimiter

Field trials are performed with the 124L truck equipped with a 6 cylinder diesel engine. An almost flat test road has been used for field trials with a minimum of changes from test to test. The focus of the tests is low gears, with low speeds and thus little impact from air drag. Reference values are generated by the computer to generate the same test situation from time to time. Only one direction of the test road is used so that there will be no difference in road inclination.

The test presented here is a velocity step response from 2.1 rad/s to 3.6 rad/s (about 1200 RPM to 2000 RPM) with gear 1. At first the smoke delimiter (see

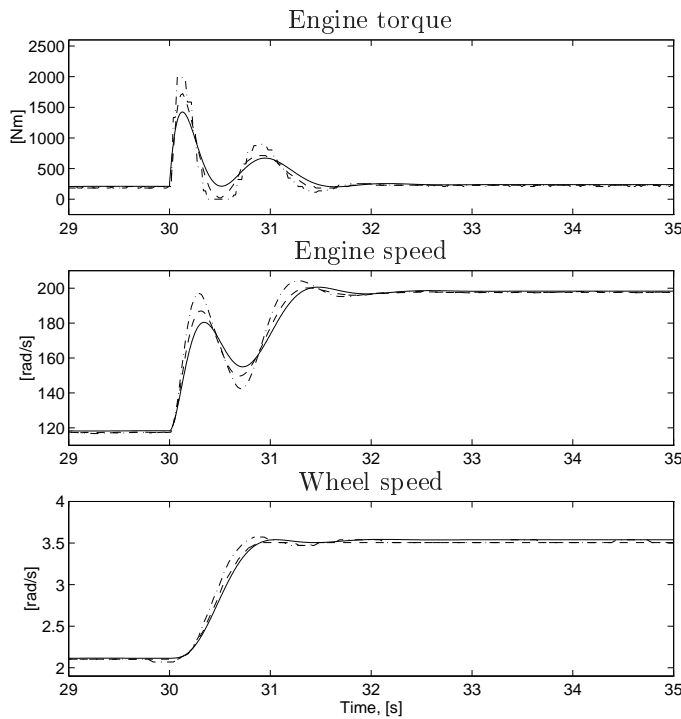


Figure 7.5 Simulation of a step response at $t=30$ s with the speed controller. Simulation in Simulink, in solid lines, is independent of sensor location. The dashed lines correspond to simulation with the real-time simulator with engine-speed feedback. The dash-dotted lines show the corresponding result when using wheel-speed feedback. The difference between the simulations is mainly a result of time delay and quantification errors.

Chapter 3) is not used in order to be able to investigate the control design with as small restrictions on the control signal as possible.

In Figure 7.6, the speed controller is compared to traditional RQV control. The engine torque, the engine speed, and the wheel speed are shown. The speed controller uses feedback from the engine speed, and the RQV controller has the gain $K_p = 50$. With this gain the rise-time and the peak torque output is about the same for the two controllers. A high torque output is possible because no smoke delimiter is used.

With RQV control, the engine speed reaches the desired speed but the wheel speed oscillates, as in the simulations made earlier. Speed control with active damping significantly reduces the oscillations in the wheel speed. This means that the controller applies the engine torque in a way that the engine inertia works in the opposite direction of the oscillation. This gives an oscillating engine speed, according to Figure 7.6. Hence, it is demonstrated that the assumption about the

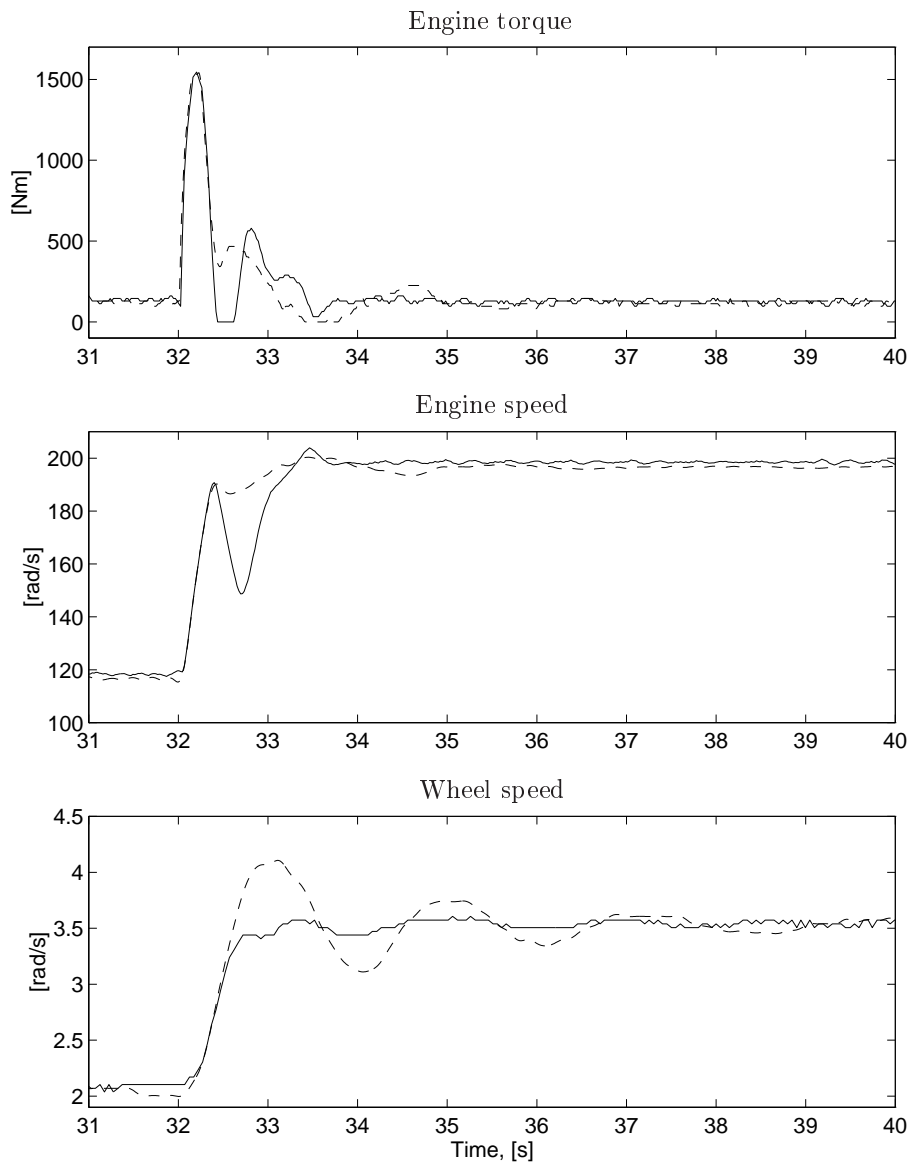


Figure 7.6 Speed step at $t=32$ s with active damping and engine-speed feedback (solid) compared to traditional RQV control with $K_p=50$ (dashed). Experiments are performed without smoke delimiter on a flat road. After 32.5 s, the control signals differ depending on control scheme. With speed control, the engine inertia works in the opposite direction of the oscillations, which are significantly reduced.

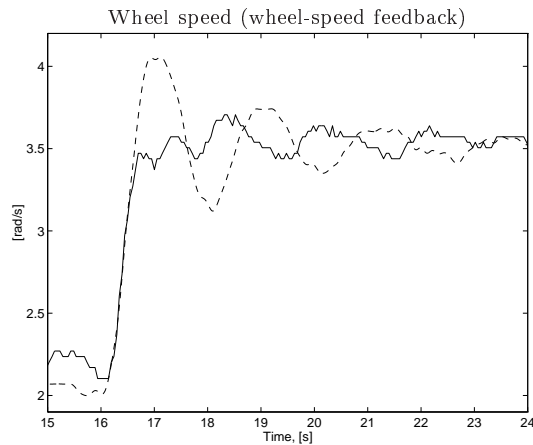


Figure 7.7 Speed control with active damping and wheel-speed feedback (solid) compared to traditional RQV control with $K_p=50$ (dashed). Experiments are performed without smoke delimiter on a flat road.

simplified model structure (Drive-shaft model) is sufficient for control design. It is further demonstrated that the design is robust against nonlinear speed dependent torque limitations (maximum torque limitations), and the assumption about static transfer function between engine torque and fuel amount is sufficient.

In Figure 7.7 the corresponding plot is shown for wheel-speed feedback. Active damping is more difficult to obtain when using the wheel speed as sensor. (Compare to Figure 7.6 where engine-speed feedback is used.) The main reason is the poor sensitivity to unmodeled dynamics (state disturbances) due to poor sensor quality, as discussed in the previous section.

7.3 Experiments with Smoke Delimiter

The design works well when no smoke delimiter is used. This results in smoke emissions at the peak values in the control signal (e.g. at $t = 32$ s in Figure 7.6). This must be avoided to reduce emissions.

The restrictions on the design imposed by the smoke delimiter are depicted in Figure 7.8. Speed control with active damping is demonstrated with and without smoke delimiter. It is seen how the maximum engine torque is restricted when using the smoke delimiter. The diesel smoke is reduced, since the peak values in the control signal are limited.

Limitations in engine torque for diesel smoke attenuation is seen to have little impact on the performance of the speed controller. Also, this case is well behaved and active damping of wheel-speed oscillations is obtained. The only detectable effect is a small reduction in bandwidth, giving larger rise-time.

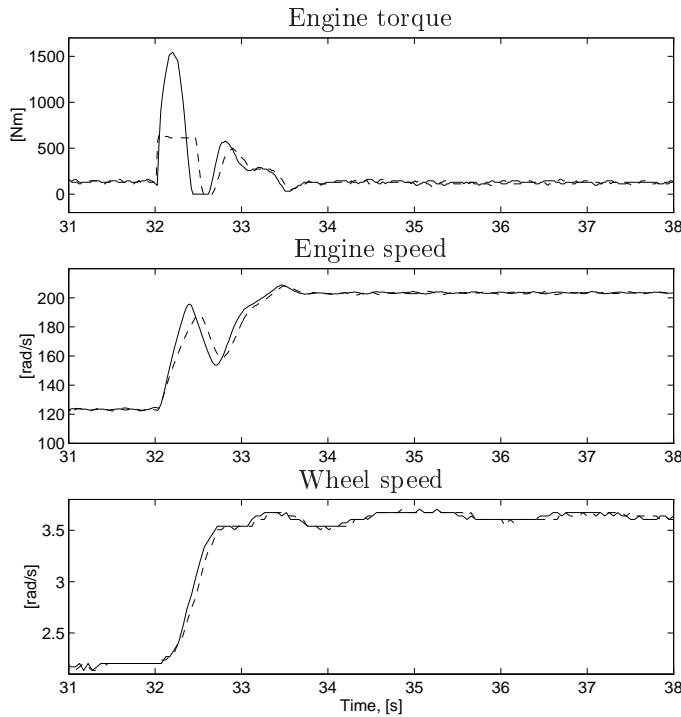


Figure 7.8 Speed control with active damping with and without smoke delimiter. The dashed lines correspond to experiments with smoke delimiter. At $t=32$ s, a speed step is commanded. When using smoke delimiter, a reduced torque level is obtained. Also the case with torque limitations is well handled and active damping is obtained.

7.4 Controller Robustness

It is important to have a design that is as robust as possible to changes in the environment like road inclination and vehicle mass. Differences in load is seen mainly as a difference in offset in the estimated drive-shaft torsion, x_1 . The vehicle mass will have greater influence on the driveline dynamics and it is necessary to have the control strategy adjusted for different weights of the vehicle.

A detailed investigation about controller robustness is not performed here, but an example of the robustness of the design against errors in conversion ratio is shown in Figure 7.9. Errors in conversion ratio means that the controller is based on an erroneous vehicle mass and load (these parameters are reduced by the conversion ratio). Since the road is flat (small load), the test emulates an error in vehicle mass. The speed controller designed for gear 1 is tested on gear 3. It is seen that the design is robust against this type of parameter errors since active damping is still obtained.

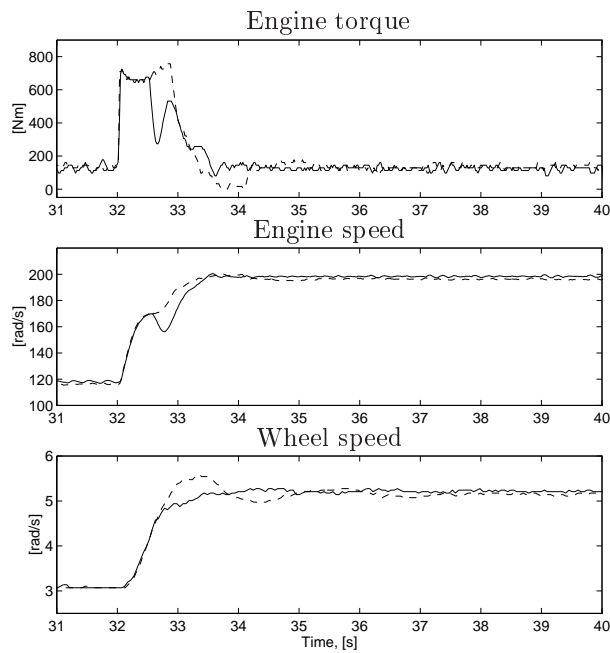


Figure 7.9 Example of robustness of the design to parameter deviations. Error in vehicle mass is emulated by testing the speed controller designed for gear 1 on gear 3 in solid. RQV control of gear 3 with $K_p=50$ is shown in dashed lines. Both experiments are with smoke delimiter. The design is robust against this types of parameter errors in vehicle mass.

7.5 Summary

Speed control is the extension of the traditionally used diesel engine speed-control scheme with engine controlled damping of wheel-speed oscillations. The simplified linear model with drive-shaft flexibility is used to derive a controller which shows significant reduction in wheel-speed oscillations in field trials with a heavy truck.

The response time of the diesel engine, with unit-pump injection system, is demonstrated to be fast enough for controlling the first resonance mode of the driveline. This means that the static torque map used for relating injected fuel amount to engine torque, together with a friction model as function of the engine speed and temperature, is sufficient for dynamic control. It is further demonstrated that the design works when restrictions in the implementation are at hand. Example of such important restrictions that are well handled are nonlinear torque limitations for maximum torque and diesel smoke reduction. The design is shown to be robust against parameter errors in vehicle mass.

To summarize, the controller improves performance and driveability since driving response is increased while still reducing vehicle shuffle.

Gear-Shift Controller Design and Simulations

Gear shifting by engine control realizes fast gear shifts by controlling the engine instead of sliding the clutch to a torque-free state in the transmission, as described in Chapter 2. This is done by controlling the internal torque of the driveline, which is the overall goal of the rest of the thesis. Internal torque control is treated in two cases, being similar strategies for gear-shift control. The topic of this chapter is to derive a control strategy based on a model of the transmitted torque in the transmission. This results in a detailed study of the dynamical behavior of the transmission torque, which should be zero in order to engage neutral gear. A transmission-torque controller is derived that controls the estimated transmission torque to zero while having engine controlled damping of driveline resonances. With this approach, the specific transmission-torque behavior for each gear is described and compensated for. This investigation is important as a principle study for understanding how to optimize gear-shift quality, and for verifying simulation studies. A secondary goal is to formulate the control problem in a way that established techniques and software can be applied to find solutions.

This transmission-torque control method requires estimation of the parameters describing the different parts in the transmission for each gear. In order to implement gear-shift control, it is desired to have a strategy that is as simple and robust as possible, but still maintains high gear-shift quality. This is the aim when deriving a second variant of internal driveline torque control, which is covered in Chapter 10.

A model of the transmission is developed in Section 8.1, where the torque transmitted in the transmission is modeled as a function of the states and the control signal of the Drive-shaft model. The controller goal was stated in Chapter 2, and is

formulated in mathematical terms as a gear-shift control criterion in Section 8.2. This is the key result of this chapter, together with the derivation of a control law in Section 8.3, that minimizes the criterion. Influence from sensor location and simulations are presented in the sections following.

8.1 Internal Driveline Torque

There are many possible definitions of internal driveline torque. Since the goal is to engage neutral gear without using the clutch, it is natural to use the minimization of the torque transferred in the transmission as a control goal. The following sections cover the derivation of an expression for this torque, called the *transmission torque*, as function of the state variables and the control signal.

8.1.1 Transmission Torque

The performance output, z , for the gear-shift controller is the transmission torque transferred between the cogwheels in the transmission. A simplified model of the transmission is depicted in Figure 8.1. The input shaft is connected to bearings with a viscous friction component b_{t1} . A cogwheel is mounted at the end of the input shaft which is connected to a cogwheel mounted on the output shaft. The conversion ratio between these are i_t , as mentioned in Chapter 4. The output shaft is also connected to bearings with the viscous friction component b_{t2} .

By using Newton's second law, the transmission can be modeled by the following two equations

$$J_{t1}\ddot{\theta}_c = M_t - b_{t1}\dot{\theta}_c - z \quad (8.1)$$

$$J_{t2}\ddot{\theta}_t = i_t z - b_{t2}\dot{\theta}_t - M_p \quad (8.2)$$

In the following subsections, the expression for the transmission torque is derived for the three models developed in Chapter 4. Furthermore, assumptions are made about the unknown variables characterizing the different parts of the transmission.

8.1.2 Transmission Torque for the Drive-Shaft Model

The Drive-shaft model is defined by Equations (4.29) and (4.30). The model is here extended with the model of the transmission depicted in Figure 8.1, and the expression for the transmission torque is derived. By using the equation describing the engine inertia (4.1)

$$J_m\ddot{\theta}_m = M_m - M_{fr:m} - M_c \quad (8.3)$$

together with (4.16)

$$M_c = M_t, \quad \theta_m = \theta_c \quad (8.4)$$

equation (8.1) is expressed in terms of engine speed

$$(J_m + J_{t1})\ddot{\theta}_m = M_m - M_{fr:m} - b_{t1}\dot{\theta}_m - z \quad (8.5)$$

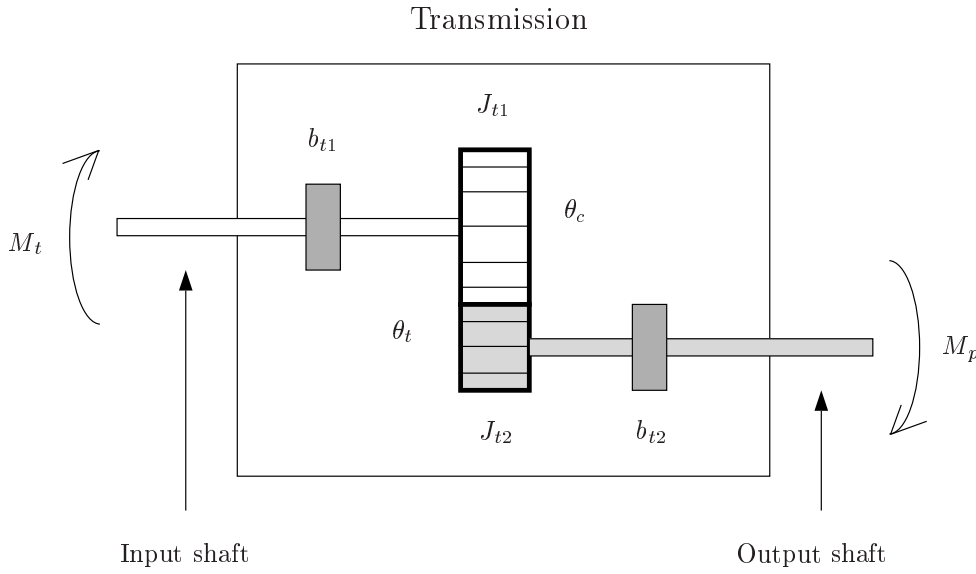


Figure 8.1 Simplified model of the transmission with two cogwheels with conversion ratio i_t . The cogwheels are connected to the input and output shafts respectively. The torque transmitted between the cogwheels is the transmission torque, z .

To describe the performance output in terms of state variables, $\ddot{\theta}_m$ (which is not a state variable) is replaced by (4.29), which is one of the differential equations describing the Drive-shaft model

$$\begin{aligned} (J_m + J_t/i_t^2 + J_f/i_t^2 i_f^2) \ddot{\theta}_m &= M_m - M_{fr:m} - (b_t/i_t^2 + b_f/i_t^2 i_f^2) \dot{\theta}_m \\ &\quad - k(\theta_m/i_t i_f - \theta_w)/i_t i_f \\ &\quad - c(\dot{\theta}_m/i_t i_f - \dot{\theta}_w)/i_t i_f \end{aligned} \quad (8.6)$$

which together with $u = M_m - M_{fr:m}$ gives

$$\begin{aligned} u - b_{t1} \dot{\theta}_m - z &= \frac{J_m + J_{t1}}{J_m + J_t/i_t^2 + J_f/i_t^2 i_f^2} \left(u - (b_t/i_t^2 + b_f/i_t^2 i_f^2) \dot{\theta}_m \right. \\ &\quad \left. - k(\theta_m/i_t i_f - \theta_w)/i_t i_f - c(\dot{\theta}_m/i_t i_f - \dot{\theta}_w)/i_t i_f \right) \end{aligned} \quad (8.7)$$

From this equation it is possible to express the performance output, z , as a function of the control signal, u , and the state variables, x , according to the state-space description (5.2) to (5.5).

Transmission Torque for the Drive-Shaft Model

$$\begin{aligned}
 z &= Mx + Du \quad \text{with} \\
 M^T &= \begin{pmatrix} \frac{(J_m + J_{t1})k}{J_1 i} \\ \frac{J_m + J_{t1}}{J_1} (b_1 + c/i^2) - b_{t1} \\ -\frac{(J_m + J_{t1})c}{J_1 i} \end{pmatrix} \\
 D &= 1 - \frac{J_m + J_{t1}}{J_1}
 \end{aligned} \tag{8.8}$$

The transmission torque, z , is modeled as a function of the states and the control signal for the Drive-shaft model, where the labels from (5.5) are used.

The unknown parameters in (8.8) are $J_m + J_{t1}$ and b_{t1} . The other parameters were estimated in Chapter 4. One way of estimating these unknowns would be to decouple the Drive-shaft model into two models, corresponding to neutral gear. Then a model including the engine, the clutch, and the input shaft of the transmission results, in which the performance output is equal to zero ($z = 0$). Trials with neutral gear would then give a possibility to estimate the unknowns. This will be further investigated in Chapter 9.

In the derivation of the Drive-shaft model in Chapter 4 the performance output, z , is eliminated. If z is eliminated in (8.1) and (8.2) and (8.4) is used, the equation for the transmission is

$$(J_{t1} i_t^2 + J_{t2}) \ddot{\theta}_m = i_t^2 M_c - i_t M_p - (b_{t1} i_t^2 + b_{t2}) \dot{\theta}_m \tag{8.9}$$

By comparing this with the equation describing the transmission in Chapter 4, (4.19)

$$J_t \ddot{\theta}_m = i_t^2 M_c - b_t \dot{\theta}_m - i_t M_p \tag{8.10}$$

the following equations relating the parameters are obtained

$$J_t = i_t^2 J_{t1} + J_{t2} \tag{8.11}$$

$$b_t = i_t^2 b_{t1} + b_{t2} \tag{8.12}$$

In order to further investigate control and estimation of the transmission torque, the unknowns are given values. It is arbitrarily assumed that the gear shift divides the transmission into two equal inertias and viscous friction components, giving

$$J_{t1} = J_{t2} \tag{8.13}$$

$$b_{t1} = b_{t2}$$

A more detailed discussion of these parameters will be performed in Chapter 10. Equations (8.11) and (8.12) then reduce to

$$J_{t1} = \frac{J_t}{1 + i_t^2} \tag{8.14}$$

$$b_{t1} = \frac{b_t}{1 + i_t^2} \tag{8.15}$$

The following combinations of parameters from the Drive-shaft model were estimated in Chapter 4

$$J_1 = J_m + J_t/i_t^2 + J_f/i_t^2 i_f^2 \quad (8.16)$$

$$b_1 = b_t/i_t^2 + b_f/i_t^2 i_f^2 \quad (8.17)$$

according to the labels from the state-space formulation in (5.5). From (8.14) and (8.16) $J_m + J_{t1}$ can be derived as

$$\begin{aligned} J_m + J_{t1} &= J_m + \frac{J_t}{1+i_t^2} = J_m + \frac{i_t^2}{1+i_t^2}(J_1 - J_m - J_f/i_t^2 i_f^2) \\ &= J_m \frac{1}{1+i_t^2} + J_1 \frac{i_t^2}{1+i_t^2} - J_f \frac{1}{i_f^2(1+i_t^2)} \end{aligned} \quad (8.18)$$

A combination of (8.15) and (8.17) gives b_{t1}

$$b_{t1} = \frac{b_t}{1+i_t^2} = \frac{i_t^2}{1+i_t^2}(b_1 - b_f/i_t^2 i_f^2) \quad (8.19)$$

For low gears i_t has a large value. This together with the fact that J_f and b_f are considerably less than J_1 and b_1 gives the following approximation about the unknown parameters

$$J_m + J_{t1} \approx J_1 \frac{i_t^2}{1+i_t^2} \quad (8.20)$$

$$b_{t1} \approx b_1 \frac{i_t^2}{1+i_t^2} \quad (8.21)$$

8.1.3 Transmission Torque for the Clutch and Drive-Shaft Model

The performance output expressed for the Clutch and drive-shaft model is given by replacing M_t in (8.1) by equation (4.49)

$$M_c = M_t = k_c(\theta_m - \theta_t i_t) + c_c(\dot{\theta}_m - \dot{\theta}_t i_t) \quad (8.22)$$

Then the performance output is

$$z = k_c(\theta_m - \theta_t i_t) + c_c(\dot{\theta}_m - \dot{\theta}_t i_t) - b_{t1} i_t \dot{\theta}_t - J_{t1} i_t \ddot{\theta}_t \quad (8.23)$$

This is expressed in terms of state variables by using (4.55)

$$(J_t + J_f/i_f^2)\ddot{\theta}_t = i_t \left(k_c(\theta_m - \theta_t i_t) + c_c(\dot{\theta}_m - \dot{\theta}_t i_t) \right) \quad (8.24)$$

$$- (b_t + b_f/i_f^2)\dot{\theta}_t - \frac{1}{i_f} \left(k_d(\theta_t/i_f - \theta_w) + c_d(\dot{\theta}_t/i_f - \dot{\theta}_w) \right) \quad (8.25)$$

leading to the following model.

Transmission Torque for the Clutch and Drive-Shaft Model

$$z = Mx \quad \text{with} \quad (8.26)$$

$$M^T = \begin{pmatrix} k_c(1 - \frac{J_{t1}i_t^2}{J_2}) \\ \frac{J_{t1}i_t k_d}{J_2 i_f} \\ c_c(1 - \frac{J_{t1}i_t^2}{J_2}) \\ \frac{J_{t1}i_t^2}{J_2}(i_t^2 c_c + b_2 + c_d/i_f^2) - c_c i_t - b_{t1} i_t \\ -\frac{J_{t1}i_t c_d}{J_2 i_f} \end{pmatrix}$$

with states and labels according to the state-space description (5.6) to (5.8).

The following combinations of parameters from the Clutch and drive-shaft model were estimated in Chapter 4

$$J_2 = J_t + J_f/i_f^2 \quad (8.27)$$

$$b_2 = b_t + b_f/i_f^2 \quad (8.28)$$

according to (5.8). From (8.14), (8.15), (8.27), and (8.28), J_{t1} and b_{t1} can be written as

$$J_{t1} = \frac{i_t^2}{1 + i_t^2}(J_2 - J_f/i_f^2) \quad (8.29)$$

$$b_{t1} = \frac{i_t^2}{1 + i_t^2}(b_2 - b_f/i_f^2) \quad (8.30)$$

which are approximated to

$$J_{t1} \approx \frac{i_t^2}{1 + i_t^2} J_2 \quad (8.31)$$

$$b_{t1} \approx \frac{i_t^2}{1 + i_t^2} b_2 \quad (8.32)$$

since J_f and b_f are considerably less than J_1 and b_1 .

8.1.4 Transmission Torque for the Nonlinear Clutch and Drive-Shaft Model

The performance output for the Nonlinear clutch and drive-shaft model is derived in the same way as for the Clutch and drive-shaft model, with the difference that (8.22) is replaced by

$$M_c = M_t = M_{kc}(\theta_m - \theta_t i_t) + c_c(\dot{\theta}_m - \dot{\theta}_t i_t) \quad (8.33)$$

where M_{kc} is the torque transmitted by the clutch nonlinearity, given by (4.59). Then the performance output is defined as

Transmission Torque for the Nonlinear Clutch and Drive-Shaft Model

$$z = (M_{kc} \quad \dot{\theta}_t/i_f - \dot{\theta}_w \quad \dot{\theta}_m \quad \dot{\theta}_t \quad \dot{\theta}_w) \begin{pmatrix} 1 - \frac{J_{t1}i_t^2}{J_2} \\ \frac{J_{t1}i_t k_d}{J_2 i_f} \\ c_c(1 - \frac{J_{t1}i_t^2}{J_2}) \\ \frac{J_{t1}i_t^2}{J_2}(i_t^2 c_c + b_2 + c_d/i_f^2) - c_c i_t - b_{t1} i_t \\ -\frac{J_{t1}i_t c_d}{J_2 i_f} \end{pmatrix} \quad (8.34)$$

The parameters not estimated in the definition above are approximated in the same way as for the performance output for the Clutch and drive-shaft model.

Model Comparison

Figure 8.2 shows the transmission torque during a test with step inputs in accelerator position with the 144L truck using gear 1. The transmission torque is calculated with (8.8) for the Drive-shaft model, and with (8.26) for the Clutch and drive-shaft model. Figure 8.3 shows the performance output in the frequency domain. The low-frequency level differs between the two models, and the main reason for this is the difficulties to estimate the viscous damping coefficients described in Chapter 4. The difference at higher frequencies is due to the clutch, which gives a second resonance peak for the Clutch and drive-shaft model. Furthermore, the roll-off rate of the Clutch and drive-shaft model is steeper than for the Drive-shaft model.

8.2 Transmission-Torque Control Criterion

Problem Formulation

The transmission-torque controller is the controller that drives the transmission torque to zero with engine controlled damping of driveline resonances. Then the time spent in the torque control phase (see Chapter 2) is minimized. The engagement of neutral gear should be at a torque level that gives no oscillations in the driveline speeds. Hereby, the disturbances to the driver and the time spent in the speed synchronization phase can be minimized. The influence on shift quality from initial driveline resonances, and torque impulses from trailer and road roughness should be minimized.

Control Criterion

The transmission-torque controller is realized as a state-feedback controller, based on the Drive-shaft model. The controller is obtained by deriving a control criterion that describes the control problem of minimizing the transmission torque. The

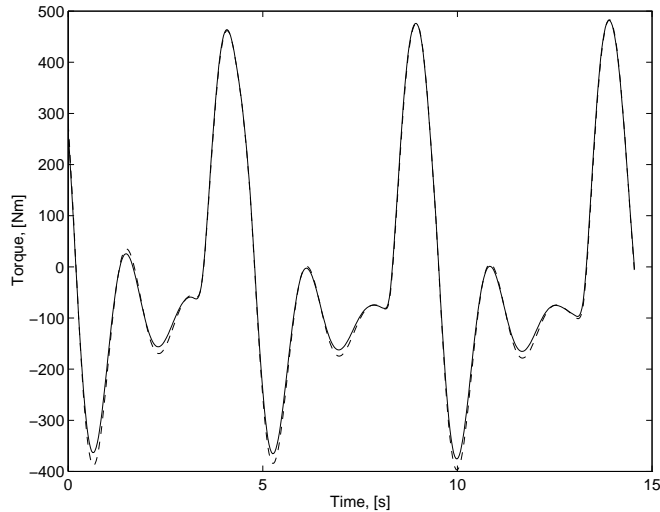


Figure 8.2 Estimated transmission torque, z , in (8.8) and (8.26) for a test with step inputs in accelerator position with the 144L truck. The solid line corresponds to the Drive-shaft model and the dashed line corresponds to the Clutch and drive-shaft model.

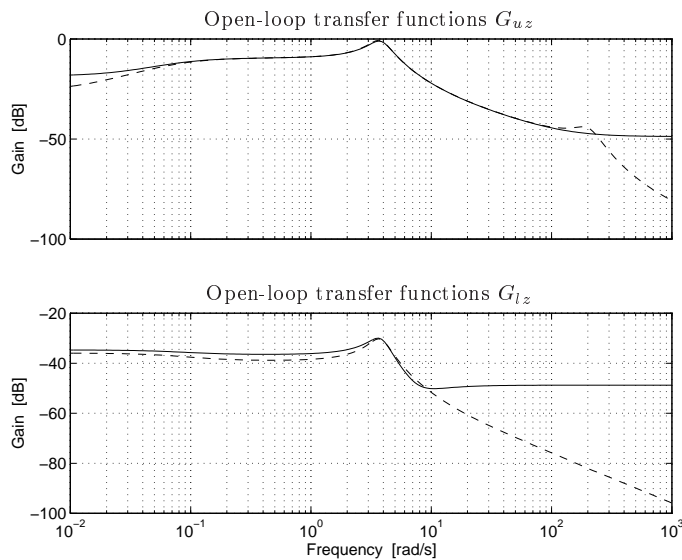


Figure 8.3 Transfer functions from control signal, u , and load, l , to transmission torque, z . The Drive-shaft model is shown in solid and the Clutch and drive-shaft model is shown in dashed lines. The modeled clutch adds a second resonance peak and a steeper roll-off rate.

criterion is then minimized by standard software for a controller solving the control problem.

The gear-shift problem can be described as minimizing the transmission torque, z , but with a control signal, u , possible to realize by the diesel engine. Therefore, the criterion consists of two terms. The first term is z^2 which describes the deviation from zero transmission torque. The second term describes the deviation in control signal from the level needed to obtain $z = 0$. Let this level be u_{shift} , which will be speed-dependent as described later. Then the criterion is described by

$$\lim_{T \rightarrow \infty} \int_0^T z^2 + \eta(u - u_{shift})^2 \quad (8.35)$$

The controller that minimizes this cost function will utilize engine controlled damping of driveline resonances (since z^2 is minimized) in order to obtain $z = 0$. At the same time, the control signal is prevented from having large deviations from the level u_{shift} . The trade-off is controlled by tuning the parameter η .

In the following subsections, the influence from each term in the criterion (8.35) will be investigated, and then how these can be balanced together for a feasible solution by tuning the parameter η .

Unconstrained Active Damping

The influence from the first term in the criterion (8.35) is investigated by minimizing z^2 . The performance output, $z = Mx + Du$, is derived in (8.8) for the Drive-shaft model as a function of the states and the control signal. The term z^2 can be minimized for a control law, since z includes the control signal and D is scalar. If u is chosen as

$$u = -D^{-1}Mx \quad (8.36)$$

$z = 0$ is guaranteed. This control law is called *unconstrained active damping* and the reason for this is illustrated in the following example.

Example 8.1 Consider the 144L truck modeled in Chapters 4 traveling at a speed of 3 rad/s (5.4 km/h) with gear 1 and a total load of 3000 Nm ($\approx 2\%$ road slope).

Figure 8.4 shows the resulting transmission torque, the control signal, the engine speed, and the wheel speed, when a gear shift is commanded at $t=1$ s, with the control signal chosen according to (8.36). Unconstrained active damping is achieved which obtains $z = 0$ instantaneously. The wheel speed decreases linearly, while the engine speed is oscillating.

Unconstrained active damping (8.36) fulfills the control goal, but generates a control signal that is too large for the engine to generate. It can be noted that despite $z = 0$ is achieved this is not a stationary point, since the speed is decreasing. This means that the vehicle is free-rolling which can be critical if lasting too long.

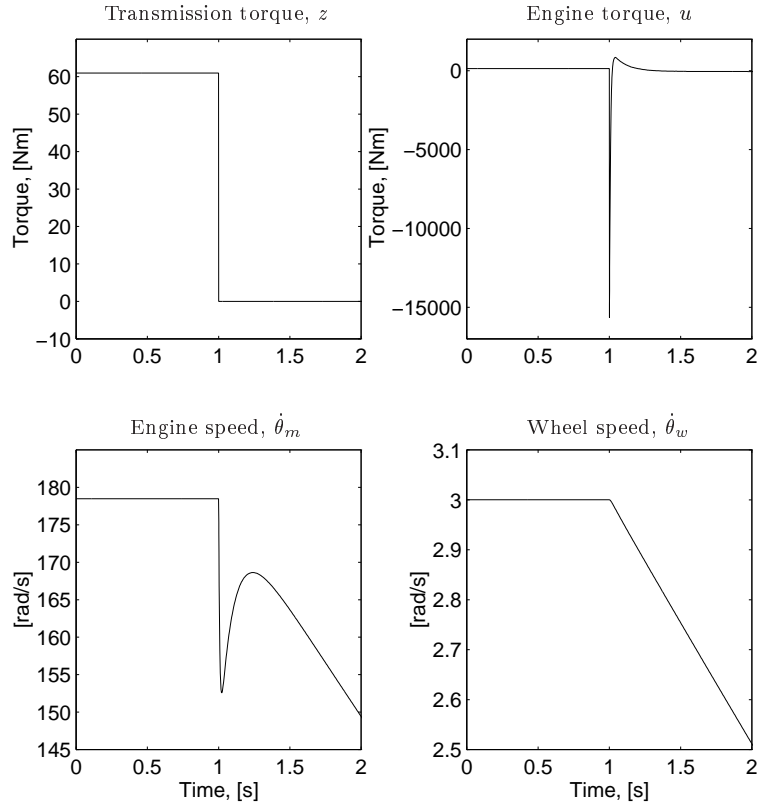


Figure 8.4 Unconstrained active damping of the Drive-shaft model. At $t=1$ s, a gear shift is commanded and the control law (8.36) calculates the engine torque such that the transmission torque is driven to zero instantaneously. The oscillations in the transmission torque are damped with an unrealizable large control signal. The wheel speed decreases linearly.

Gear-Shift Condition

The influence from the second term in the criterion (8.35) is investigated by minimizing $(u - u_{shift})^2$, resulting in the control law

$$u = u_{shift} \quad (8.37)$$

where the torque level u_{shift} is the control signal needed to obtain zero transmission torque, without using active damping of driveline resonances. Hence, u_{shift} can be derived from a stiff driveline model, by solving for $z = 0$.

By using the labels according to Chapter 5, the differential equation describing the stiff driveline is

$$(J_1 i + J_2/i)\ddot{\theta}_w = u - (b_1 i + b_2/i)\dot{\theta}_w - l/i \quad (8.38)$$

This equation is developed by using the Drive-shaft model in (4.29) and (4.30), and eliminating the torque transmitted by the drive shaft, $k(\theta_m/i - \theta_w) + c(\dot{\theta}_m/i - \dot{\theta}_w)$. Then, by using $\dot{\theta}_m = \dot{\theta}_w i$ (i.e. stiff driveline), (8.38) results.

Equation (8.5) expressed in terms of wheel speed is

$$z = u - b_{t1} i \dot{\theta}_w - (J_m + J_{t1}) i \ddot{\theta}_w \quad (8.39)$$

Combining (8.38) and (8.39) gives the performance output for the stiff driveline.

$$z = \left(1 - \frac{(J_m + J_{t1}) i^2}{J_1 i^2 + J_2}\right) u - \left(b_{t1} i - \frac{(J_m + J_{t1}) i}{J_1 i^2 + J_2} (b_1 i^2 + b_2)\right) \dot{\theta}_w + \frac{(J_m + J_{t1}) i}{J_1 i^2 + J_2} l \quad (8.40)$$

The control signal to force $z = 0$ is given by solving (8.40) for u while $z = 0$. Then the torque level u_{shift} becomes

$$\begin{aligned} u_{shift}(\dot{\theta}_w, l) &= \mu_x \dot{\theta}_w + \mu_l l \quad \text{with} \\ \mu_x &= \left(b_{t1} i - \frac{(J_m + J_{t1}) i}{J_1 i^2 + J_2} (b_1 i^2 + b_2)\right) \left(1 - \frac{(J_m + J_{t1}) i^2}{J_1 i^2 + J_2}\right)^{-1} \\ \mu_l &= -\frac{(J_m + J_{t1}) i}{J_1 i^2 + J_2} \left(1 - \frac{(J_m + J_{t1}) i^2}{J_1 i^2 + J_2}\right)^{-1} \end{aligned} \quad (8.41)$$

This control law is called the *gear-shift condition*, since it implies zero transmission torque. The following example illustrates the control performance when using (8.41).

Example 8.2 Consider the 144L truck in the same driving situation as in Example 8.1. The stationary point is obtained by using (6.3) and (6.4).

$$x_{30} = 3, \quad l = 3000 \quad \Rightarrow \quad x_0 = (0.0511 \quad 178 \quad 3.00), \quad u_0 = 138 \quad (8.42)$$

Figure 8.5 shows the resulting transmission torque, the control signal, the engine speed, and the wheel speed when a gear shift is commanded at $t=1$ s, with the control signal chosen according to (8.41).

This control law achieves $z = 0$ with a realizable control signal, but the oscillations introduced are not damped. Therefore, the time needed to obtain zero transmission torque is not optimized. The performance of this approach is worse if the driveline is oscillating at the time for the gear shift, or if there are disturbances present.

Final Control Criterion

The final cost criterion for the transmission-torque controller is obtained by including (8.41) in the cost criterion (8.35)

$$\begin{aligned} & \lim_{T \rightarrow \infty} \int_0^T z^2 + \eta(u - u_{shift}(\dot{\theta}_w, l))^2 \\ &= \lim_{T \rightarrow \infty} \int_0^T (Mx + Du)^2 + \eta(u - \mu_x \dot{\theta}_w - \mu_l l)^2 \end{aligned} \quad (8.43)$$

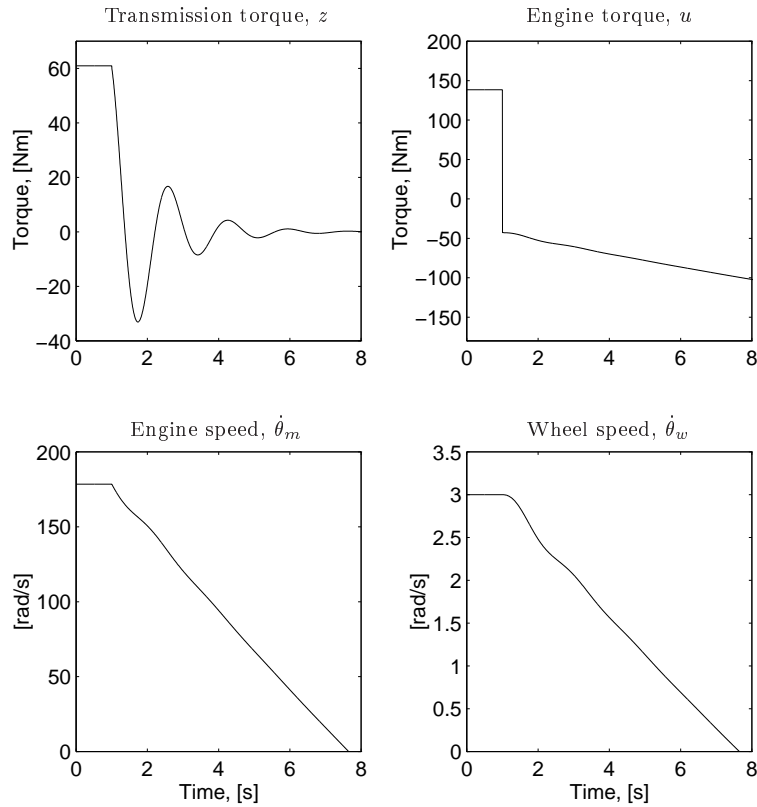


Figure 8.5 The Drive-shaft model controlled with the gear-shift condition (8.41). At $t=1$ s, a gear shift is commanded. The speed dependent realizable control signal drives the transmission torque to zero. Undamped oscillations in the transmission torque increase the time needed to fulfill the goal of controlling the transmission torque to zero.

If the driveline is stiff, there is no difference between the two terms in the cost function (8.43). Furthermore, the point at which the cost function is zero is no stationary point, since the speed of the vehicle will decrease despite $z = 0$ and $u = u_{shift}$.

8.3 Transmission-Torque Control Design

The new idea for gear-shift control is in this section given efficient treatment by solving (8.43) for a control law by using LQG technique, and available software. This is done by linearizing the driveline model and rewriting (8.43) in terms of the linearized variables. A state-feedback matrix is derived that minimizes (8.43) by

solving a Riccati equation. The derived feedback law is a function of η , which is chosen such that high bandwidth together with a feasible control signal is obtained.

The linearized driveline model is given by (6.8) and (6.9) in Section 6.3. The cost function is expressed in terms of Δx and Δu by using (6.9)

$$\begin{aligned} & \lim_{T \rightarrow \infty} \int_0^T (M \Delta x + D \Delta u + M x_0 + D u_0)^2 \\ & + \eta (\Delta u - \mu_x \Delta x_3 + u_0 - \mu_x x_{30} - \mu_l l)^2 \\ & = \lim_{T \rightarrow \infty} \int_0^T (M \Delta x + D \Delta u + r_1)^2 + \eta (\Delta u - \mu_x \Delta x_3 + r_2) \end{aligned} \quad (8.44)$$

with

$$\begin{aligned} r_1 &= M x_0 + D u_0 \\ r_2 &= u_0 - \mu_x x_{30} - \mu_l l \end{aligned} \quad (8.45)$$

The constants r_1 and r_2 are expressed as state variables, by augmenting the plant model (A, B) with models of the constants r_1 and r_2 . This was done in (6.13) to (6.16).

By using these equations, the cost function (8.44) can be written in the form

$$\lim_{T \rightarrow \infty} \int_0^T x_r^T Q x_r + R \Delta u^2 + 2x_r^T N \Delta u \quad (8.46)$$

with

$$\begin{aligned} Q &= (M \ 1 \ 0)^T (M \ 1 \ 0) + \eta (0 \ 0 \ -\mu_x \ 0 \ 1)^T (0 \ 0 \ -\mu_x \ 0 \ 1) \\ N &= (M \ 1 \ 0)^T D + \eta (0 \ 0 \ -\mu_x \ 0 \ 1)^T \\ R &= D^2 + \eta \end{aligned} \quad (8.47)$$

The cost function (8.46) is minimized by the state-feedback gain

$$K_c = Q^{-1} (B_r^T P_c + N^T) \quad (8.48)$$

where P_c is the stabilizing solution to the Riccati equation (6.21). The resulting control law is

$$\Delta u = -K_c x_r = - \begin{pmatrix} K_{c1} & K_{c2} & K_{c3} \end{pmatrix} \Delta x - K_{c4} r_1 - K_{c5} r_2 \quad (8.49)$$

which by using (8.45) gives

$$u = K_0 x_{30} + K_l l - \begin{pmatrix} K_{c1} & K_{c2} & K_{c3} \end{pmatrix} x \quad (8.50)$$

with

$$\begin{aligned} K_0 &= \begin{pmatrix} \lambda_x & \delta_x & \mu_x \end{pmatrix} \Gamma \\ K_l &= \begin{pmatrix} \lambda_l & \delta_l & \mu_l \end{pmatrix} \Gamma \end{aligned} \quad (8.51)$$

where Γ is given by

$$\Gamma = \begin{pmatrix} 1 - K_{c4}D - K_{c5} \\ (K_{c1} \ K_{c2} \ K_{c3}) - K_{c4}M \\ K_{c5} \end{pmatrix} \quad (8.52)$$

with λ , δ , and μ given by (6.3), (6.4), and (8.41).

The solution to the gear-shift criterion (8.43) is the transmission-torque controller (8.50), which obtains active damping with a realizable control signal. The parameter η is tuned to balance the behavior of the unconstrained active damping solution (8.36) and the gear-shift condition (8.41). The transmission-torque controller with tuned η is studied in the following example.

Example 8.3 Consider the 144L truck in the same driving situation as in Example 8.1. The transmission-torque controller (8.50) then becomes

$$u = 2.37 \cdot 10^{-4} x_{30} - 0.0327l - \begin{pmatrix} 4.2123 & 0.0207 & -1.2521 \end{pmatrix} x \quad (8.53)$$

where $\eta = 0.03$ and $\sigma = 0.0001$ are used. With this controller the phase margin is guaranteed to be at least 60° and the amplitude margin is infinite [14].

Figure 8.6 shows the resulting transmission torque, the control signal, the engine speed, and the wheel speed when a gear shift is commanded at $t=1$ s, with the control signal chosen according to (8.53).

The transmission-torque controller achieves $z = 0$ with a realizable control signal. The oscillations in the driveline are damped, since the controller forces the engine inertia to work in the opposite direction of the oscillations. Therefore, the time needed for the torque control phase and the speed synchronization phase is minimized, since resonances are damped and engagement of neutral gear is commanded at a torque level giving no oscillations in the transmission speed.

8.4 Influence from Sensor Location

The transmission-torque controller investigated in the previous section uses feedback from all states ($x_1 = \theta_m/i_t i_f - \theta_w$, $x_2 = \dot{\theta}_m$, and $x_3 = \dot{\theta}_w$). A sensor measuring shaft torsion (e.g. x_1) is not used, and therefore an observer is needed to estimate the unknown states. In this work, either the engine speed or the wheel speed is used as input to the observer. This results in different control problems depending on sensor location. Especially the difference in disturbance rejection is investigated.

The observer gain is calculated using Loop-Transfer Recovery (LTR) [14]. The unknown load can be estimated as in Section 6.4.3.

The transmission-torque control law (8.50) becomes

$$u = K_0 x_{30} + K_l l - \begin{pmatrix} K_{c1} & K_{c2} & K_{c3} \end{pmatrix} \hat{x} \quad (8.54)$$

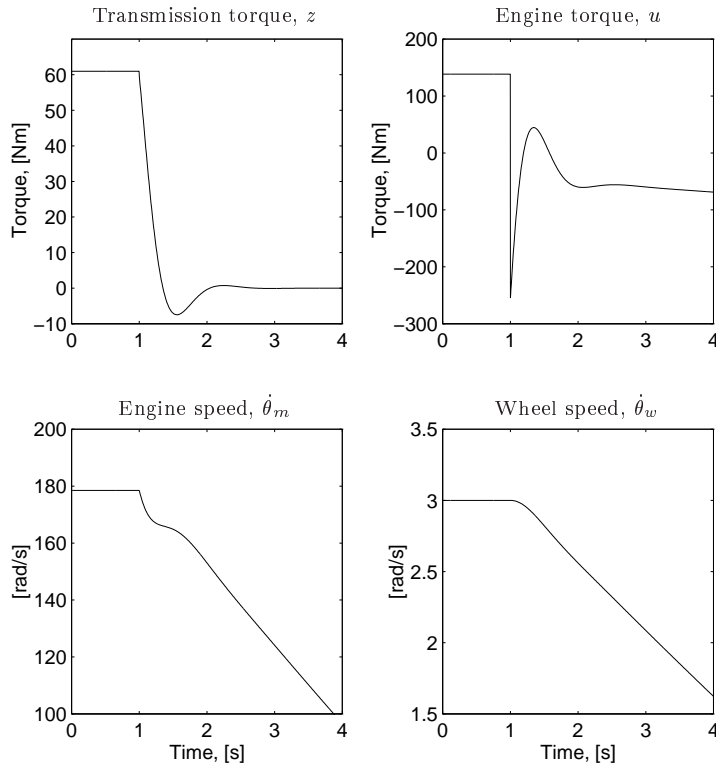


Figure 8.6 The Drive-shaft model controlled with the transmission-torque controller (8.53), solving the gear-shift criterion (8.43). At $t=1$ s, a gear shift is commanded. A realizable control signal is used such that the transmission torque is driven to zero, while oscillations are actively damped.

with K_0 and K_l given by (8.51). The estimated state \hat{x} is given by the Kalman filter

$$\Delta \dot{\hat{x}} = A\Delta \hat{x} + B\Delta u + K_f(\Delta y - C\Delta \hat{x}) \quad (8.55)$$

$$K_f = P_f C^T V^{-1} \quad (8.56)$$

where P_f is found by solving the Riccati equation (6.30).

When using a LQG-controller with feedback from all states, the phase margin, φ , is at least 60° , and the amplitude margin, a , is infinite, as stated before. This is obtained also when using the observer by increasing ρ towards infinity. For Example 8.3 the following values are used

$$\rho_m = 10^4 \Rightarrow \varphi_m = 77.3^\circ, \quad a_m = 2.82 \quad (8.57)$$

$$\rho_w = 10^{11} \Rightarrow \varphi_w = 74.3^\circ, \quad a_w = 2.84 \quad (8.58)$$

where the aim has been to have at least 60° phase margin.

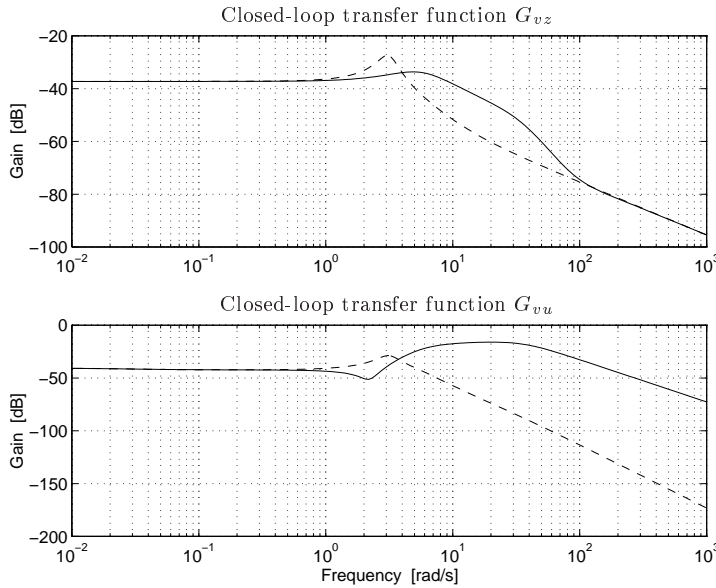


Figure 8.7 Closed-loop transfer functions from load disturbance, v , to performance output, z , and to control signal, u . Feedback from $\hat{\theta}_w$ is shown in solid and feedback from $\hat{\theta}_m$ is shown in dashed lines. With $\hat{\theta}_m$ -feedback the transfer functions have a resonance peak, resulting from the open-loop zeros.

The observer dynamics is cancelled in the transfer functions from reference value, r , to performance output, z , and to control signal, u . Hence, these transfer functions are not affected by the sensor location. However, the dynamics will be included in the transfer functions from disturbances to both z and u .

8.4.1 Influence from Load Disturbances

Figure 8.7 shows how the performance output and the control signal are affected by load disturbances, v . In Section 6.4 it was shown that for the speed controller, the resonant open-loop zeros become poles of the closed-loop system when feedback from the engine-speed sensor is used. The same equations are valid for the transmission-torque controller with the minor difference that the D matrix in the performance output, (8.8), is not equal to zero, as for the speed controller. Hence, also the transfer function DG_{vu} should be added to (6.33). The closed-loop transfer function G_{vu} is given by

$$(G_{vu})_{cl} = -\frac{F_y G_{vy}}{1 + F_y G_{uy}} \quad (8.59)$$

according to (5.18) and the matrix inversion lemma. Thus, the closed-loop transfer function from v to u also has the controller F_y in the numerator. Hence, the closed-loop transfer function from v to z has the open-loop zeros as poles. For

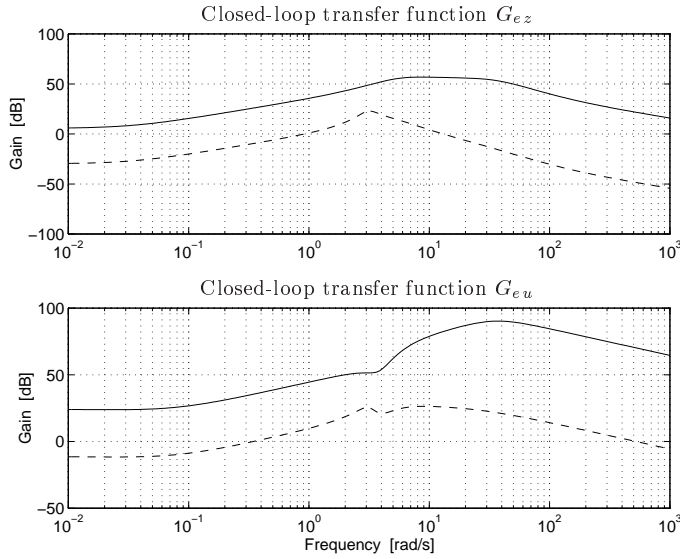


Figure 8.8 Closed-loop transfer functions from measurement noise, e , to performance output, z , and control signal, u . Feedback from $\dot{\theta}_w$ is shown in solid and feedback from $\dot{\theta}_m$ is shown in dashed. The difference between the two feedback principles are described by the dynamic output ratio. The effect increases with lower gears.

$\dot{\theta}_m$ -feedback, this means that a resonance peak is present in the transfer functions from v to performance output and to control signal.

8.4.2 Influence from Measurement Disturbances

The influence from measurement disturbances e are shown in Figure 8.8. According to (6.39) the closed-loop transfer function from e to z is

$$(G_{ez})_{cl} = -\frac{G_{uz}F_y}{1 + G_{uy}F_y} \quad (8.60)$$

Then

$$(G_{ez})_{cl} = -T_w \frac{G_{uz}}{G_{uw}} \quad \text{with } \dot{\theta}_w\text{-feedback} \quad (8.61)$$

$$(G_{ez})_{cl} = -T_m \frac{G_{uz}}{G_{um}} \quad \text{with } \dot{\theta}_m\text{-feedback} \quad (8.62)$$

with the transfer functions T_w and T_m given by (6.40).

When ρ in (6.31) is increased towards infinity, $T_m = T_w$, as was discussed in Section 6.4. Then (8.61) and (8.62) give

$$(G_{ez})_{cl,m} = (G_{ez})_{cl,w} G_{w/m} \quad (8.63)$$

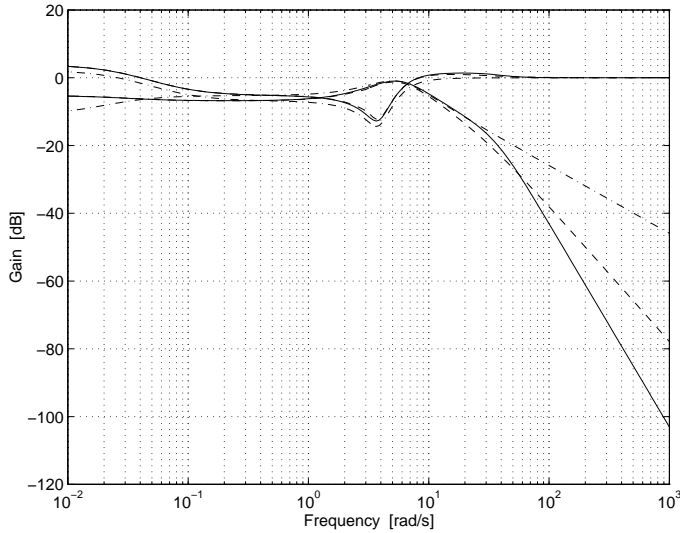


Figure 8.9 Sensitivity function S and complementary sensitivity function T . The dash-dotted lines correspond to the case with all states known. When only one velocity is measured, the solid lines correspond to $\dot{\theta}_w$ -feedback, and the dashed lines correspond to $\dot{\theta}_m$ -feedback.

where cl, m and cl, w denote closed loop with feedback from $\dot{\theta}_m$ and $\dot{\theta}_w$ respectively. The dynamic output ratio $G_{w/m}$ was defined in Definition 5.1, and is given by (6.43).

The frequency range in which the relation $T_m = T_w$ is valid depends on how large ρ in (6.31) is made, as discussed in Section 6.4. Figure 8.9 shows the sensitivity functions (6.45) and the complementary sensitivity functions T_w and T_m (6.40) for the two cases of feedback. It is seen that $T_m = T_w$ is valid up to about 10 rad/s (≈ 1.6 Hz). The roll-off rate at higher frequencies differ between the two feedback principles. This is due to that the open-loop transfer functions G_{uw} and G_{um} have different relative degrees. T_w has a steeper roll-off rate than T_m , because that G_{uw} has a relative degree of two, and G_{um} has a relative degree of only one.

Hence, the difference in G_{ez} depending on sensor location is described by the dynamic output ratio $G_{w/m}$. The difference in low-frequency level is equal to the conversion ratio of the driveline. Therefore, this effect increases with lower gears.

8.5 Simulations

As in the case of the speed controller in Section 6.5, the feasibility of the gear-shift controller is studied by simulating a more complicated vehicle model than it was designed for. Also here, the disturbances that are difficult to systematically generate in real experiments are treated in the simulations. The control design is

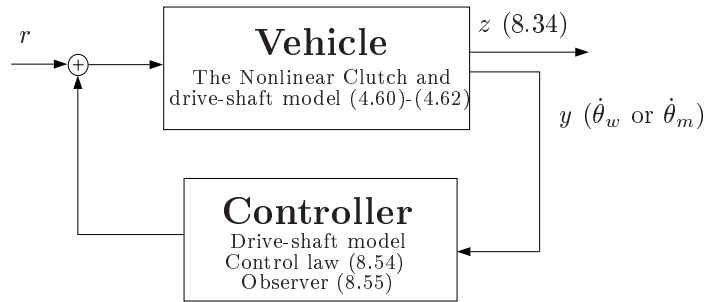


Figure 8.10 Simulation configuration. As a step for demonstrating feasibility for real implementation, the Nonlinear clutch and drive-shaft model is simulated with the controller based on the Drive-shaft model.

simulated with the Nonlinear clutch and drive-shaft model, according to Figure 8.10. The effects from different sensor locations are also studied in accordance with the discussion made in Section 8.4.

The Nonlinear clutch and drive-shaft model is given by Equations (4.60) to (4.62). The steady-state level for the Nonlinear clutch and drive-shaft model is calculated by solving the model equations for the equilibrium point when the load and speed are known. By using the parameter relationship (8.13), the equation for the transmission torque is computed by (8.34).

The transmission-torque controller used is based on the Drive-shaft model, and was developed in the previous sections. The wheel speed or the engine speed is input to the observer (8.55), and the control law (8.54) generates the control signal.

Three simulations are performed with the driving situation as in Example 8.3, (i.e. with wheel speed $\dot{\theta}_w = 3$ rad/s, and load $l = 3000$ Nm). In the simulations, a gear shift is commanded at $t = 2$ s. The first simulation is without disturbances. In the second simulation, the driveline is oscillating prior to the gear shift. The oscillations are a result of a sinusoid disturbance acting on the control signal. The third gear shift is simulated with a load impulse at $t = 3$ s. The disturbance is generated as a square pulse with 0.1 s width and 1200 Nm height.

In order to simulate the nonlinear model, the differential equations (4.60) to (4.62) are scaled such that the five differential equations (one for each state) have about the same magnitude. The model is simulated using the Runge Kutta (45) method [26] with a low step size to catch the effect of the nonlinearity.

Figure 8.11 shows the simulation without any disturbances. This plot should be compared to Figure 8.6 in Example 8.3, where the design is tested on the Drive-shaft model. The result is that the performance does not critically depend on the simplified model structure. The design still works if the extra nonlinear clutch dynamics is added. In the simulation, there are different results depending on which sensor that is used. The model errors between the Drive-shaft model and the Nonlinear clutch and drive-shaft model are better handled when using the wheel-speed sensor.

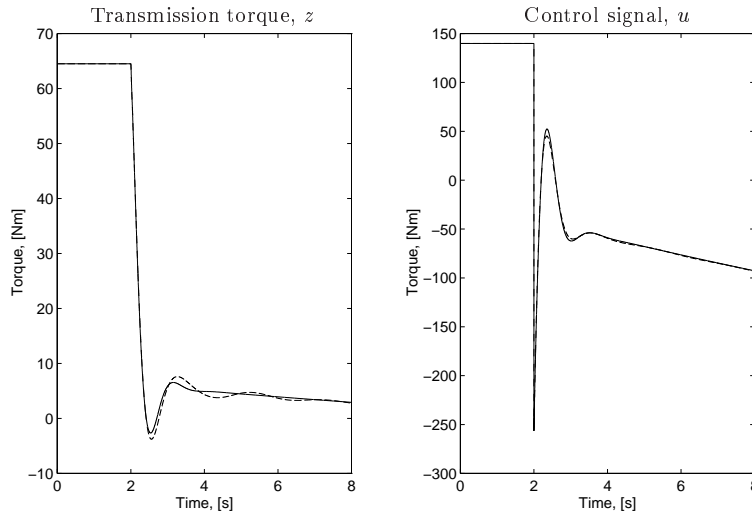


Figure 8.11 Simulation of the Nonlinear clutch and drive-shaft model with observer and control law based on the Drive-shaft model. A gear shift is commanded at $t=2$ s. Feedback from the wheel-speed sensor is shown in solid lines, and feedback from the engine-speed sensor is shown in dashed lines. The design still works when simulated with extra clutch dynamics.

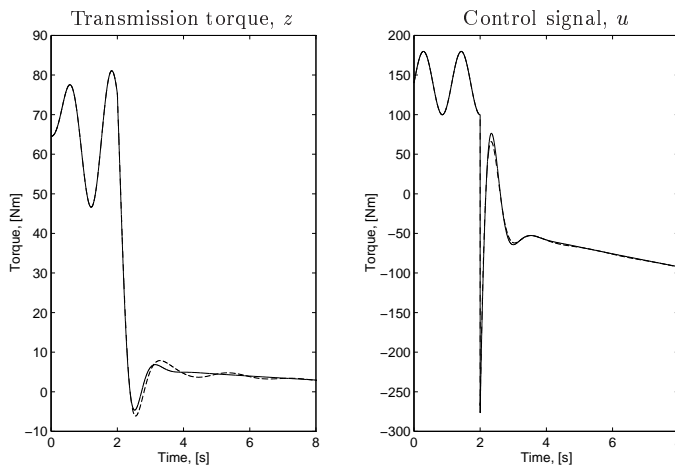


Figure 8.12 Same simulation case as in Figure 8.11, but with driveline oscillations at the start of the transmission-torque controller. Feedback from the wheel-speed sensor is shown in solid lines, and feedback from the engine-speed sensor is shown in dashed lines. The conclusion is that the control law works well despite initial driveline oscillations.

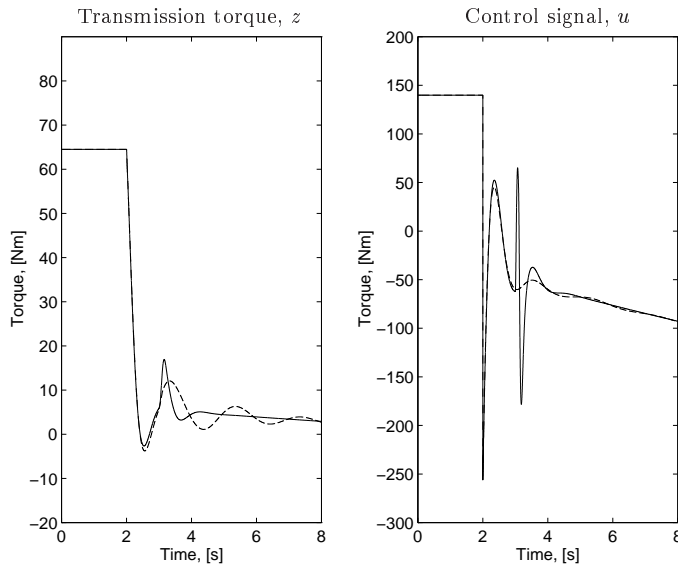


Figure 8.13 Same simulation case as in Figure 8.11, but with a load disturbance at $t=3$ s. Feedback from the wheel-speed sensor is shown in solid lines, and feedback from the engine-speed sensor is shown in dashed lines. The conclusion is that the load disturbance is better attenuated when using feedback from the wheel-speed sensor.

However, neither of the sensor alternatives reaches $z = 0$. This is due to the low-frequency model errors discussed in Section 8.1. In Figure 8.12 the simulation with driveline oscillations prior to the gear shift is shown. The result is that the performance of the controller is not affected by the oscillations. Figure 8.13 shows the simulation with a load disturbance. The disturbance is better damped when using feedback from the wheel-speed sensor, than from the engine-speed sensor, which is a verification of the discussion in Section 8.4.

8.6 Summary

Driveline oscillations are a limiting factor in gear shifting by engine control. Internal driveline torque control is a new idea for handling resonances and optimizing shift quality. A criterion for a gear-shift controller is obtained, based on a model of the transmitted torque in the transmission, characterizing the behavior for each gear. The resulting transmission-torque controller drives the transmission torque to zero with damped driveline resonances.

When using a linear driveline model with drive-shaft flexibility, it is possible to solve the criterion for a control law that minimizes the cost function. The control law is derived with LQG/LTR technique. Simulations show that the controller,

based on the simplified model, works well for a more complicated model with a nonlinear clutch characteristics. However, there can be problems with a low-frequency level that gives a stationary error. This difference in level is a result of the difficulty to estimate driveline friction parameters.

An investigation of the influence that different sensor locations have on the control design results in the same conclusions as in Chapter 6. When using LQG/LTR design methodology the open-loop zeros are cancelled by the controller. This results in undamped load disturbances when engine-speed feedback is used. Therefore, load disturbances are better attenuated with feedback from the wheel-speed sensor.

Measurement disturbances are better attenuated when the engine-speed sensor is used, than when using the wheel-speed sensor. This effect increases with lower gears. Two different closed-loop transfer functions result, depending on feedback configuration. The difference between these two is captured by the dynamic output ratio. As mentioned before, both sensors are normally available on a driveline, but the principle study can be used as a guideline on where to invest in improved sensor quality.

In conclusion, actively damped transmission-torque control works well also in the case of existing initial oscillations. Furthermore, disturbances occurring during the control action are actively damped, and thus reducing the time needed for a gear shift.

Additional Modeling and Analysis for Gear-Shift Control

Gear-shift control is based on control of internal torque in the driveline. A basic question when evaluating field tests is how to validate the controller performance since a measurement of the torque of interest is not available. A number of other indicators must then be used, e.g. the possibility of disengaging a gear, indicating low torque in the transmission. Another important basis for validation is the dynamic behavior of the driveline before and after going from a gear to neutral. This requires additional modeling of the driveline since it is separated in two parts when in neutral. This is the topic of this chapter together with an analysis of the possible oscillation patterns of the decoupled driveline. Besides being used for validation in the next chapter, this analysis will cast light on the sometimes, at first sight, surprising oscillations that occur in an uncontrolled driveline. It will also be used as a further indication for the value of feedback control.

The oscillations in the driveline speeds, following a gear shift, are investigated by performing a number of field trials in Section 9.1. Experiments with three different types of oscillations are presented, which are analyzed in Section 9.2.

9.1 Open-Loop Gear-Shift Experiments

The field-trial platform was described in Chapter 3, and neutral gear is engaged by sending a specific CAN message to the transmission node, which then performs the shift by using a gear lever actuator, driven by air pressure. A delay-time from commanded gear shift to activated gear-lever movement is seen in the experiments. This is a combined effect from a delay in the actuator, and a delay in building up the air pressure needed to overcome friction.

9.1.1 Stationary Trials

First, a series of gear-shifts with a stationary driveline are performed without using driveline torque control. This means that an RQV speed controller controls the engine speed to a desired level, and when the driveline speeds have reached stationary levels, engagement of neutral gear is commanded.

Figure 9.1 shows two of these trials where the engine speed is 1400 RPM and 2100 RPM respectively, on a flat road with gear 1. The behavior of the engine speed, the transmission speed, and the wheel speed is shown in the figure. At $t = 14$ s, a shift to neutral is commanded and there is a delay time before the engagement is completed. This delay is longer the higher the speed is.

After the shift, the driveline is decoupled into two parts. The movement of the engine speed is independent of the movement of the transmission speed and the wheel speed, which are connected by the propeller shaft and the drive shaft, according to Figure 4.1. The RQV controller maintains the desired engine speed also after the gear shift. The transmission speed and the wheel speed, on the other hand, are only affected by the load (rolling resistance, air drag, and road inclination), which explains the decreasing speeds in the figure.

The transient behavior of the transmission speed and the wheel speed differ however, and the energy built up in the shafts is seen to affect the transmission speed more than the wheel speed, giving an oscillating transmission speed. The higher the speed is, the higher amplitude of the oscillations is obtained. The amplitude value of the oscillations for 1400 RPM is 2.5 rad/s, and 5 rad/s for 2100 RPM.

9.1.2 Dynamical Trials

In the previous trials there was no relative speed difference, since the driveline was in a stationary mode. If a relative speed difference is present prior to the gear-shift, there will be a different type of oscillation. Figures 9.2 and 9.3 describe two trials where neutral gear is engaged with an oscillating driveline without torque control. The oscillations are a result of an engine torque pulse at 11.7 s.

There is only a small difference between the measured engine speed and transmission speed prior to the gear shift. This difference was in Chapter 4 explained to be a result of a sensor filter and a stiff clutch flexibility. After the gear shift, the energy built up in the shafts is released, which generates the oscillations and minimizes the difference between the transmission speed and the wheel speed. The two speeds then decrease as a function of the load. Hence, a relative speed difference between the transmission speed and the wheel speed at the shift moment gives oscillations in the transmission speed. The larger the relative speed difference is, the higher the amplitude of the oscillating transmission speed will be.

Figure 9.3 shows a similar experiment as in Figure 9.2, but with neutral gear engaged at 13.2 s. The relative speed difference has opposite sign compared to that in Figure 9.2. The transmission speed transfers to the wheel speed, and these two decrease as a function of the load. However, initially the transmission speed

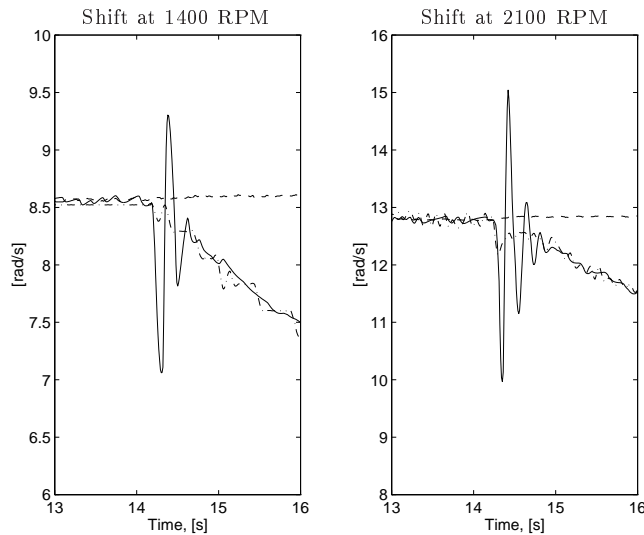


Figure 9.1 Engagement of neutral gear commanded at 14 s, with stationary driveline at 1400 RPM and 2100 RPM on a flat road with gear 1. Engine speed (dashed) and wheel speed (dash-dotted) are scaled to transmission speed which is seen in solid lines. After a delay time, neutral gear is engaged, causing the driveline speeds to oscillate. The amplitude of the oscillating transmission speed is higher the higher the speed is.

deviates in the opposite direction compared to how the relative speed difference indicates, which seems like a surprising behavior.

The three different types of oscillations described by Figures 9.1, 9.2, and 9.3 will in the following be analyzed and explained.

9.2 Predicting Gear-Shift Quality

Engaging neutral gear can be described as in Figure 9.4. Before the gear shift, the driveline dynamics is described by the Drive-shaft model (derived in Chapter 4). This model assumes a lumped engine and transmission inertia, as described previously. When neutral gear is engaged, the driveline is separated into two parts as indicated in the figure. The two parts move independent of each other, as mentioned before. The engine side of the model consists of the engine, the clutch, and part of the transmission (characterized by the parameters J_{t1} and b_{t1} according to Chapter 8). The parameters describing the lumped engine, clutch, and part of transmission are \bar{J}_1 and \bar{b}_1 according to the figure. The wheel side of the model consists of the rest of the transmission (characterized by the parameters J_{t2} and b_{t2}) and the drive-shaft flexibility out to the wheels, which is named the Decoupled model. The model is described by the following equations.

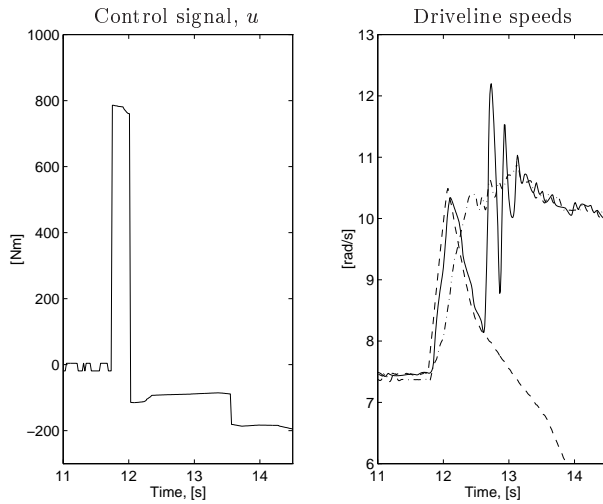


Figure 9.2 Engaged neutral gear without torque control at 12.5 s in a trial with oscillating driveline as a result of a provoking engine torque pulse at 11.7 s in the left figure. Engine speed (dashed) and wheel speed (dash-dotted) are scaled to transmission speed (solid) in the right figure. After the gear shift the transmission speed oscillates.

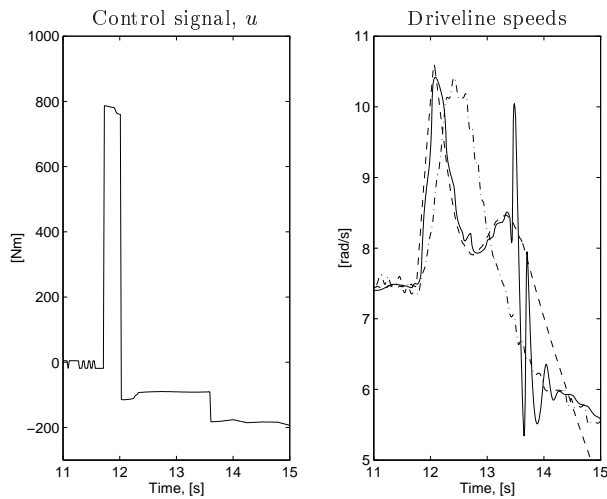


Figure 9.3 Same field trial as in Figure 9.2, but with engaged neutral gear at 13.2 s. Engine speed (dashed) and wheel speed (dash-dotted) are scaled to transmission speed (solid) in the right figure. After the gear shift the transmission speed oscillates.

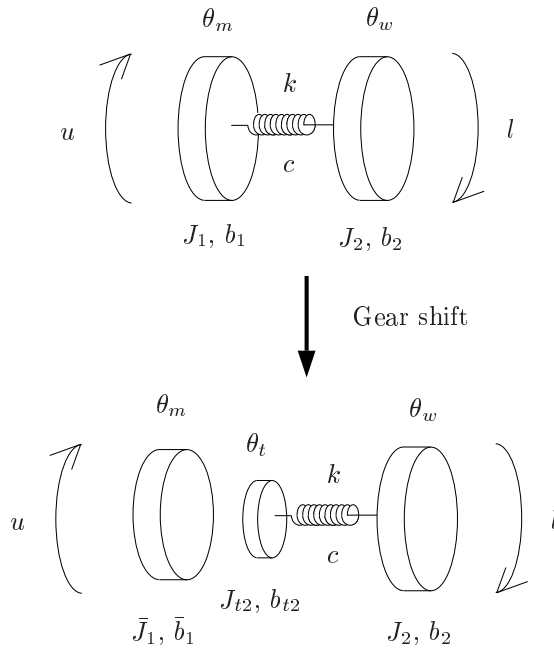


Figure 9.4 Description of how the driveline model changes after engagement of neutral gear. The first model is the *Drive-shaft model* (see Chapter 4), which is then separated into two sub-models when neutral gear is engaged. The left part consists of the engine and one part of the transmission. The right part of the model consists of the rest of the transmission and the drive shaft out to the wheels, called the *Decoupled model*.

The Decoupled Model

$$J_{t2}\ddot{\theta}_t = -b_{t2}\dot{\theta}_t - k(\theta_t/i_f - \theta_w)/i_f - c(\dot{\theta}_t/i_f - \dot{\theta}_w)/i_f \quad (9.1)$$

$$J_2\ddot{\theta}_w = k(\theta_t/i_f - \theta_w) + c(\dot{\theta}_t/i_f - \dot{\theta}_w) - b_2\dot{\theta}_w - l \quad (9.2)$$

The model equipped with the sensor filter in (4.48) gives the true sensor outputs (y_t, y_w) .

All these parameters were estimated in Chapter 4, except the unknown parameters J_{t2} and b_{t2} . The model is written in state-space form by using the states $x_1 =$ drive-shaft torsion, $x_2 =$ transmission speed, and $x_3 =$ wheel speed.

This section is concentrated to the study of the behavior of the Decoupled model after the gear shift. The model structure is the same as the Drive-shaft model, but with the difference that the first inertia is considerable less in the Decoupled model, since the engine and part of the transmission are decoupled from the model.

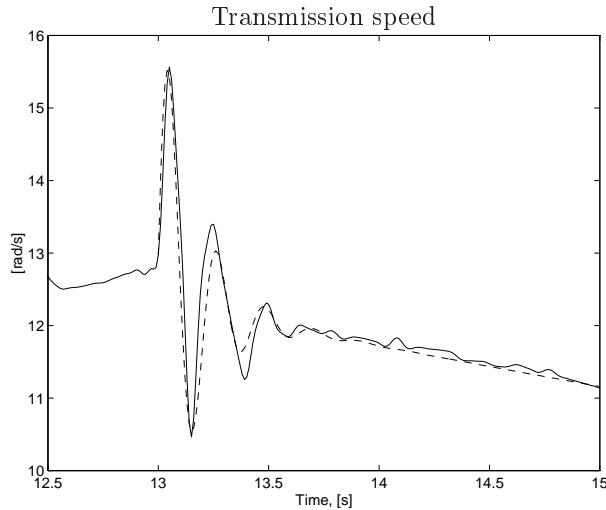


Figure 9.5 Measured oscillations after a gear shift at 13.0 s in solid line. The outputs of the Decoupled model are fitted to data, shown in dashed line. The Decoupled model is able to capture the main resonance in the oscillating transmission speed after the gear shift.

9.2.1 Quality of the Decoupled Model

The unknown parameters J_{t2} and b_{t2} can be estimated if the dynamics described by the Decoupled model is excited. This is the case when engaging neutral gear at a transmission torque level different from zero, giving oscillations. One such case is seen in Figure 9.5, where the oscillating transmission speed is seen together with the Decoupled model with estimated parameters J_{t2} and b_{t2} , and initial drive-shaft torsion, x_{10} . The rest of the parameters are the same as in the Drive-shaft model, which were estimated in Chapter 4. The rest of the initial condition of the states (transmission speed and wheel speed) are the measured values at the time for the gear shift. The model output (y_t and y_w with sensor filter) are fitted to the measured transmission speed and wheel speed. The conclusion is that the Decoupled model is able to capture the main resonance in the oscillating transmission speed.

If the initial states (drive-shaft torsion, transmission speed, and wheel speed) of the Decoupled model are known at the time for engaging neutral gear, the behavior of the speeds after the shift can be predicted. In order to explain the different behavior in the transmission speed seen in Section 9.1, a simulation study with different initial values are performed in the following two subsections.

9.2.2 Simulation of Gear Shifts with Stationary Driveline

First, the Decoupled model is simulated with a stationary driveline, i.e. without relative speed difference between the transmission speed and the wheel speed. The

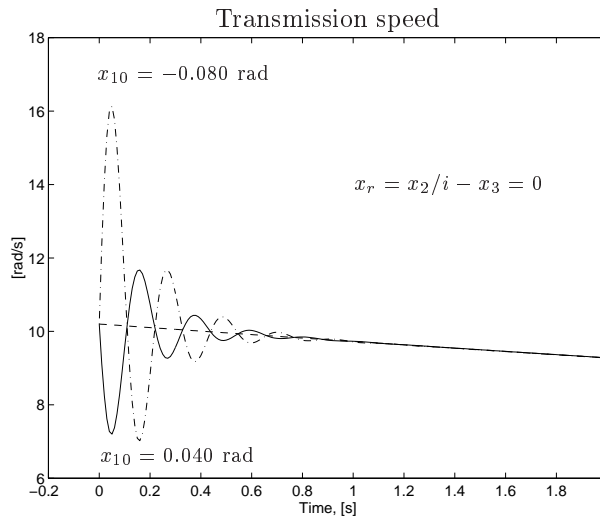


Figure 9.6 Transmission speed oscillations after engagement of neutral gear. The Decoupled model is simulated with different initial values of the drive-shaft torsion, x_{10} . The relative speed difference, $x_r = x_2/i - x_3$, is equal to zero. The dashed line with no oscillations has the initial value $x_{10} = -0.004$ rad. The higher the drive-shaft torsion is, the higher the amplitude of the oscillations will be.

influence from different initial drive-shaft torsions on the transmission speed are studied in Figure 9.6.

The higher the drive-shaft torsion is, the higher the amplitude of the oscillations will be. This was also the case in the experiments shown in Section 9.1 (Figure 9.1), since a higher speed requires a higher drive-shaft torsion to maintain the speed. However, in order to have no oscillations in the transmission speed, there must be a small negative drive-shaft torsion ($x_{10} = -0.004$ rad in the figure). The reason for this is to balance the torque resulting from the viscous friction component b_{t2} . This effect is seen in the simulations, but in experiments, the effect is not detectable together with measurement disturbances.

9.2.3 Simulation of Gear Shifts with Driveline Oscillations

To analyze gear shifts with oscillating driveline, simulations are performed with a constant relative speed difference. Figure 9.7 shows the transmission speed for three simulations with the same initial speed difference, $x_r = 3$ rad/s, but with different initial drive-shaft torsions, x_{10} .

The transmission speed oscillates also when the drive-shaft torsion has a value that gave no oscillations in the stationary simulations (Figure 9.6). The reason for this is that the energy stored in the drive shaft is transferred to speed oscillations, and since the first inertia of the Decoupled model is almost 900 times smaller than

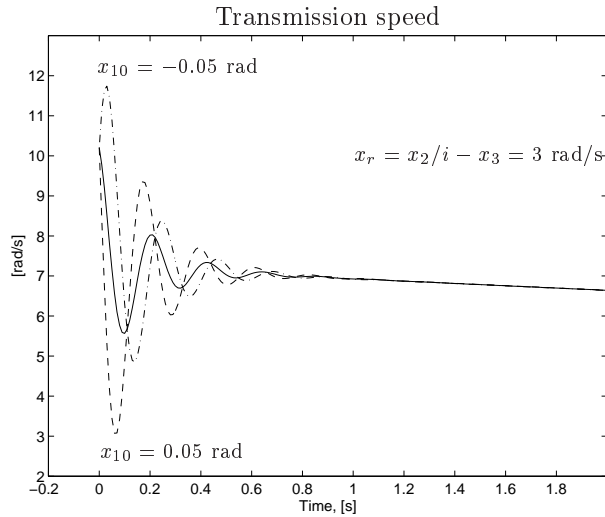


Figure 9.7 Transmission speed oscillations after engagement of neutral gear. The Decoupled model is simulated with a relative speed difference, $x_r = x_2/i - x_3$, equal to 3 rad/s, and with three different initial values of the drive-shaft torsion, $x_{10} = -0.050$ rad (dash-dotted), $x_{10} = -0.004$ rad (solid), and $x_{10} = 0.050$ rad (dashed).

the wheel inertia, almost all energy is released as transmission speed oscillations. The transmission speed is transferred to wheel speed, and the higher the speed difference is, the higher the oscillations will be before the difference between the speeds is minimized.

If the drive-shaft torsion is different from zero, the oscillation is a combined effect from the relative speed difference and the drive-shaft torsion. This means that the oscillation is increased if x_1 has a value greater than zero (according to the dashed line in Figure 9.7). If x_1 has a value less than zero, the initial direction of the oscillation will be opposite the oscillation resulting from the relative speed difference (according to the dashed-dotted line in Figure 9.7). This analysis explains the different characteristics seen in Section 9.1 (Figures 9.2 and 9.3).

Summary

The different characteristic oscillations seen in the experiments after engaged neutral gear are explained by the value of the drive-shaft torsion and the relative speed difference at the time of engagement. The Decoupled model can be used to predict the behavior of the driveline speeds if these initial variables are known. The demonstration of problems with an uncontrolled driveline motivates the need for feedback control in order to minimize the oscillations after a gear shift.

Gear-Shift Controller Experiments

The quality of gear shifts can be optimized by internal driveline torque control when using automatic gear shifting by engine control. This was demonstrated in Chapter 8 where a transmission-torque controller was derived, based on a model of the transmission. In order to implement this strategy and validate the results, the unknown parameters describing the transmission torque must be estimated for each gear. The values of these parameters are difficult to estimate, since the truck used for experiments has no sensor measuring the transmission torque.

A different variant of internal driveline torque control is proposed in this chapter, where control of the drive-shaft torsion to zero is assumed to give sufficient gear-shift quality. This is motivated by the fact that the drive shaft is the main flexibility of the driveline, according to Chapter 4. If this torsion is small it is reasonable to believe that the transmission torque also is small, if the dynamical effects in the transmission are neglected. The estimation of the drive-shaft torsion is easier performed than estimating the transmission torque. No extra parameters are requested, because the drive-shaft torsion is one of the states in the **Drive-shaft model**. The controlling of the drive-shaft torsion is a more robust method, since the different behavior for each gear is neglected, and the drive shaft is the same for all gears. Another advantage with using a simpler scheme, utilizing a consistent physical variable, is that extensions to monitoring, supervision, and adaptive control are simpler.

In order to validate these assumptions, it is necessary to demonstrate that the estimated drive-shaft torsion is sufficiently accurate for gear-shift control. Since there is no transmission-torque sensor that can be used for validation, the only measure of gear-shift quality is to use the measured driveline speeds. If neutral gear

is engaged at an improper torque level, there will be oscillations in the transmission speed as discussed in Chapter 9.

The reasons for using control of the drive-shaft torsion are further motivated in Section 10.1. The derivation and validation of a virtual drive-shaft torsion sensor is covered in Section 10.2. The torsion is estimated by using the measured engine speed and wheel speed in a Kalman filter and is validated in field trials. Finally, the controlling of the drive-shaft torsion to zero is given experimental and theoretical treatment in Section 10.3, which forms a major contribution of the chapter.

10.1 Internal Driveline Torque

In Chapter 8, internal torque control was investigated by controlling the estimated transmitted torque in the transmission. The aim of this chapter is to develop a simpler and more robust scheme, that is feasible for implementation with standard automotive sensors, as mentioned before. The proposed strategy is to control the drive-shaft torsion to zero with the use of a virtual drive-shaft torsion sensor, derived later. This section will give further motivation for selecting the drive-shaft torsion as internal driveline torque, together with a demonstration of the problems of estimating the correct parameters describing the transmission torque. In Section 10.3, the choice of control scheme will be validated in closed-loop tests.

Estimation of transmission-torque parameters

The transmission torque, z , for the Drive-shaft model is derived as a function of the control signal, u , and the states, x_1 , x_2 , and x_3 in (8.8) as

$$\begin{aligned} z &= Mx + Du \quad \text{with} \\ M^T &= \begin{pmatrix} \frac{(J_m + J_{t1})k}{J_1 i} \\ \frac{J_m + J_{t1}}{J_1} (b_1 + c/i^2) - b_{t1} \\ -\frac{(J_m + J_{t1})c}{J_1 i} \end{pmatrix} \\ D &= 1 - \frac{J_m + J_{t1}}{J_1} \end{aligned} \quad (10.1)$$

The unknown parameters in the transmission are J_{t1} , J_{t2} , b_{t1} , and b_{t2} . The relation between these is given by (8.11) and (8.12) as

$$J_t = i_t^2 J_{t1} + J_{t2} \quad (10.2)$$

$$b_t = i_t^2 b_{t1} + b_{t2} \quad (10.3)$$

where J_t and b_t are the total inertia and viscous friction components of the transmission, according to Chapter 8. The parameters J_{t2} and b_{t2} were estimated in Section 9.2 and therefore J_{t1} and b_{t1} in (10.1) can be solved for if J_t and b_t are known, by using (10.2) and (10.3).

The first inertia of the Drive-shaft model has the estimated parameters

$$J_1 = J_m + J_t/i_t^2 + J_f/i_t^2 i_f^2 \quad (10.4)$$

$$b_1 = b_t/i_t^2 + b_f/i_t^2 i_f^2$$

Hence, J_t and b_t are not directly estimated by the procedure used in Chapter 4. Tests have been performed in order to fully estimate the unknowns in (10.1), but with poor results. The main reason is that there is no actual measure of the transmitted torque in the transmission.

Influence from drive-shaft torsion

Real experiments and a simulation study in the previous chapter have concluded that the oscillation in the transmission speed is a function of the drive-shaft torsion, x_1 , and the relative speed difference, x_r , at the moment of engagement. Is it the same thing to have $z = 0$ in (10.1) as to have no oscillations in the transmission speed? Equation (10.1) shows that the answer is no, since the transmission torque is also a function of the control signal, which has no influence on the Decoupled model (9.1) and (9.2). However, this effect is probably very small since the term $u(1 - (J_m + J_{t1})/J_1)$ is small compared to other terms in (10.1).

The dominating term in (10.1) is $x_1(J_m + J_{t1})k/J_1 i$, which is an indication of how important the drive-shaft torsion is for describing the transmission torque. Further support to this is seen in Figures 10.1 and 10.2, where the estimated drive-shaft torsion, x_1 , and the measured relative speed difference, x_r , are shown. It is demonstrated that the delay time from commanded to engaged neutral gear, which is a measure of how easily neutral gear can be engaged, depends strongly on how close to zero x_1 is. The figures show that neutral gear is not engaged until x_1 is close to zero again.

Influence from relative speed difference

The actual torque transferred in the drive-shaft is also a function of the relative speed difference, x_r , due to internal damping (the torque transferred is $kx_1 + cx_r$). However, the relative speed difference has little influence on the ability to engage neutral gear, which can be seen in Figure 10.1. During the delay time from commanded to engaged neutral gear, x_r varies from negative to positive values, but neutral gear is not engaged until x_1 is small again. Another motivation is seen in Figure 10.2. Neutral gear is engaged at a low drive-shaft torsion, $x_1 = -0.0078$ rad, after a short delay time, but at the moment of engagement, x_r has a negative value.

Hence, neutral gear can successfully be engaged if the drive-shaft torsion, x_1 , is close to zero. This is true also if the relative speed difference is different from zero. The rest of this chapter treats the hypothesis that it is sufficient to control the drive-shaft torsion to zero for gear shifts with acceptable quality.

10.2 Virtual Drive-Shaft Torsion Sensor

Control of the drive-shaft torsion is performed with a virtual drive-shaft torsion sensor, since the truck used for experiments uses no torsion sensor. The derivation

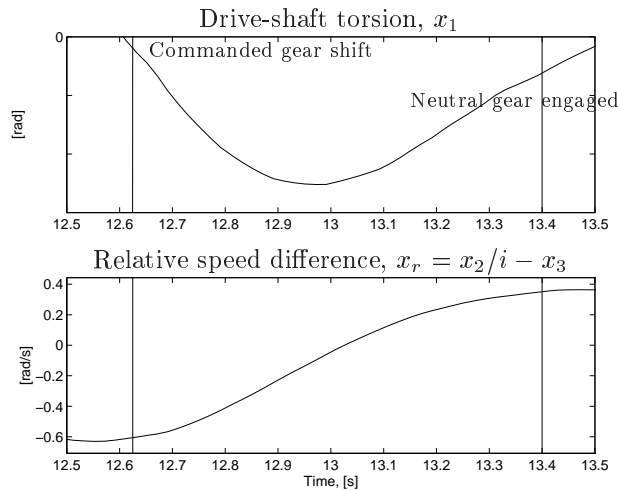


Figure 10.1 Field trial with gear shift when the driveline is oscillating. The estimated drive-shaft torsion and the measured relative speed difference between the transmission speed and the wheel speed are shown for a gear shift commanded at 12.63 s. Neutral gear is not engaged until x_1 is close to zero (at 13.40 s indicated by the second vertical line), after a large delay time.

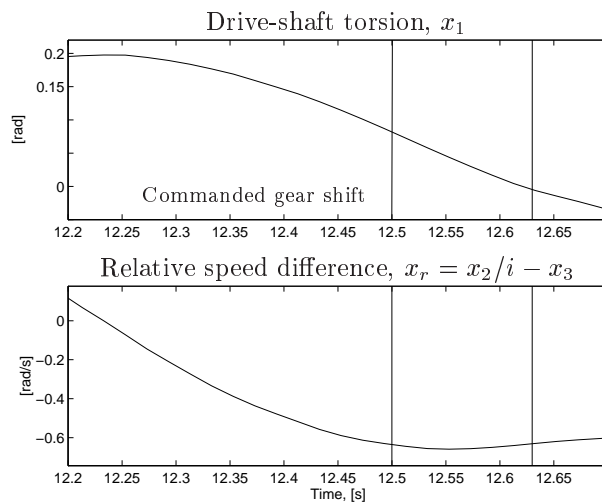


Figure 10.2 Field trial with gear shift when the driveline is oscillating. The estimated drive-shaft torsion and the measured relative speed difference are shown for a gear shift commanded at 12.50 s. Neutral gear is engaged after 12.63 s, indicated by the second vertical line, after a small delay time.

and validation of this sensor is the topic of this section. The modeling in Chapter 4 concluded that the Drive-shaft model estimated a drive-shaft torsion with realistic values. A virtual sensor is constructed by using this model together with the measured engine speed and wheel speed.

The drive-shaft torsion has in previous chapters been estimated by an observer with either the engine speed or the wheel speed as input. The quality of the torsion estimate is in this chapter of central importance, and to eliminate sources of errors, both engine speed and wheel speed measurements are used as inputs to the observer in this chapter. (By this way, not only the drive-shaft torsion is estimated, but also the total torque transmitted in the drive shaft, which is equal to $kx_1 + c(x_2/i - x_3)$.)

The observer gain was determined by solving a Riccati equation with weights adjusted such that the engine speed and wheel speed are estimated as close as possible, without following quantification errors and measurement errors. The observer was implemented in the same way as the observer with one input in Chapter 7.

An example of how the observer with engine speed and wheel speed inputs performs on-line is seen in Figure 10.3. It is shown how the measured signals are closely estimated, which gives support to the estimated drive-shaft torsion.

In the following subsections, the estimated drive-shaft torsion will be validated. There is no direct way of validating the estimate, since there is no sensor to compare with. On the other hand, the previous chapter described a way in which the drive-shaft torsion could be found by studying the oscillations in the transmission speed after neutral gear is engaged. The on-line estimated drive-shaft torsion should be equal to the initial drive-shaft torsion explaining the oscillations in the transmission speed after neutral gear is engaged. Hence, a series of experiments with engagement at different on-line estimated values of x_1 are performed in the following subsections.

10.2.1 Validation in Stationary Trials

The estimated drive-shaft torsion is validated by first performing field trials with stationary driveline, of the form described in Section 9.1 (Figure 9.1). Neutral gear is engaged with different stationary speeds. For every trial, the initial drive-shaft torsion, x_{10} , and the parameters J_{t2} and b_{t2} of the Decoupled model, derived in Chapter 9, are fitted to the measured oscillation after the shift.

The result is that the estimated x_{10} agree well with the on-line estimates of the drive-shaft torsion. However, validation with this type of experiments only covers a small range of drive-shaft torsions. To maintain the stationary speed, it only requires a small torque amount, which means that the drive-shaft torsion is small.

10.2.2 Validation in Dynamical Trials

To validate the estimated torsion in dynamical trials, the driveline is set to oscillate by an engine torque pulse, as described before (see e.g. Figure 10.3). Neutral gear is then commanded at different time delays after the torque pulse has occurred.

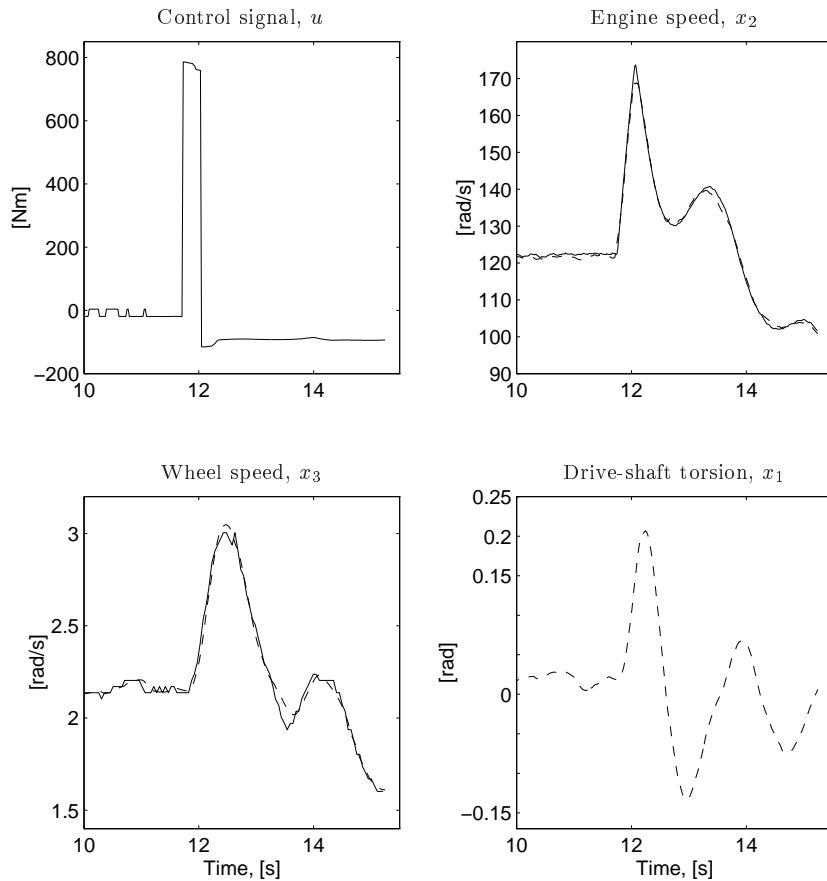


Figure 10.3 Field trial with driveline oscillations excited by an engine torque pulse (at 11.7 s). Measured engine torque, engine speed, and wheel speed are represented by solid lines. The observer estimates the engine speed, the wheel speed, and the drive-shaft torsion, on-line (dashed lines).

Figures 10.4, 10.5, and 10.6 show three different trials generated in the same way, with the only difference that the gear-shift is commanded after 0.50, 0.60, and 0.63 s after the engine torque pulse has occurred.

The measured transmission speed and the on-line estimated drive-shaft torsion, x_1 , are seen in the figures. From the oscillation after the gear shift, the initial drive-shaft torsion x_{10} is estimated and this value agrees well with the on-line estimate, which is a validation of the virtual drive-shaft sensor.

In Figure 10.4, the delay time from commanded shift to completed shift is small due to a low transmission torque at the shift moment. In Figures 10.5, the gear shift is commanded 0.1 s later, but neutral gear is not engaged until after

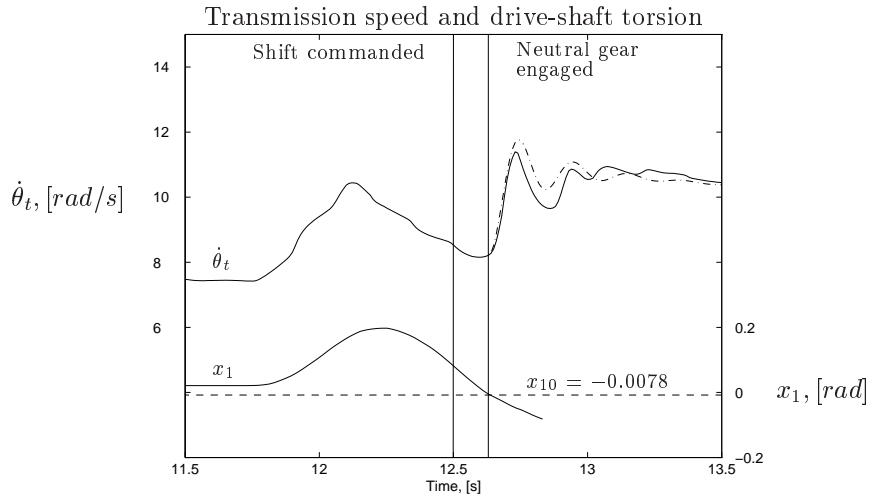


Figure 10.4 Measured transmission speed and estimated drive-shaft torsion during a test with oscillating driveline and a commanded gear shift at 12.5 s. Neutral gear is engaged at 12.63 s. The output of the fitted *Decoupled model* is the dash-dotted line with the estimated initial drive-shaft torsion value, x_{10} , plotted as a dashed horizontal line. The estimated initial value x_{10} agrees well with the on-line estimated x_1 at the time of engagement.

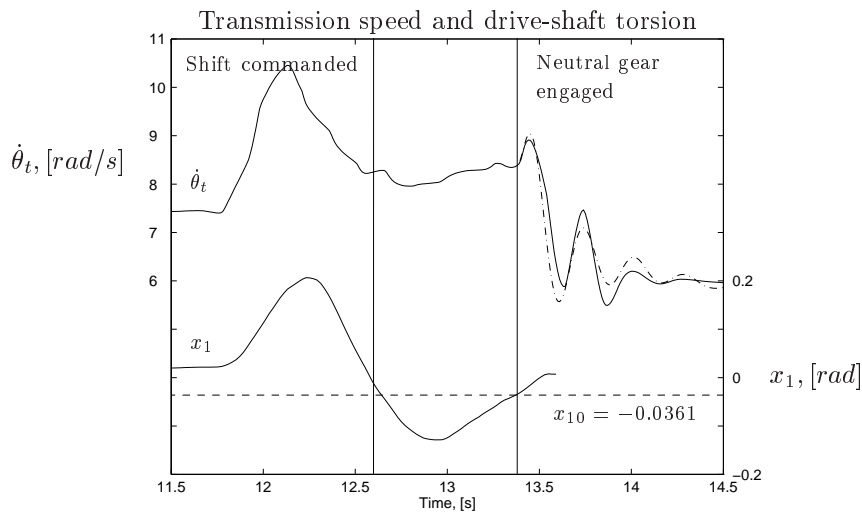


Figure 10.5 Similar experiment as in Figure 10.4, but the gear shift is commanded at 12.60 s, and neutral gear is engaged at 13.38 s. The long delay time from commanded to completed shift is due to the large negative values of x_1 .

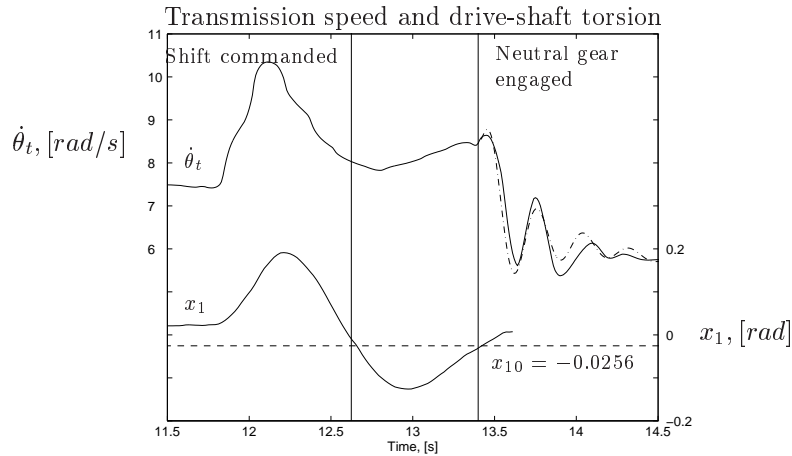


Figure 10.6 Similar experiment as in Figure 10.4, but the gear shift is commanded at 12.63 s, and neutral gear is engaged at 13.40 s. The long delay time from commanded to completed shift is due to the large negative values of x_1 .

0.78 s, indicating a high transmission torque during the delay time. About the same observation can be seen in Figure 10.6. For these trials, where there is a long time delay from commanded to engaged gear, the on-line estimated torsion, x_1 , sometimes has a higher value than the initial value of the Decoupled model, x_{10} .

10.3 Drive-Shaft Torsion Control

The goal is now to control the drive-shaft torsion to zero with damped driveline resonances, and verify that sufficient gear-shift quality is obtained. The controller goal means that both x_1 and x_r are driven to zero, since the driveline resonances are minimized. The oscillations in the transmission speed and the wheel speed after the gear shift are then minimized, according to Section 9.2.

10.3.1 Controller Structure for Active Damping

Active damping was in Chapter 8 achieved by minimizing a criterion, giving a state-feedback law that calculates the fuel amount. Before selecting controller structure for drive-shaft torsion control, the open-loop transfer function from control signal, u , to drive-shaft torsion, x_1 , is investigated. The poles and zeros of the transfer function are shown in Figure 10.7. One interesting fact is that the zero and the real pole are close to cancel each other. If they do cancel, the third order system will act as if it is a second order system with no zero. The same result is also valid for higher gears. When controlling a second order system with no zero, it is sufficient to have a second order controller in order to be able to move the poles to any location.

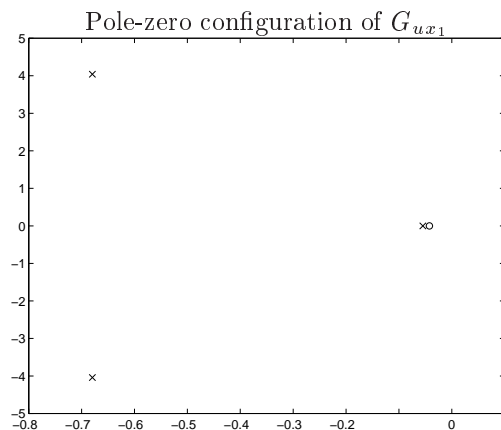


Figure 10.7 Poles and zeros of the transfer function from control signal to drive-shaft torsion. (Calculated from the *Drive-shaft model* fitted to data in Chapter 4 for gear 1.) The third order model is reduced to a second order model by the cancellation of the real pole by the zero. Similar results are found for higher gears.

A PID controller controlling the drive-shaft torsion is simulated with a gear shift commanded at a stationary speed of 1900 RPM and gear 1. The resulting drive-shaft torsion with and without derivative part is shown in Figure 10.8. The controller parameters are obtained by first tuning the proportional parameter such the negative peak values of the engine torque is possible to generate for the diesel engine. The integral parameter is then adjusted so that $x_1 = 0$ is obtained after the oscillations are damped out. Finally, the derivative parameter is tuned until the drive-shaft torsion is well damped, according to Figure 10.8.

Hence, active damping can be obtained with a simple PID controller structure. This controller structure has natural parameter tuning properties with a derivative part that determines the amount of active damping of driveline resonances. The integral part guarantees that the control signal is such that there is no stationary error. This means that the procedure of calculating the gear-shift condition (8.41) (as a function of the working point) is not needed.

10.3.2 Demonstration of Active Damping in Field Trials

A PID controller with anti-windup is implemented which controls the output of the virtual sensor to zero. Figure 10.9 shows a first trial with a PI controller in dashed lines. The proportional part of the controller gives the speed of the controller, but is not sufficient for damping out the oscillations in the driveline. This was also demonstrated in the simulations, and is due to the resonant pole-pair seen in Figure 10.7, which cannot be damped by a proportional controller. Finally, the derivative part is adjusted to obtain active damping, which is seen in Figure 10.9 in solid lines.

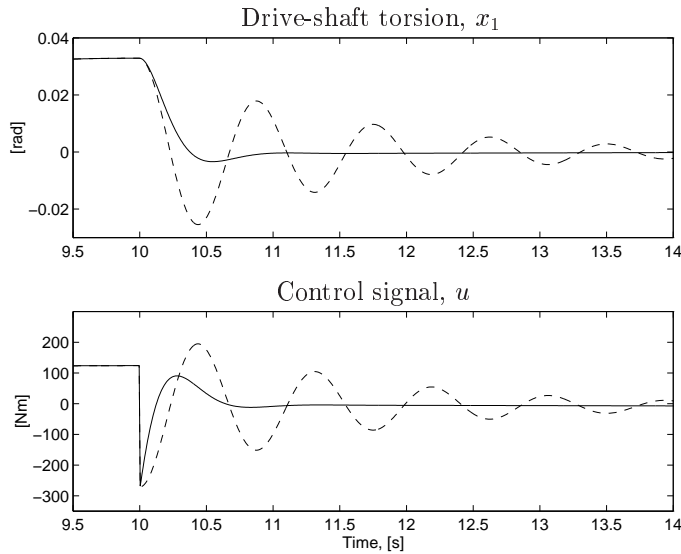


Figure 10.8 Simulated control of the drive-shaft torsion to zero with a PID controller starting at 10.0 s. Prior to that, the engine has the stationary speed 1900 RPM with gear 1 engaged. A PI controller (dashed lines) is used that obtains $x_1 = 0$, but with undamped driveline resonances. The solid lines are extension with derivative part in the controller. Active damping is obtained with a simple PID controller structure.

Hence, active damping is obtained in field trials with a PID controller and a virtual sensor measuring the drive-shaft torsion. This gives additional support to the Drive-shaft model structure and parameters, derived in Chapter 4, since the observation with cancellation of a pole and a zero also holds in field trials.

10.3.3 Validation of Controller Goal

The drive-shaft torsion is controlled to zero with damped driveline resonances, which was the goal of the controller. However, it is not yet proved that this actually is sufficient for engaging neutral gear with sufficient quality (short delay and no oscillations). The way to prove this is to use the controller demonstrated in Figure 10.9, and engage neutral gear and measure the oscillations in the transmission speed. This is done in Figures 10.10 to 10.12, where the controller is started at 12.0 s and gear shifts are commanded every 0.25 s, starting at 12.25 s.

From these figures, it is clear that controlling the drive-shaft torsion to zero is sufficient for obtaining gear shifts with short delay time (compare this with the results in Figures 10.5 and 10.6). Oscillations in transmission speed are minimized to under 1 rad/s in amplitude with different signs, which is well in the range for giving no disturbance to the driver. Furthermore, the speed synchronization phase,

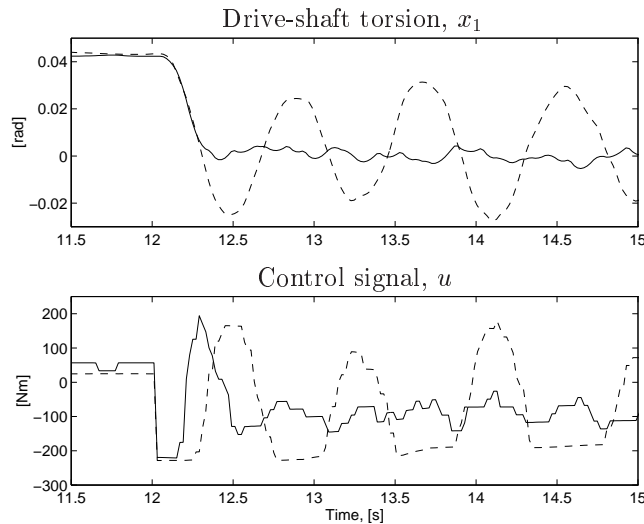


Figure 10.9 Control signal and drive-shaft torsion when using the gear-shift controller that controls the drive-shaft torsion to zero, started at 12.0 s. Prior to that, the engine has the stationary speed 1900 RPM with gear 1 engaged. In dashed lines, a PI controller is used that gives $x_1 = 0$, but with undamped driveline resonances. The solid lines are extension with derivative part in the controller. A PID controller structure is sufficient for obtaining active damping in field trials.

where the engine speed is controlled to match the propeller shaft speed, can be done fast, since there are only minor oscillations in the transmission speed.

Figure 10.10 also shows that a gear shift can be commanded after only 0.25 s after the controller has started, and an acceptable shift quality is obtained. These results are for gear 1, where the problems with oscillations are largest. The time to a commanded engagement of neutral gear can be decreased further for higher gears.

10.3.4 Gear Shifts with Initial Driveline Oscillations

One important problem, necessary to handle, is when a gear shift is commanded at a state where the driveline is oscillating. This was discussed in Chapter 8 where the controller was simulated with initial driveline oscillations. To verify that the PID controller structure can handle this situation and that it also works in real experiments, driveline resonances are excited by an engine torque pulse at 11.7 s, according to Figure 10.13.

Figures 10.13 to 10.15 show the same type of experiments, but the controller is started at different time delays after the engine torque pulse has occurred. For all three experiments, the resulting engine torque, calculated by the feedback controller, actively damps the initial driveline oscillations and obtains $x_1 = 0$.

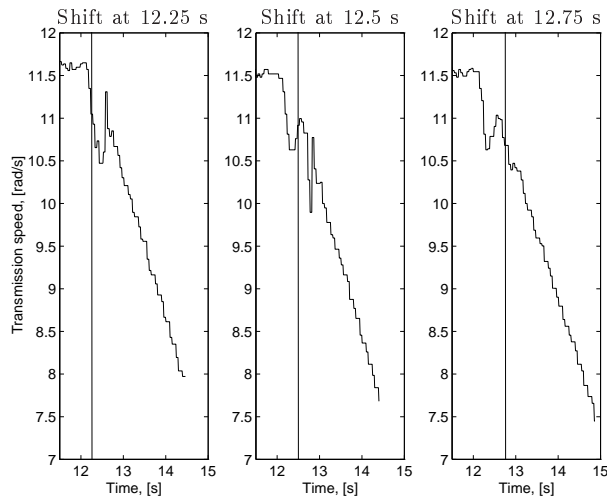


Figure 10.10 Field trials with start of the gear-shift controller at 12.0 s, all with the same PID controller controlling the drive-shaft torsion to zero. Engagement of neutral gear is commanded every 0.25 s after the start of the controller, indicated by the vertical lines. The transmission speed is seen when neutral gear is engaged after a delay time. The amplitudes of the transmission speed oscillations after the gear shift are less than 1 rad/s with different signs, which is an acceptable level.

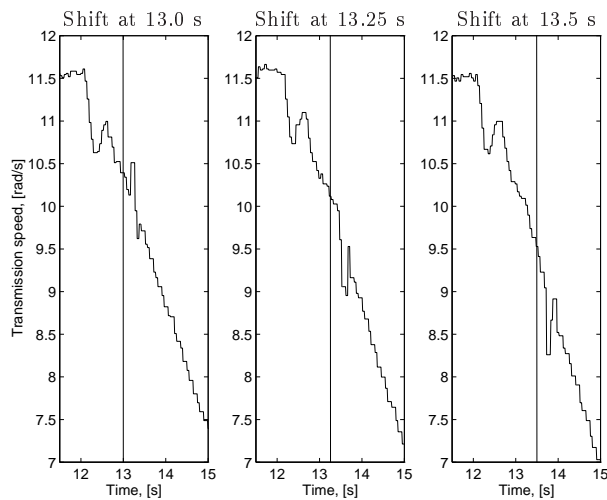


Figure 10.11 Same type of field experiment as in Figure 10.10, but with commanded engagement of neutral gear at 13.0, 13.25, and 13.5 s. The amplitudes of the transmission speed oscillations after the gear shift are less than 1 rad/s with different signs, which is an acceptable level.

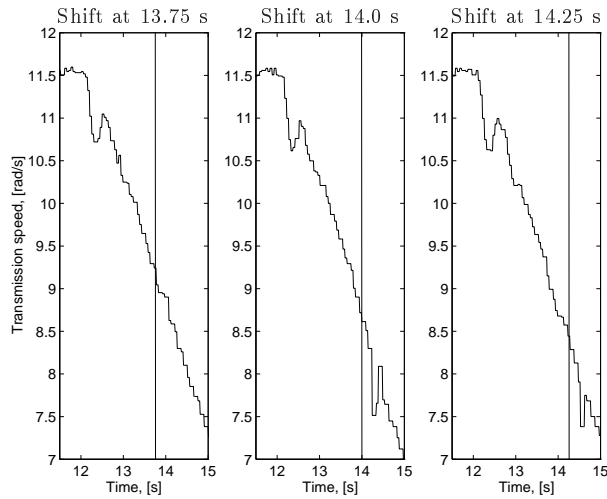


Figure 10.12 Same type of field experiment as in Figure 10.10, but with commanded engagement of neutral gear at 13.75, 14.0, and 14.25 s. The amplitudes of the transmission speed oscillations after the gear shift are less than 1 rad/s with different signs, which is an acceptable level.

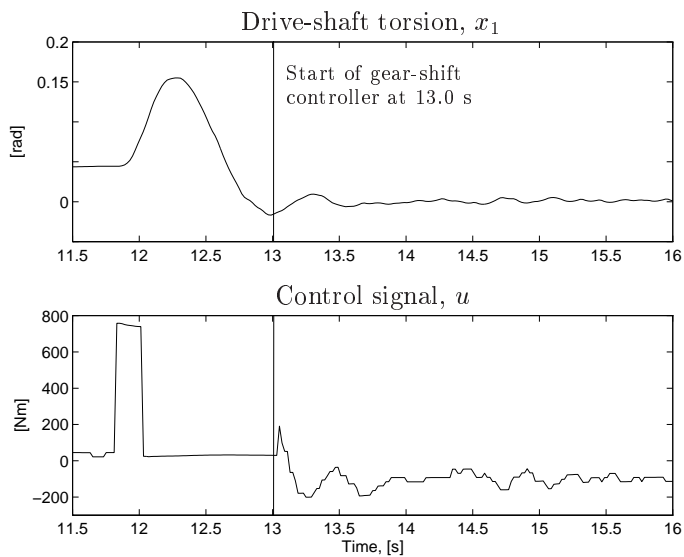


Figure 10.13 Control signal and drive-shaft torsion during field trials with start of the gear-shift controller at 13.0 s. The driveline is oscillating prior to the gear shift due to an engine torque pulse at 11.7 s. The controller controls the drive-shaft torsion to zero with damped resonances despite initial driveline oscillations.

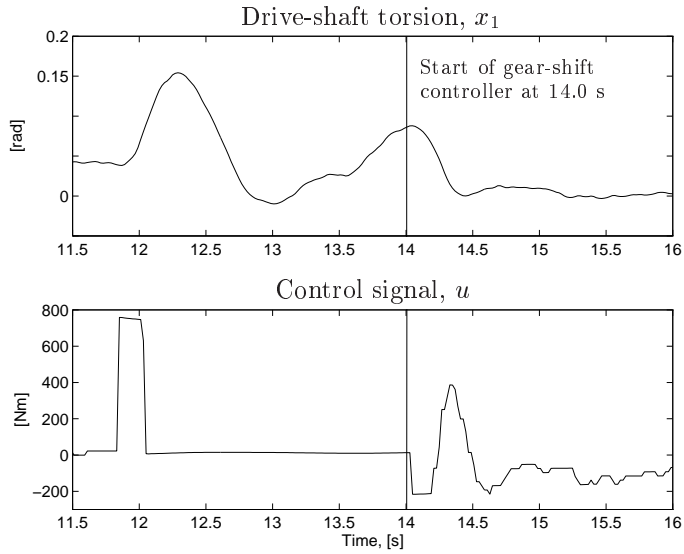


Figure 10.14 Control signal and drive-shaft torsion during field trials with start of the gear-shift controller at 14.0 s. The controller controls the drive-shaft torsion to zero with damped resonances despite initial driveline oscillations.

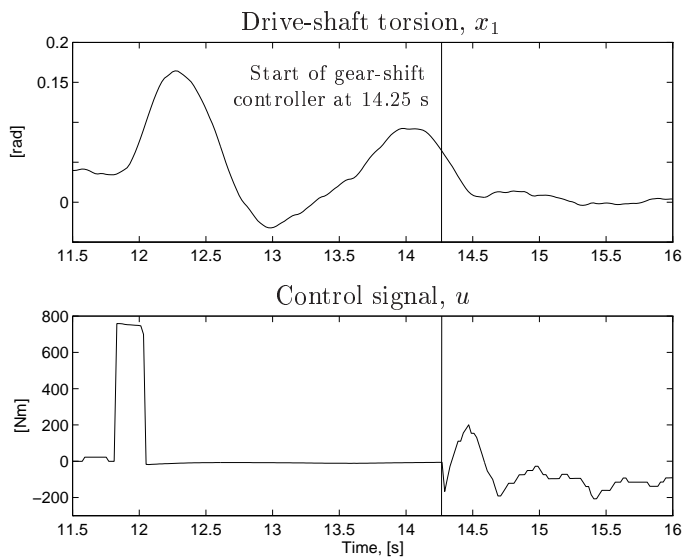


Figure 10.15 Control signal and drive-shaft torsion during field trials with start of the gear-shift controller at 14.25 s. The controller controls the drive-shaft torsion to zero with damped resonances despite initial driveline oscillations.

The difference in control signal in Figures 10.13 to 10.15 is a strong evidence that driveline dynamics affects shift performance so much that feedback control is motivated. An open-loop scheme would not be able to handle these initial oscillations, leading to longer time for gear shifts.

10.4 Summary

The main contribution of this chapter is a demonstration of gear-shift control with optimized shift quality, implemented with standard automotive sensors. The idea used is that gear-shift control can be obtained by controlling the drive-shaft torsion to zero. This approach is motivated by the following two main advantages

- When the drive-shaft torsion is zero, neutral gear can be engaged fast, with only small oscillations in the transmission speed and no oscillations in the wheel speed.
- By controlling the drive-shaft torsion, it is sufficient to use an observer in combination with a PID controller structure, with simple tuning rules, for obtaining active damping of driveline resonances. The reason for this is that the third order system can be treated as a second order system when considering the drive-shaft torsion as output.

Control of the drive-shaft torsion is implemented by estimating the drive-shaft torsion from the measured engine speed and wheel speed. This is shown to give sufficient accuracy for gear-shift control.

Active damping of driveline resonances gives a way of optimizing the time needed for the torque control phase, and since there will be no oscillations in the transmission speed, the new gear can be engaged with a minimum of time spent in the speed synchronization phase, and thus leading to a minimized time for a gear shift.

The problems with low-frequency errors due to friction parameter errors, described in Chapter 8, are avoided by the use of feedback. This also means that there is a measure of gear-shift quality, since the deviation from zero in drive-shaft torsion implies a gear shift with oscillating transmission speed.

By using feedback control, initial driveline oscillations are handled independently of the state at which the gear shift is commanded. The difference in control signal, depending on the start time of the gear shift, is another strong motivation that feedback control is necessary, since an open-loop scheme would not be able to handle these oscillations.

Conclusions

The theme of this work is speed control and torque control of a vehicular driveline with engine controlled damping of driveline resonances. Novel strategies for two driveline management applications are derived and validated in field trials with a heavy truck.

One application is automatic gear shifting utilizing engine control to shift to neutral and synchronize speeds during the shift sequence, without using the clutch. The main contribution of the thesis is the derivation and implementation of a new strategy for fast engine control to a torque-free state in the transmission. The idea behind the strategy is to use internal driveline torque control. A key contribution is the derivation of a transmission-torque control strategy, based on a model describing the transmission torque, and a criterion for a controller that drives this torque to zero. This gives a way of systematically disengaging the gear with minimized driver disturbances and faster speed synchronization, despite disturbances and driveline resonances at the start of the gear shift. Field-trial demonstrations show that it is sufficient to control the drive-shaft torsion to zero, and still maintain high gear-shift quality. This scheme is simple and robust against variations among different gears. Furthermore, damping of driveline resonances can be obtained with an observer in combination with a PID feedback structure, with simple tuning rules for active damping. The strategy has successfully been implemented with a virtual drive-shaft torsion sensor based on standard automotive speed sensors and a Kalman filter. Another advantage with using the simpler scheme, utilizing a consistent physical variable, is that extensions to monitoring, supervision, and adaptive control are simpler.

Another application is wheel-speed control using engine control, aiming at reduced vehicle shuffle. A new speed-control strategy, that includes the behavior of the driveline in the control scheme, is proposed. The derived model-based state-feedback controller calculates the fuel amount such that driveline oscillations are reduced. At the same time the speed is maintained with the same type of velocity lag (when going uphill or downhill) as with the traditional control scheme. Implementation shows significantly reduced driveline oscillations, also when facing nonlinear torque limitations from maximum torque and diesel smoke delimiters.

A common basis for the two control strategies is the modeling conclusions. Three driveline models of increasing complexity are derived that explain the oscillations in the measured driveline speeds. The main flexibility of the driveline is shown to be the drive shaft, located between the final drive and the wheels. A key result is that a simple linear model with a drive-shaft flexibility can capture the first main resonance of the driveline. The derived strategies are based on this model, which is shown to be sufficiently detailed for control design, and is easy to implement with only three states.

Successful implementations show that the response time of the diesel engine is clearly sufficient for reducing low-frequent driveline oscillations, despite the simplified treatment of the dynamical behavior of the engine. Sufficient accuracy in the estimated values can be obtained with standard automotive sensors. However, an investigation about how different sensor locations influence control performance has demonstrated the importance of the wheel-speed sensor for disturbance rejection and robustness properties. This investigation aims at understanding where to invest in increased sensor quality in future driveline management systems, which is interesting since successful field trials have demonstrated the advantage of active damping.

References

- [1] K. J. Åström and B. Wittenmark. *Computer Controlled Systems, Theory and Design*. Prentice-Hall, 1984.
- [2] Automotive Handbook. Robert Bosch GmbH, 1993.
- [3] A. Björnberg, M. Petterson, and L. Nielsen. Nonlinear driveline oscillations at low clutch torques in heavy trucks. *Presented at Reglermötet '96 in Luleå, Sweden*, 1996.
- [4] CAN Specification. Version 2.0. Philips GmbH, Hamburg, Germany, 1991.
- [5] Diesel Fuel Injection. Robert Bosch GmbH, 1994.
- [6] S. Edlund and T. Henriksson. User's manual and technical documentation of Vehicular Systems's realtime system. Vehicular Systems, Linköping University, Sweden, 1996.
- [7] G. F. Franklin, J. D. Powell, and M. L. Workman. *Digital Control of Dynamical Systems*. Addison-Wesley, 1990.
- [8] T. D. Gillespie. *Fundamentals of Vehicle Dynamics*. SAE International, 1992.
- [9] T. Henriksson, M. Petterson, and F. Gustafsson. An investigation of the longitudinal dynamics of a car, especially air drag and rolling resistance. Technical Report LiTH-ISY-R-1506, Department of Electrical Engineering, Linköping University, 1993.
- [10] T. Kailath. *Linear Systems*. Prentice Hall, 1980.

-
- [11] C.S. Kubrusly and H. Malebranche. Sensors and controllers location in distributed systems - a survey. *Automatica*, 21:117–128, 1985.
 - [12] L. Ljung. Control Theory 1984-1986. *Automatica*, 24:573–583, 1988.
 - [13] L. Ljung. *System Identification Toolbox. User's Guide*. MathWorks, Inc., 1995.
 - [14] J. M. Maciejowski. *Multivariable Feedback Design*. Addison-Wesley, 1989.
 - [15] J. L. Meriam and L. G. Kraige. *Engineering Mechanics, Dynamics*. John Wiley & Sons, 1987.
 - [16] C. Y. Mo, A. J. Beaumont, and N. N. Powell. Active control of driveability. SAE Paper 960046, 1996.
 - [17] K. Nordgård and H. Hoonhorst. Developments in automated clutch management systems. SAE Paper 950896, 1995.
 - [18] C. O. Nwagboso. *Automotive Sensory Systems*. Chapman & Hall, 1993.
 - [19] L. Orehall. Scania OptiCruise: Mechanical gearchanging with engine control. Truck and Commercial Vehicle International '95, 1995.
 - [20] M. Pettersson. Driveline modeling and principles for speed control and gear-shift control. Licentiate Thesis ISBN: 91-7871-744-2, 1996.
 - [21] M. Pettersson and L. Nielsen. Sensor placement for driveline control. *Preprint of the IFAC-Workshop on Advances in Automotive Control, Ascona, Switzerland*, 1995.
 - [22] M. Pettersson and L. Nielsen. Driveline modeling and RQV control with active damping of vehicle shuffle. SAE Paper 970536, 1997.
 - [23] M. Pettersson, L. Nielsen, and L.-G. Hedström. Transmission-torque control for gear-shifting with engine control. SAE Paper 970864, 1997.
 - [24] PPCan. User's guide. Mecel AB, Göteborg, Sweden, 1996.
 - [25] RTKernel. Real-time multitasking kernel 4.5. On Time Informatik GMBH, 1996.
 - [26] Simulink. User's guide. MathWorks, Inc., 1993.
 - [27] M. W. Spong and M. Vidyasagar. *Robot Dynamics and Control*. John Wiley & Sons, 1989.
 - [28] K. Suzuki and Y. Tozawa. Influence of powertrain torsional rigidity on NVH of 6x4 trucks. SAE Paper 922482, 1992.

Notations

Variables

r	Radius, reference signal
u	Control signal
z	Performance output
x	State vector
y	Sensor output
v	State disturbance, velocity
e	Measurement disturbance
n	Input disturbance
l	Load
θ	Angle
α	Road slope
F_a	Air resistance force
F_r	Rolling resistance force

Symbols

J	Mass moment of inertia
-----	------------------------

i	Conversion ratio
k	Torsional stiffness
c	Torsional damping
b	Viscous friction component
m	Vehicle mass
c_{r1}, c_{r2}	Rolling resistance coefficients
c_w	Air drag coefficient
ρ_a	Air density
A_a	Vehicle cross-section area
M	Torque, performance output state matrix
A	State-space matrix
B	Input state matrix
C	Output state matrix
H	Load state matrix
D	Performance-output control-signal matrix
G	Transfer function
$G_{w/m}$	Dynamic output ratio
S	Sensitivity function
T	Complementary sensitivity function
K_c	State-feedback gain
K_f	Observer gain
φ	Phase margin
a	Amplitude margin
γ	Sensor filter constant

Subscripts

m	Engine
c	Clutch
t	Transmission
p	Propeller shaft
f	Final drive
d	Drive shafts
w	Wheel
fr	Friction
0	Stationary value
$t1$	Transmission input
$t2$	Transmission output

Index

A
automatic gear shifting 2, 6, 127
Åström, K. J. 90

B
basic driveline equations 24
Beaumont, A. J. 1, 23
Björnberg, A. 45, 78

C
CAN-bus 18–20, 90, 119
Clutch and drive-shaft model 41,
42, 50, 64, 101, 103
clutch nonlinearity 43, 46, 78, 115
complementary sensitivity fcn. . . . 56,
60, 61, 74, 77, 89, 114

D
Decoupled model 123
diesel smoke delimiter 11, 16, 90,
92–94
disturbance description 51, 52
Drive-shaft model 32, 38, 47,
50, 64, 78, 98, 103, 115, 128
drive-shaft torsion control 3, 127,
134, 136–140

driveline load 26, 45, 51, 64, 70, 94
dynamic output ratio 57, 58, 62,
74, 76, 81, 114, 118

E
Edlund, S. 18
engine friction 11, 17, 24, 28, 95
Euler’s method 28

F
Franklin, G. F. 84
fuel-injection strategy 1, 5, 7

G
gear shifting by engine control . . . 2, 6,
7, 97, 127
gear-shift condition 107, 135
gear-shift control 3, 10, 97,
108, 127, 134
Gillespie, T. 23, 26
Gustafsson, F. 27

H
Hedström, L.-G. 3
Henriksson, T. 18, 27

I

in-line pump injection system 2,
11, 14, 28
internal driveline torque . . . 3, 97, 98,
127, 128

K

Kailath, T. 54, 56, 73
Kraige, L. G. 24
Kubrusly, C.S. 49

L

Ljung, L. 27, 49
Loop-transfer recovery, LTR 60,
72, 86, 110
LQG/LTR 3, 54, 67, 108

M

Maciejowski, J. M. 53, 54, 56,
59, 68, 69, 72, 110
Malebranche, H. 49
maximum torque delimiter . . . 11, 16,
17, 93
Meriam, J. L. 24
Mo, C. Y. 1, 23
modified compl. sensitivity fcn. . . 57,
60–62

N

Nielsen, L. 1, 3, 23, 45, 50, 78
Nonlinear clutch and drive-shaft model
44, 46, 78, 102, 115
Nwagboso, C. O. 17

O

OptiCruise 14, 15
Orehall, L. 2, 14

P

parameter estimation. 32, 41, 44, 121
parameter estimation software. . . . 27
performance output 52, 64, 98
Pettersson, M. 1, 3, 23, 27, 45, 50, 78
Powell, J. D. 84
Powell, N. N. 1, 23
pre-filtering ref. value. 57, 85, 87

R

real-time simulator 90, 91
return ratio 53, 59, 74
RQ control 5
RQV control . . . 1, 3, 5, 48, 64, 70, 91

S

Scania 124L truck . 13, 14, 29, 47, 90
Scania 144L truck 14, 16, 29, 30
Scania DSC12 engine 13, 15
Scania DSC14 engine 14
Scania GRS900R transmission 13–15
sensitivity function 56, 60, 61,
75, 77, 89, 114
sensor dynamics 17, 37, 38, 47
sensor location. . . 2, 3, 49, 54, 62, 71,
78, 87, 90, 93, 110, 115, 131
speed control 3, 9, 54, 63,
64, 69, 83, 92, 95
speed synchronization phase 7,
8, 10, 103, 110, 137, 141
Spong, M. W. 49
state-space description 50
Suzuki, K. 23

T

torque control phase . . . 7, 8, 10, 103,
110, 141
Tozawa, Y. 23
transmission torque . . . 2, 97, 98, 127
transmission-torque control 3, 97,
103, 110
Tustin's method 84

U

unconstrained active damping . . . 105
unit-pump injection system . . . 2, 11,
13, 28, 95

V

Vidyasagar, M. 49
virtual drive-shaft torsion sensor 129,
132

W

Wittenmark, B. 90
Workman, M. L. 84